DOKUZ EYLÜL UNIVERSITY

GRADUATE SCHOOL OF NATURAL AND APPLIED SCIENCES

MODELLING AND OPTIMIZATION OF DIFFERENT HYDRAULIC SCHEMES OF A HEATING APPLIANCE FOR DOMESTIC HOT WATER (DHW) COMFORT AND EFFICIENCY

by

Ayşe Uğurcan ATMACA

August, 2013

İZMİR

MODELLING AND OPTIMIZATION OF DIFFERENT HYDRAULIC SCHEMES OF A HEATING APPLIANCE FOR DOMESTIC HOT WATER (DHW) COMFORT AND EFFICIENCY

A Thesis Submitted to the
Graduate School of Natural and Applied Sciences of Dokuz Eylül University
In Partial Fulfillment of the Requirements for the Degree of Master of Science in Mechanical Engineering, Thermodynamics Program

by

Ayşe Uğurcan ATMACA

August, 2013

İZMİR

M.Sc THESIS EXAMINATION RESULT FORM

We have read the thesis entitled **"MODELLING AND OPTIMIZATION OF DIFFERENT HYDRAULIC SCHEMES OF A HEATING APPLIANCE FOR DOMESTIC HOT WATER (DHW) COMFORT AND EFFICIENCY"** completed by **AYŞE UĞURCAN ATMACA** under supervision of **ASSOC. PROF. DR. AYTUNÇ EREK** and we certify that in our opinion it is fully adequate, in scope and in quality, as a thesis for the degree of Master of Science.

Assoc. Prof. Dr. Aytunç EREK

Supervisor

Arif Hepbaşlı, Prof. Dr.

(Jury Member)

Doç. Dr. Moghtada MOBEDI

(Jury Member)

Prof. Dr. Ayşe OKUR
Director
Graduate School of Natural and Applied Sciences

ACKNOWLEDGMENTS

The author wishes to express her sincere gratitude to her advisor Assoc. Prof. Dr. Aytunç Erek from Dokuz Eylül University, and her section manager Dr. Hürrem Murat Altay from Bosch Termoteknik Sanayi ve Ticaret A. Ş., R&D Centre. This project would not have been possible without their invaluable assistance, support, and guidance.

The author would also like to convey her thanks to the colleagues from Bosch Termoteknik Sanayi ve Ticaret A. Ş., R&D Centre., Mr. Cenk Acar and Dr. Turgut Oruç Yılmaz for their valuable discussions, Mr. Bruno A. R. Ribeiro for his helps in experiments, Mr. Özkan Dağlıöz and Mr. Halil Ufuk Özboğa for their technical support.

Special thanks are also to her beloved family for their endless support in her entire life; especially her mother Tekay Atmaca has a very special role in her life with her encouragement, suggestions, motivations, and friendship.

Deepest gratitude is also due to the greatest leader of the world and the Republic of Turkey, Mustafa Kemal ATATÜRK for the brilliant Turkish revolution achieved by his unique genius, well-planned strategies and confidence in Turkish public; for his principles still being the most important guidelines of Turkey as an independent country; and for the biggest proud that each Turkish person has as being a child of him.

Ayşe Uğurcan Atmaca

MODELLING AND OPTIMIZATION OF DIFFERENT HYDRAULIC SCHEMES OF A HEATING APPLIANCE FOR DOMESTIC HOT WATER (DHW) COMFORT AND EFFICIENCY

ABSTRACT

In this study, dual function heating appliances, commonly known as combi boiler type heating appliances, have been investigated. Combi boilers are used for both space heating and cold usage water heating and generally use natural gas as their energy source. The hot water requested by the users is called as domestic hot water (DHW). Throughout this study, only DHW supply function of a combi boiler type heating appliance has been investigated from the comfort and efficiency points of view.

Firstly, water heating appliances have been categorized generally. Gas-fired integrated space/water heating appliances which are one branch of this classification have been divided into different groups by considering the differences in their DHW supply function. From these groups, standard combi boilers and primary DHW concepts have been chosen for the efficiency and comfort comparison.

Later on, a mathematical model of the standard combi boilers has been employed by taking all system parameters into consideration in terms of their DHW supply function. 1D energy equations of the heat exchangers in a standard combi boiler have been established using thermodynamic laws and solved simultaneously in Matlab.

The numerical results obtained from the theoretical analyses have been compared with the experimental results and the constructed mathematical model has been verified for a standard combi boiler. After experimental verification, a similar mathematical model has been established for the primary DHW concepts. Through the constructed mathematical models, efficiency values and comfort levels of the appliance concepts have been compared theoretically. Besides, the effects of some

common parameters on the system behavior have been investigated and optimized for each appliance concept.

Finally, in the primary DHW concepts, DHW outlet temperature reaches the steady-state temperature more rapidly and they have higher efficiency in addition to lower wasted energy/useful energy ratio when compared to the standard combi boilers.

Keywords: Water heating appliances, combi boiler type heating appliances, domestic hot water (DHW), DHW comfort, DHW efficiency, mathematical modelling

SICAK KULLANIM SUYU (SKS) KONFORU VE VERİMLİLİĞİ İÇİN BİR ISITMA CİHAZININ DEĞİŞİK HİDROLİK SİSTEMLERİNİN MODELLENMESİ VE OPTİMİZASYONU

ÖZ

Bu çalışmada, yaygın olarak kombi tipi ısıtma cihazları olarak bilinen çift fonksiyonlu ısıtma cihazları incelenmiştir. Kombiler mahallerin ve kullanım suyunun ısıtılmasında kullanılırlar ve genellikle enerji kaynağı olarak doğal gaz kullanırlar. Kullanıcı tarafından talep edilen sıcak su sıcak kullanım suyu/ev sıcak suyu (SKS/ESS) olarak adlandırılır. Bu araştırma boyunca, kombi tipi bir ısıtma cihazının sadece sıcak kullanım suyu sağlama fonksiyonu verimlilik ve konfor özellikleri açısından incelenmiştir.

Öncelikle, su ısıtma cihazları genel olarak sınıflandırılmıştır. Bu genel sınıflandırmanın bir dalı olan gaz yakıtlı birleşik mahal/kullanım suyu ısıtma cihazları, kullanım suyu sağlama fonksiyonlarındaki farklılıklar dikkate alınarak kendi içerisinde gruplara ayrılmıştır. Bu gruplardan standart kombiler ve kullanım suyu öncelikli sistemler konfor ve verimlilik kıyaslaması için seçilmiştir.

Daha sonra kullanım suyu sağlama fonksiyonu açısından tüm sistem parametreleri dikkate alınarak standart kombi cihazları için matematiksel bir model kurulmuştur. Termodinamik yasalar kullanılarak standart bir kombideki ısı değiştiricilerinin bir boyutlu enerji denklemleri elde edilmiştir ve Matlab ortamında eş zamanlı olarak çözülmüştür.

Teorik analizler sonucu elde edilen sayısal sonuçlar deneysel sonuçlarla karşılaştırılmıştır ve kurulan matematik model standart bir kombi için doğrulanmıştır. Deneysel doğrulama yapıldıktan sonra, benzer bir matematik model kullanım suyu öncelikli sistemler için kurulmuştur. Kurulan matematik modeller üzerinden, cihaz sistemlerinin verimlilik değerleri ve konfor seviyeleri teorik olarak

karşılaştırılmıştır. Ayrıca bazı ortak parametrelerin sistem davranışı üzerindeki etkileri araştırılmış ve her bir cihaz sistemi için optimize edilmiştir.

Sonuç olarak, kullanım suyu öncelikli sistemlerde, kullanım suyu çıkış sıcaklığı daha hızlı bir şekilde kararlı durum sıcaklığına ulaşır ve bu cihazlar standart kombilerle kıyaslandığında, düşük atık enerji/faydalı enerji oranına ek olarak daha yüksek verimlilik değerlerine sahip olurlar.

Anahtar kelimeler: Su ısıtma cihazları, kombi tipi ısıtma cihazları, sıcak kullanım suyu (SKS), SKS konforu, SKS verimliliği, matematik modelleme

CONTENTS

Page

LIST OF FIGURES

Page

LIST OF TABLES

Page

CHAPTER ONE
INTRODUCTION

1.1 General Introduction

Stringent customer and governmental demands are continuously shaping the water heating industry; resulting in large product portfolio with new high efficiency boilers (Atmaca, Altay, Ribeiro, & Erek, 2013). In this study, dual function heating appliances used for both space and domestic hot water (DHW) heating have been investigated. In the case of DHW heating, hot water is used for purposes such as showers, baths and personal hygiene (ablution), washing of cooking and eating utensils and general cleaning purposes including clothes washing, whereas in the case of space heating, heated water is usually distributed via a pipe system (loop) to provide heating via radiators that are placed around the dwelling (Waide, 2011). This kind of appliances generally uses natural gas as their energy source. Therefore, from the combination of these characteristics, they are also called as gas-fired integrated space/water heating appliances. The main topic that has been focused on this study is the usage water supply function of this kind of appliances.

In terms of space heating function; highly efficient condensing appliances have been manufactured; however there is still room for challenge to increase the DHW comfort levels and efficiency. In some markets the DHW comfort level expectation of the end-user is significantly high, shaping the competition of the heating industry; i.e. the end user desires the set temperature to be reached very rapidly, without any fluctuation in the hot water temperature by not spending extra cost on high-tech sensors, etc. (Atmaca et al., 2013).

First of all, after a detailed classification of gas-fired integrated space/water appliances has been proposed, all branches have been explained broadly. In this classification, standard combi boilers and primary DHW concepts are the ones that have been modeled theoretically. Standard combi boilers and primary DHW concepts include two heat exchangers as primary and secondary heat exchangers. In standard

combi boiler, primary heat exchanger (P-HE) mainly heats the central heating (CH) water sent through the radiators to warm up the surrounding air. At the time of usage water request, CH water is sent to secondary heat exchanger (S-HE) (not to radiators) to give its energy to domestic cold water (DCW); thereby increasing the temperature of the cold usage water. However, in primary DHW concept, P-HE heats directly the tapping water (DCW) when there is user demand of hot water; and in other times it heats up the water sent through the S-HE where CH water is heated for space heating. In summary, in the standard combi boiler, P-HE heating the CH water and S-HE heating the DHW has been modeled, whereas in the other appliance system, the primary DHW concept, only P-HE has been modeled for DHW function of the appliances.

1.2 Objectives, Motivations, and Methodology

The main objective of the study is to model DHW supply function of two kinds of gas-fired integrated space/water heating appliances, the standard combi boiler and primary DHW concept to evaluate and compare their comfort levels and efficiency values with theoretical calculations.

The gain of constructing such kind of mathematical models is mainly estimating the results of the laboratory tests of new appliance concepts or proposed changes on regular appliance to evaluate their comfort levels and efficiency values. With these estimations the software parameters and heat exchanger design of combi boilers could be optimized during the design phase to minimize the trial-and-error procedure while developing a new boiler, thereby decreasing the number of the laboratory tests, saving prototype costs (if the appliance is on design phase), and saving time and energy spent on testing.

As the method of this study, 1D time dependent energy equations have been established for P-HE and S-HE of the standard combi boiler concept. The time dependent (transient) energy equations have been solved simultaneously in Matlab. Thermodynamic properties of the gas mixture (flue gases at the end of the

combustion) and water have been obtained via open source software Cantera (Goodwin, 2002). After mathematical model of the standard combi boiler has been constructed and the numerical results have been obtained, they also have been verified with the experiments. Therefore, the numerical results at the end of the theoretical analyses have been compared with the experimental results of the two separate primary and secondary heat exchanger combinations in economic and comfortable working modes of the combi boilers. Later on, the equations of the primary DHW concept have been constructed and solved in the same way. On the other hand, the primary DHW concept has no experimental verification since it is only proposed as a new concept and it is on the evaluation phase. Subsequently, the comfort level and efficiency value of both concepts have been compared theoretically.

When the comfort and efficiency comparison has been completed, a parametric study for both of the appliance concept has been conducted with the calculation algorithms of the appliance concepts. Common critical parameters thought to have essential effects on the comfort level of the appliance concepts such as (i) material type of P-HE, (ii) inlet temperature of the DCW, and (iii) water and gas volume capacity of the P-HE have been investigated.

CHAPTER TWO
BACKGROUND INFORMATION ABOUT WATER HEATING TECHNOLOGIES

2.1 Hot Water Demand of the Buildings

A typical home's energy use for heating water accounts for approximately 15% of the total consumption. When compared to the standard models, high efficiency water heaters use 10% to 50% less energy (High efficiency water heaters, n.d.).

In 2010, 9.1% of the total energy used by all buildings in the United States was consumed for water heating. As can be seen in Figure 2.1, water heating was the fourth largest energy end-use in the U.S. building stock (Research and development roadmap for water heating technologies, 2011).

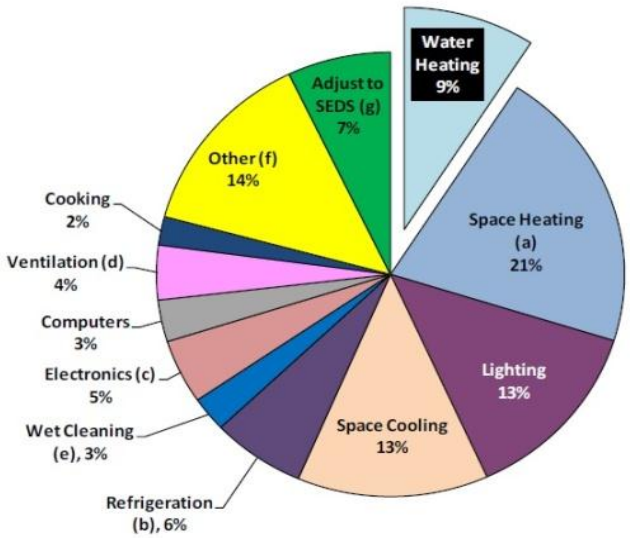

Figure 2.1 2010 U.S. Buildings energy end-use splits.

With reference to the statistics of the same year, in residential buildings water heating was responsible for 13.2% of the total energy consumption. As it is obvious from Figure 2.2, after space heating and cooling, water heating is the third energy end-use (Research and development roadmap for water heating technologies, 2011).

Additionally, from the same point of view, commercial buildings water heating consumption was about 4.3% of the total energy used by the commercial sector as it is shown in Figure 2.3. Commercial water heating consumption was concentrated in just a few building types. Hotels, hospitals, and food service together consume over 75% of the commercial sector's water heating energy (Research and development roadmap for water heating technologies, 2011).

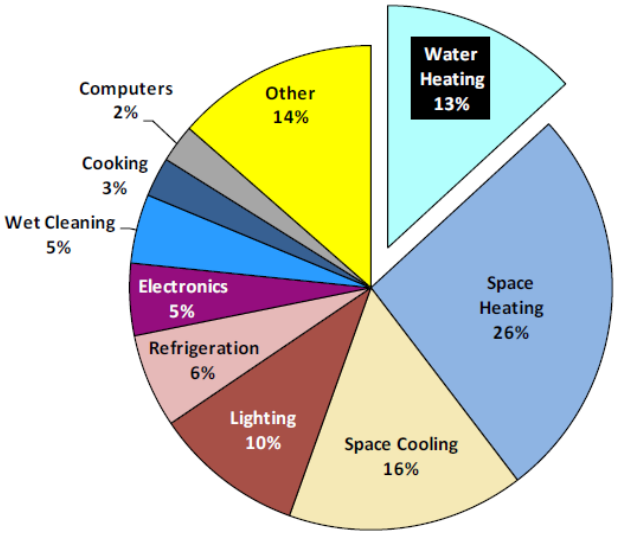

Figure 2.2 Residential buildings energy use by end-use.

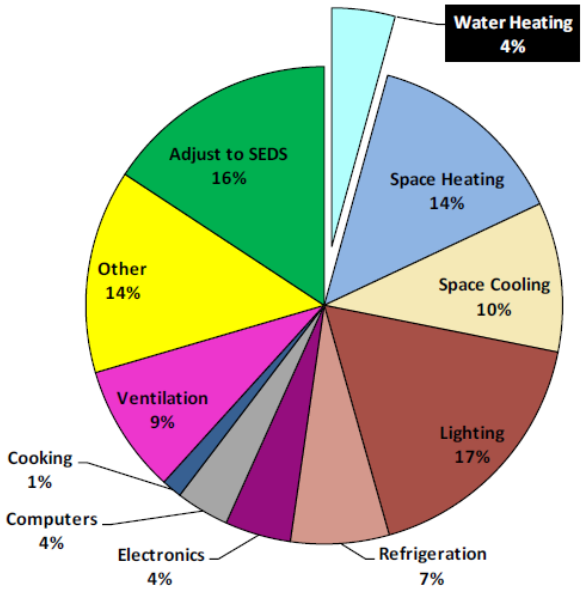

Figure 2.3 Commercial buildings energy use by end-use.

2.2 Classification of Water Heaters

Water heating appliances include an extremely diverse range of product types that are used primarily for domestic hot water, space heating or both of these functions. Water heating appliances are very popular product types for developed and developing countries.

Two kinds of classifications for water heating appliances have been given. In Figure 2.4, water heating technologies are classified according to energy sources commonly used and the working configuration of the heating system (Waide, 2011).

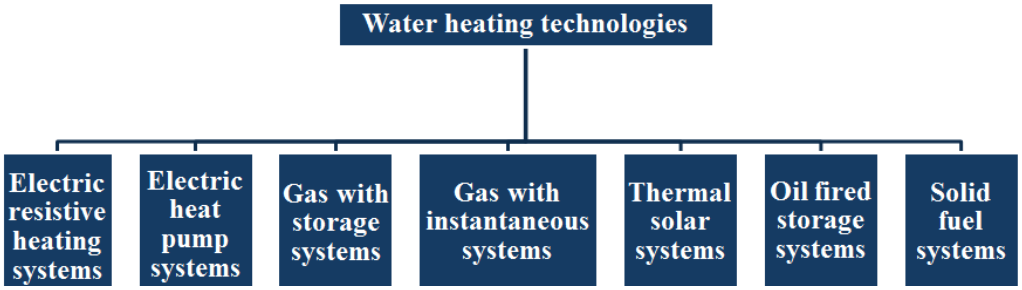

Figure 2.4 Classification of water heating technologies according to energy source and working configurations of the appliances (Waide, 2011).

The most common configurations are storage systems, instantaneous systems, circulation systems, and combinations systems.

In storage systems, water is heated and stored in an insulated tank or vessel for use when required. Heat can be added to the water using any of the above-mentioned technologies. Within the storage type, there are displacement water heaters and heat exchange types. In displacement water heaters, the hot water in the storage tank is supplied directly to the users and cold water displaces the consumed hot water to be heated up for further requirements. However, in heat exchange types, incoming cold water is heated using stored hot water in a vessel, and a heat exchanger. Then, energy is transferred from hot water to the cold tapping water and supplied to the users (Waide, 2011).

Instantaneous systems generate hot water when hot water demand is created. These kinds of systems include little or no hot water is stored. Typically, very high power inputs are required to meet the hot water demand and these are usually limited to gas systems (Waide, 2011).

In circulation systems, hot water is pumped in a loop and the temperature in the hot water loop is maintained by a water heating appliance. These kinds of systems are usually used for space heating applications (Waide, 2011).

In combination systems, domestic hot water and space heating functions are supplied with one water heater (Waide, 2011).

Water heating appliances has extremely large product range all around the world. In most regions, products tend to be designed for and adapted to local requirements, conditions, and available fuels (Waide, 2011).

A classification given in Figure 2.5 shows several types of water heaters according to working configuration and heating technology (Types of water heaters, n.d.).

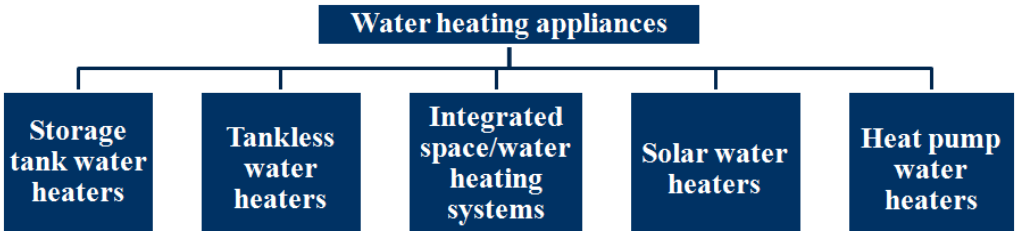

Figure 2.5 Classification of water heaters according to the working configurations and heating technology (Types of water heaters, n.d.).

In addition to the above-given information, efficient storage tank water heaters can perform as much as 40% better when compared to conventional models. Extra tank insulation for better heat retention and less standby losses, a better heat exchanger to transfer more heat from the energy source to the water, and factory-installed heat traps used for avoiding flow of hot water out of the tank are the

features that an energy-efficient model must primarily have. Tankless water heaters are the same as instantaneous water heaters. The water is heated when it is need to avoid standby heat loss through tank walls and water pipes. Integrated space/water heating systems are the combination systems defined in the previous classification. Furthermore, solar water heaters use the sun's energy to heat water as their energy source. Solar systems can supply up to 50% of the energy requirement of a household. Solar water heaters can significantly reduce a household's water heating costs since energy from the sun is free. Lastly, heat pump water heater technology uses electricity to move heat from one place to another instead of generating heat directly. Heat is transferred from one environment to another via a refrigerant (Types of water heaters, n.d.).

As emphasized from the beginning of this study, gas-fired integrated space/water heating appliances have been investigated in this study. In the following section a detailed classification of this appliance group is expressed.

2.3 Classification of Integrated Space/Water Heating Appliances

Integrated space/water heating systems supply both household heating and the hot water requirements thereby saving money on total system installation. They use generally natural gas as their energy source. The heater is sized to produce enough heat to warm a house on the coldest winter day (Types of water heaters, n.d.). They are also called *combi boilers* since they combine space and DHW heating requirements of a household.

In terms of DHW supply function; this appliance group includes a variety of sub-groups since all of them have different hydraulic concepts. An example classification is given in Figure 2.6. However, making other reasonable classifications is possible.

Each of the appliance concepts given in the example classification of the integrated space/water heating systems is explained in the following sections.

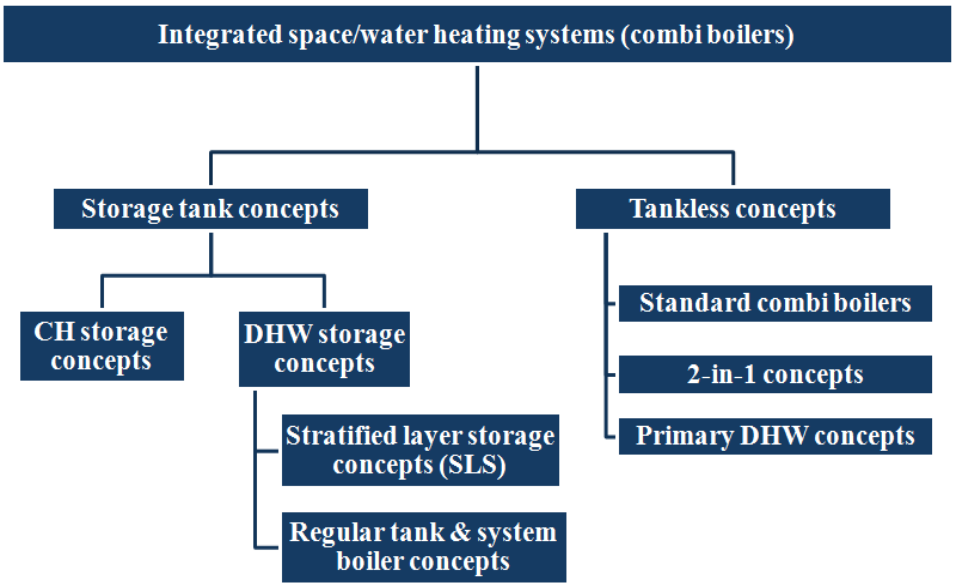

Figure 2.6 Classification of integrated space/water heating appliances in terms of DHW supply function.

2.3.1 Tankless Concepts

Heating appliances producing hot water instantaneously according to the demand of the users are divided into three groups according to their hydraulic scheme as standard combi boilers, 2-in-1 concepts, and primary DHW concepts.

2.3.1.1 Standard Combi Boilers

The most important components of an ordinary gas-fired combi boiler in addition to its control unit are: (i) a primary heat exchanger, (ii) a secondary heat exchanger, (iii) a pump, and (iv) a diverter valve as shown in Figure 2.7.

The primary heat exchanger and the secondary heat exchanger heat up the CH water and the DHW, respectively. In space heating mode, CH water heated by the primary heat exchanger is sent to the radiators to warm up the surrounding air. When there is domestic hot water demand, i.e. in the DHW mode, the diverter valve changes its position so that the heated CH water in the HE flows through the secondary heat exchanger (instead of flowing to the radiators) to warm up the tap water (domestic cold water (DCW)) to produce DHW (Atmaca et al., 2013).

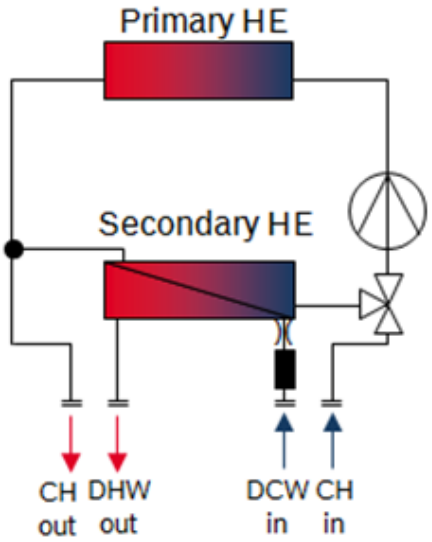

Figure 2.7 Schematic view of a standard combi boiler.

The basic component, primary heat exchanger is called heat cell (HC) and has combustion inside. Energy from hot combustion products is transferred to the CH water flowing around the HC. One of the reference HCs that has been modeled in this study is given in Figure 2.8.

Figure 2.8 Cross-sectional view of one of the reference heat cell (HC).

The secondary heat exchanger is plate heat exchanger, as shown in Figure 2.9. A plate heat exchanger has layer by layer structure. Hot CH water heated by the HC transfers its energy to the cold tapping water, DCW in the PHE.

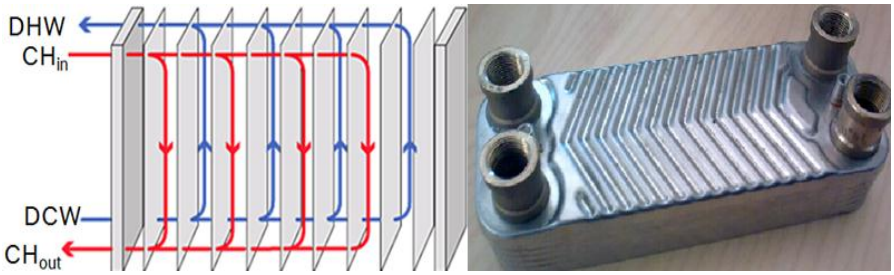

Figure 2.9 Plate heat exchanger and its working principle.

Basically, there are two working modes in a standard combi boiler as eco and comfort mode for DHW supply function. In eco mode, when tapping is created, the CH water and DHW is heated up instantaneously. On the other hand, comfort mode has regular pre-heat periods for increasing CH water temperature in the system to an upper temperature limit in case there is a user-demand; therefore DHW set temperature is reached rapidly and waiting period to produce DHW from cold tapping water is diminished. As it is also obvious from Figure 2.10, whether there is tapping or not, with these pre-heat phases the CH water is always kept between critical upper and lower temperature limits.

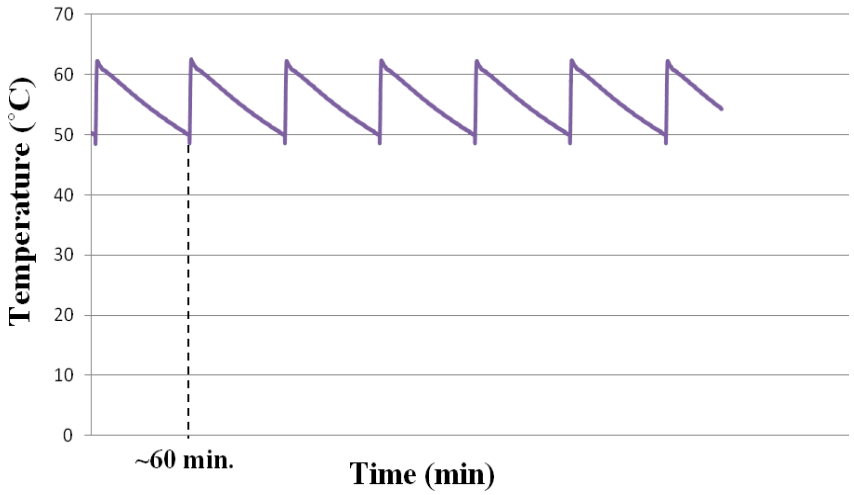

Figure 2.10 Regular heating periods of CH water because of losses to the environment (no hot water demand).

Thanks to the pre-heat phases, DCW is heated up to the desired set temperature levels in a shorter time when compared to eco mode as shown experimentally in Figure 2.11.

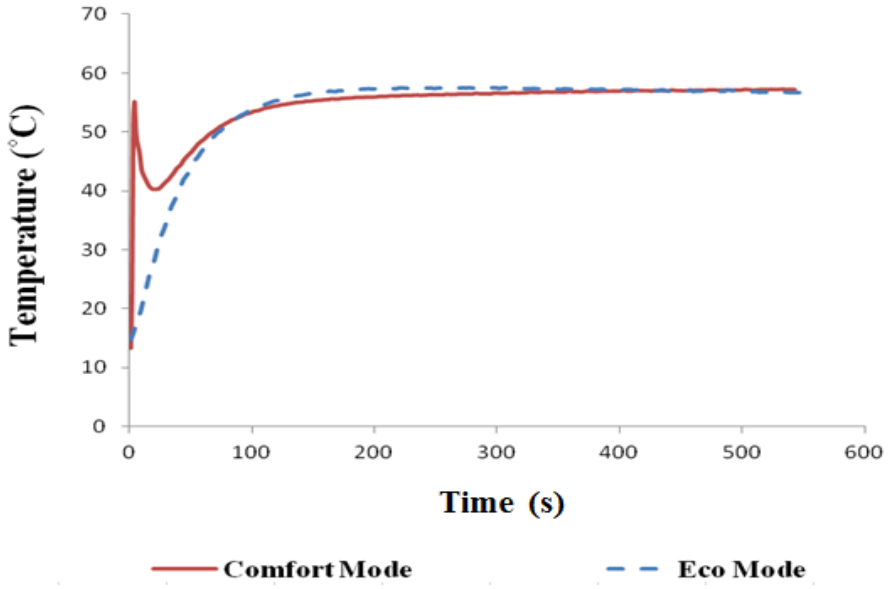

Figure 2.11 Comparison of experimental DHW outlet temperature in eco and comfort mode.

2.3.1.2 2-in-1 Concepts

Another tankless concept is 2-in-1 concept and as it is obvious from its name, there is only one heat exchanger including pipes of both DHW and CH water. The schematic view of this concept is shown in Figure 2.12.

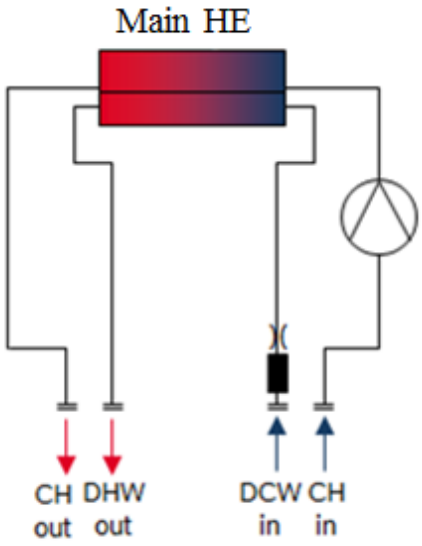

Figure 2.12 Schematic view of a 2-in-1 concept.

In the nested structure of the heat exchanger, DHW pipes are located in the CH pipes as seen in Figure 2.13.

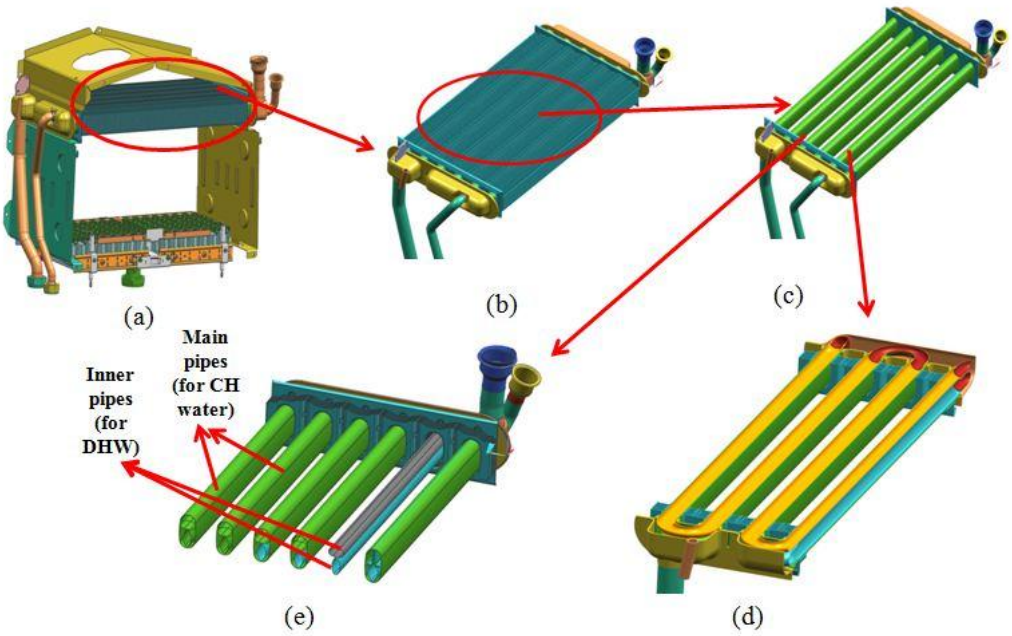

Figure 2.13 Structure of the heat exchanger of 2-in-1 concept; (a) heat exchanger assembly with burner, (b) heat exchanger with fins, (c) heat exchanger pipes, (d) top cross-sectional view of CH and DHW pipes in the heat exchanger, (e) front cross-sectional view of CH and DHW pipes in the heat exchanger.

This concept is also called “tube-in-tube” concept since DHW pipes are located in CH pipes. The above-given sketches belong to longitudinal pipe configuration. With the same working principle of this concept, another tube-in-tube appliance can be designed in spiral pipe configuration as shown in Figure 2.14.

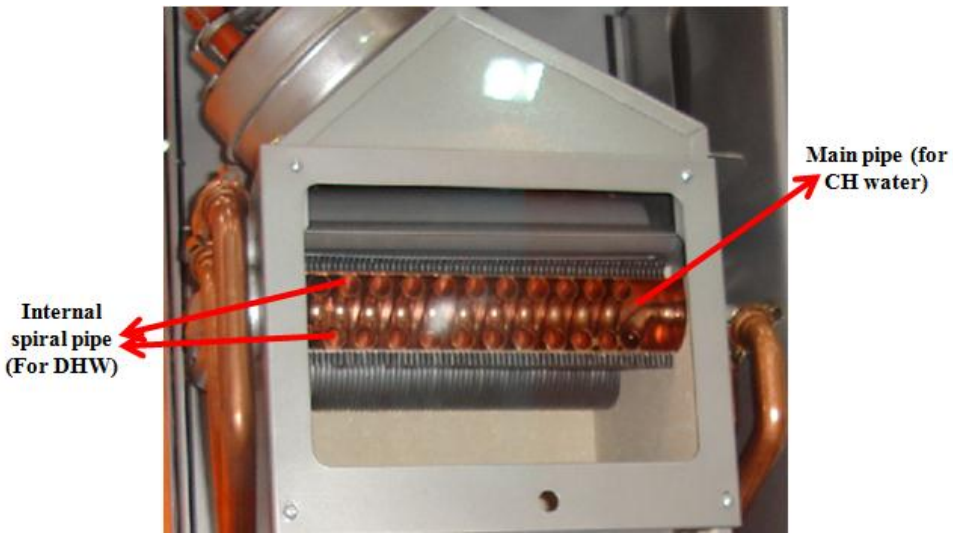

Figure 2.14 Spiral pipe configuration of the tube-in-tube concept (Ferroli patented heat exchanger).

Basically, when the appliance is in space heating mode, the heated CH water in the main pipe flows to the radiators, transfers its energy to the surrounding air, cools down and turns back to the heat cell to be heated up again. If DHW request is created, the pump stops circulating the CH water through the radiators. The CH water in the main pipe is used to heat DCW (demanded water). When compared to standard combi boilers, this concept also does not have a diverter valve. Space heating mode is activated with the pump in winter times.

2.3.1.3 Primary DHW Concept

This concept is similar to standard combi boiler concept; but DHW is heated in the P-HE and CH water is heated in the S-HE. Working configuration of this concept is opposite to the standard combi boilers' as it is shown in Figure 2.15. This kind of concept is proposed for increasing the comfort level of the users by heating DHW in a shorter time since DHW request is always of priority importance.

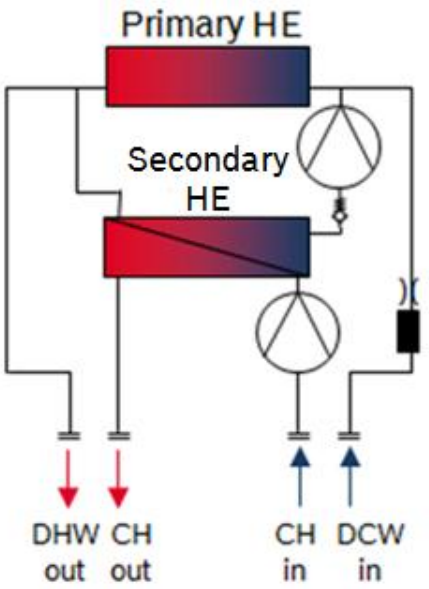

Figure 2.15 Schematic view of a primary DHW concept.

Similar to tube-in-tube concept, this concept also does not include a diverter valve. However, as opposed to previously defined concepts, this one has an additional pump.

In space heating mode, CH water is heated in the S-HE by the hot water sent from the P-HE. When DHW request is created, tapping water is heated by the P-HE. However, this appliance concept has some disadvantages. Standard combi boilers have calcification and blockage problems in S-HE due to the precipitation of some elements in DCW such as $CaCO_3$, $MgCO_3$, $CaSO_4$, and $MgSO_4$. In primary DHW concept, this time P-HE will have the same calcification problem. Another important point that is needed to be considered while converting a standard combi boiler into a primary DHW appliance concept is related to the pressure of the CH water and DHW circuits. Pressure of the DHW line is about 10 bar (Basınç düşürücüler, n.d.), whereas pressure of the CH water circuit is about 2-3 bar. Therefore, the P-HE and its circuit will be designed according to the requirements of the high pressure systems.

2.3.2 Storage Tank Concepts

Some systems have additional storage tanks for increasing the comfort level of the appliances. These systems are divided into two groups according to the types of water that is stored, as CH water and DHW storage concepts.

An additional storage tank is a must for fulfilling the requirements of some markets since the appliances have to get high scores at the end of the comfort tests to be sold in those markets.

2.3.2.1 CH Water Storage Concepts

Typical storage models in the market store DHW; so this is a completely different concept and aiming to introduce a new storage type heating appliance. As it is shown in Figure 2.16, it is simply the expansion of the standard combi boiler with a second diverter valve and a storage vessel.

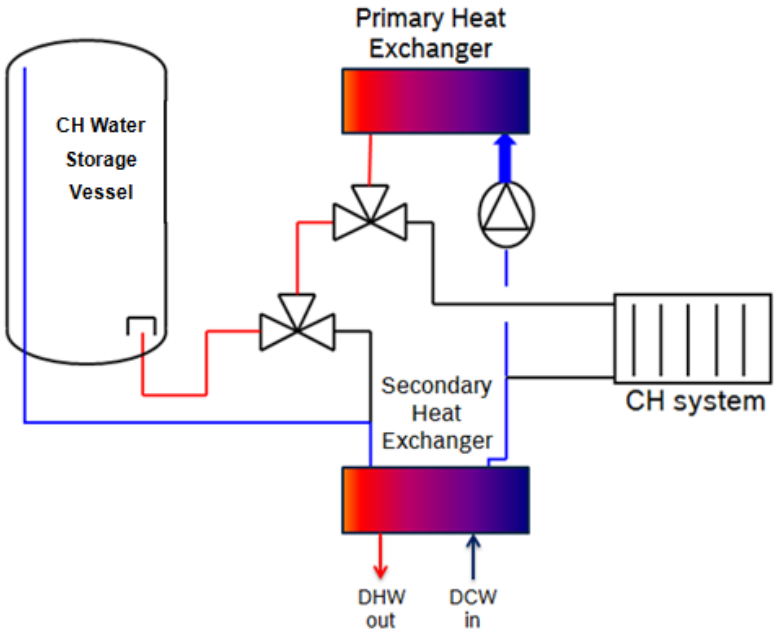

Figure 2.16 Schematic view of a CH water storage concept.

The volume of the storage vessel depends on DHW requirement. P-HE is directly connected to CH water storage tank (vessel). The water in CH storage tank is heated by the P-HE. When there is no DHW requirement, the cold water returns over S-HE by completing the circuit. This CH water storage load mode is also described by the colors of the lines in Figure 2.16. When there is DHW requirement, diverter valve changes direction. CH water goes through S-HE. The tapping water is heated. DHW mode is nearly the same as the standard combi boiler. At the beginning of DHW tapping or eco mode (just for small tapings) P-HE does not start; hot water heating the tapping water comes from storage. For big tappings, hot water supply starts from storage. For allowing high DHW peak, both P-HE and storage water can supply heat to S-HE. After tapping, storage tank will be reloaded by the P-HE again. Space heating mode is identical to the standard combi boilers. When high temperature space heating is demanded, the space heating function and the DHW function can be activated at the same time.

2.3.2.2 DHW Storage Concepts

As it is obvious from the title, ready-to-use DHW is kept in a storage tank; thereby increasing the comfort level of the users. Most commonly seen DHW storage

concepts are regular tank & system boiler concepts and stratified layer storage (SLS) tank concepts.

2.3.2.2.1 Regular Tank & System Boiler Concepts. The regular tank & system boiler concept is a kind of conventional storage concept including a standard tank for DHW storage. As shown in Figure 2.17, the DHW storage tank has copper coils inside.

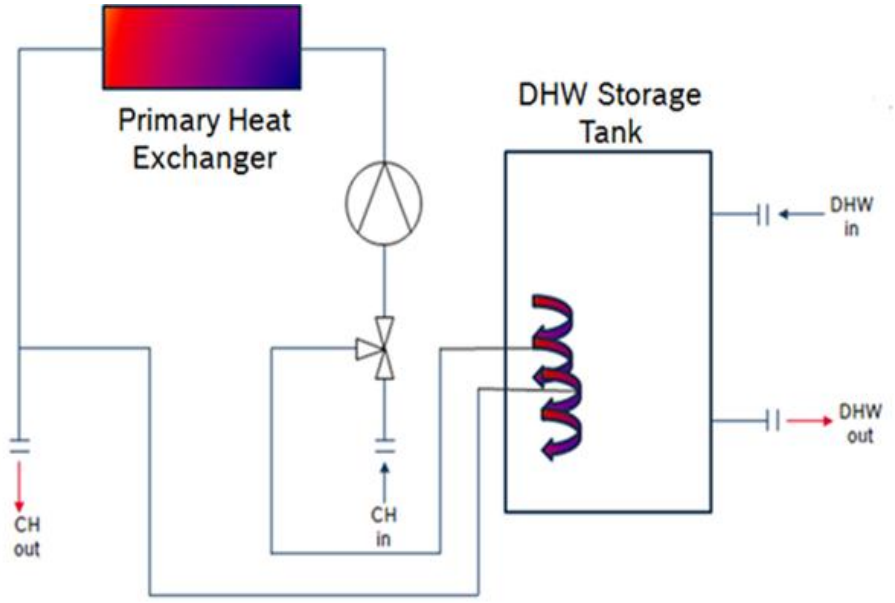

Figure 2.17 Schematic view of a regular tank & system boiler concept.

Different from the other concepts, this model does not include a S-HE. The temperature of the stored DHW in the tank is always kept above a critical limit in terms of comfort by the circulation of the CH water through the coils and P-HE.

Space heating mode is the same as the standard combi boiler. When there is DHW request, the diverter valve changes direction. At the time of tapping, DCW directly enters the tank and while it is being heated by the energy of the CH water circulating in the coils of the tank, previously heated DHW in the storage tank is supplied to the users.

2.3.2.2.2 Stratified Layer Storage (SLS) Tank Concepts. Generally speaking, stratified layer storage (SLS) tank concept appliances have high comfort level since they have both PHE and an additional storage tank as shown in Figure 2.18.

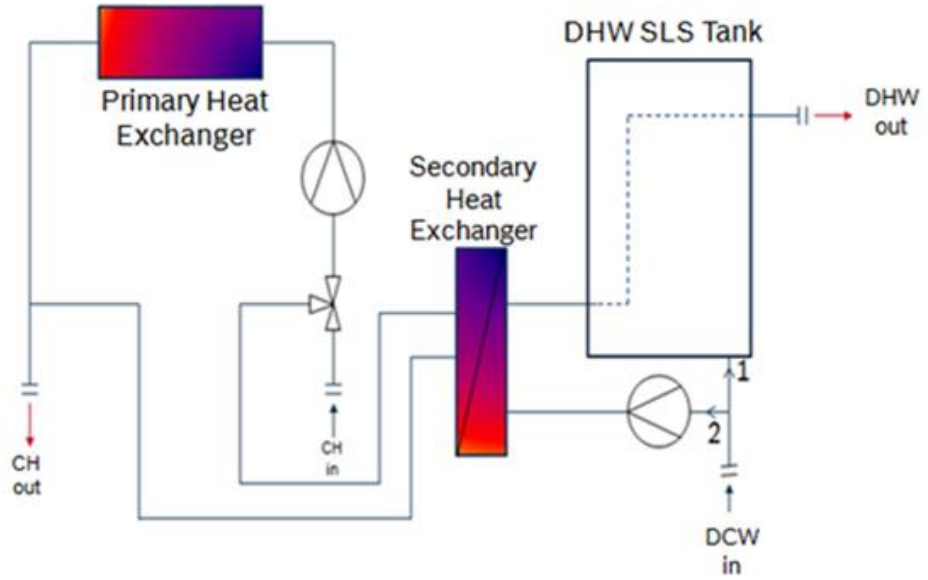

Figure 2.18 Schematic view of a stratified layer storage (SLS) tank concept.

Similar to other concepts, P-HE heats up the CH water and hot CH water is used for space heating in the radiators. When there is DHW request, the DCW directly enters the SLS tank (1. way shown in Figure 2.18) if the temperature distribution of the tank is above a critical limit defined according to the comfort level of the appliance. Otherwise, if temperature distribution of the tank falls below that comfort limit, the DCW enters the S-HE (2. way shown in Figure 2.18) to be heated and later sent to the tank for continuous supply of DHW at the desired conditions.

The typical models in the market stores DHW other than CH water. However, CH water storage concept is also an option for the future markets since it has some advantages over the DHW storage concepts. A simple storage tank is used in CH water storage concept, whereas stainless steel tank completely filled with copper is used for regular tank & system boiler concept. Furthermore, also when compared to the SLS tank concept, a DHW pump, a PHE, sensors, etc. costs are added to the stainless steel tank. Since CH water storage concept is less complex when compared to other ones, service costs will also reduce.

Integrated space/water heating appliances are categorized and explained broadly. Only two of these appliance types from tankless concepts, the standard combi boilers and the primary DHW concepts have been investigated and compared for their comfort level and efficiency of DHW supply function. Then, only both of these concepts have been expressed with mathematical equations. Since P-HE and S-HE have been modeled for the standard combi boiler and P-HE has been modeled for the primary DHW concept, a comprehensive literature review will be mentioned related to the mathematical Modelling of the heat exchangers in the next chapters.This literature review will be beneficial to give a general idea about the way of thinking while constructing the models of the heat exchangers of a combi boiler type of heating appliance.

CHAPTER THREE
LITERATURE REVIEW ABOUT MODELLING OF HEAT EXCHANGERS

The objective of this study is to establish a mathematical model, which takes all system parameters into consideration during operation in the DHW mode, to be able to simulate the DHW comfort level and efficiency value. Differential equations representing the energy balances in the primary and the secondary heat exchangers are constructed, and numerically solved. Then, numerical results are compared with the experimental results for validation. The most important step of the construction of the mathematical model is obtaining correct energy equations including all heat transfer processes in and out of the inspected domain. The literature has plenty of similar studies related to the mathematical Modelling issues of different types of heat exchangers under different operating conditions.

Bunce, & Kandlikar (1995) modeled a two-fluid counter-flow heat exchanger by deriving governing differential equations with some idealizations to simplify the problem. They compared different models in the literature and came up with specific recommendations regarding to their suitability to different types of problems. Different predicting schemes were evaluated for their suitable range of operation. In this study, energy balance was applied to the incremental control volumes around the hot fluid, the cold fluid, and the wall of the counter flow heat exchanger. After simplification of the equations of hot, cold, and wall media, solution of the transient heat exchanger problem was obtained by solving three simultaneous partial differential equations for temperature as a function of time and position. As the main objective, emphasize was placed on the application of previously presented major solutions (in literature) to the practical engineering problems.

Junxiao, Guiping, & Xiugan (1998) created a lumped parameter model for a two-pass gas-to-gas cross-flow heat exchanger to investigate its transient behaviours. This model could be used to investigate the effects of changes of both inlet temperature and flow rate on the outlet temperature. The calculation results under typical

conditions were compared with the experimental results and a good agreement is achieved. The effects of heat transfer perpendicular to the flow direction were not considered in this model since the flow at both the cold and hot sides of the heat exchanger were one dimensional. On the basis of the assumptions of one dimensional heat transfer process and neglected conduction resistance of the wall, three partial differential equations were obtained by applying energy balance to both fluids and the wall. In order to verify the reliability of the model, a test rig was constructed and the transient variation of the outlet temperature was measured. Finally, good agreement was achieved between the numerical and the experimental results.

Mishra, Das, & Sarangi (2006) investigated numerically the transient temperature response of cross-flow heat exchangers having finite wall capacitance with unmixed fluids, while providing perturbations in both temperature and flow. Transient performance of a direct transfer, single pass, two-fluid, cross-flow, multilayer plate-fin heat exchanger was analyzed under some simplifications. Applying the assumptions, conservation of energy for the wall and the two fluids could be expressed in non-dimensional form. The conservation equations were discretized using the implicit finite difference technique. The temperature response of the fluid streams as well as the separator plate was inspected solving the conservation equations by finite difference formulation for step, ramp as well as exponential variation of the hot fluid inlet temperature and step and ramp variation in flow rates. As a result, a numerical scheme was developed for determining the transient behavior of cross flow heat exchangers using finite difference method. The validity of the numerical scheme was checked by comparing the results of the present investigation with the available analytical results obtained with Laplace transform for balanced gas-to-gas cross-flow heat exchangers. The dynamic performance of the heat exchanger was investigated over a wide range of parameters. Numerical results were calculated for sufficient time duration so that steady state conditions were obtained for each individual excitation.

Ünal (1998) modeled triple concentric-tube heat exchangers providing better heat transfer efficiencies compared to double concentric-tube heat exchangers. The

physical model of the system was composed of three concentric tubes, forming one circular flow passage and two concentric annular flow passages. This theoretical study arose to decide on the diameters of three tubes for an optimum design. A set of equations were derived for well insulated triple tube heat exchangers under fully developed flow conditions in a rather straightforward way and using some properly defined parameters such as heat capacity flow rates, number of transfer units, and some other non-dimensional parameters. The derived governing equations were two second order differential equations and a first order ordinary differential equation. Second order ordinary differential equations were belong to the inner pipe flow and the flow in outer annulus, whereas the first order ordinary differential equation was for the fluid that flows through inner annulus. The differential equations were solved numerically. The model was constructed to investigate the bulk temperature variations of the three fluid streams along the heat exchanger. The triple concentric-tube heat exchanger was expressed in terms of all system parameter to analyze the effects of the changes created in the parameters on the exchanger performance or exchanger size. Under some similar assumptions mentioned in the previous literature studies while applying simple energy balance to the control volumes of each fluid domain, the governing ordinary differential equations were obtained. Consequently, the equations derived in this study could be used for both design calculations and performance calculations. Furthermore, they could be used for the determination of bulk temperature variations of the fluids along the exchanger.

Ataer, İleri, & Göğüş (1995) developed three different approaches for the prediction of transient performance of cross-flow, finned-tube liquid-gas heat exchangers for the step change in the temperature of the hot fluid. The first method was named as zero solid capacity (ZCA) and in the analysis made by using this method; the heat capacities of the wall and the fins were added to the capacities of the cold and hot fluids. The second method was called one solid capacity (OCA) and in this method the fins and tube wall were considered as one thermal capacity and the thermal resistance between them was neglected. The last method was two solid capacity (TCA) and in the analysis using TCA, the capacities of the fins and tube

wall were considered separately. Energy equations of the hot and cold fluids and if necessary according to the chosen approach, wall and fins were constructed. After obtaining the equations for each approach they were solved numerically with finite-difference method. A step change in the temperature of the hot fluid was created to investigate the variation of the dimensionless exit temperature. To show the availability of these approaches, an experimental study was performed, and numerical results were compared with the experimental results. The typical assumptions which were valid also for investigating steady-state behavior of the heat exchangers were made. However, some of the assumptions were specific to the type of the chosen approach. In the ZCA approach, energy equations of the hot fluid and the cold fluid were written. In the OCA approach, energy balances were obtained for the tube wall, the hot fluid and the cold fluid by considering the combined capacity of the tube and the fins. In TCA approach, energy balances were given in a similar way as the previously defined OCA method and the energy equations were obtained for the tube wall, the hot fluid, and the cold fluid. However, the masses of the tube wall and fins were considered separately and the total thermal resistances of the hot side, cold side, and the fin were expressed. In addition to the energy equations for the hot and cold fluids and the wall of the tube, the energy equation for the fin was also constructed. The energy equations were solved analytically in the ZCA method. A finite difference method was used for discretization of the above energy equations of OCE and TCA. After comparing the numerical results with the experimental results, it could be concluded that the TCA predictions were in best overall agreement with the experimental results. On the other hand, the results obtained by OCA were not as good as the results of the TCA method and the ZCA was possible to fail to provide sufficiently accurate results in some cases. As a result, OCA or TCA methods could be used to determine the gain and time constant of heat exchangers and to predict the effects of fins. These methods could also easily be modified for other heat exchanger types.

Gut, & Pinto (2003) developed a mathematical model in algorithmic form for steady-state simulation of gasketed plate heat exchangers with generalized configurations. The configuration parameters were the number of channels, number

of passes at each side, fluid locations, feed connection locations and type of channel-flow. The main objectives of this model were to study the configuration effects on the exchanger performance and as the next step to develop a method for configuration optimization. Temperature profiles in all channels, thermal effectiveness, distribution of the overall heat transfer coefficients, and pressure drop were the major simulation results which were aimed to be investigated. Furthermore, the assumption of the overall heat transfer coefficient was analyzed. Under some common simplifications, the mathematical model was derived by applying energy balances to the control volumes. The overall heat transfer coefficient between the channels was a function of the fluid convective heat transfer coefficient, the plate thermal conductivity, the thickness of the plate, and the fouling factors for hot and cold streams. There were two models in this study; overall heat transfer coefficient was considered as a function of temperature, whereas in the other model, constant overall heat transfer coefficient assumption was made. Both of the models were reduced to a linear system of ordinary differential equations which can be solved analytically. As summary, based on the defined parameters, a detailed mathematical model for the simulation of a PHE in steady-state with a general configuration was developed to simulate and compare different configurations. The assumption of constant overall heat transfer coefficient throughout the exchanger, which is commonly used in Modelling issues of heat exchangers, was tested and shows little influence over the main simulation results such as thermal effectiveness and outlet temperatures.

Galeazzo, Miura, Gut, & Tadini (2006) developed a virtual prototype of a four-channel plate heat exchanger with flat plates using computational fluid dynamics (CFD). Parallel and series flow arrangements were tested and experimental results were compared to the numerical predictions for heat load. As the first step of the CFD simulation, the meshes were generated on the geometrical domain where the equations for heat and momentum transfer were solved. The models contain approximately one million hexahedral elements and were created with the software GAMBIT (FLUENT Inc., Lebanon, USA). Then, boundary conditions and material properties were introduced as the second step. The problem was numerically solved

using the finite volume method with the software FLUENT 6.1.22 (FLUENT, Lebanon, USA). As a result, it was concluded that it was possible to build a virtual prototype of a PHE with four channels and flat plates by using a CFD tool. The simulation results were composed of outlet temperatures, heat load, 3D temperature and velocity distribution. The CFD results for parallel flow were in better agreement with experimental data.

Gögüş, & Ataer (1988) studied the effect of the fins on transient behaviour of cross-flow air-liquid heat exchangers. The well-known finite volume method was used to predict time response of a cross-flow heat exchanger to step change in the liquid temperature in order to determine the effective values of the coefficients of an approximate response function. Experiments were conducted to show the good agreement and verify the method used to take the effects of the fins into consideration. Preliminary results show that the time lag of the water exit temperature was smaller than the time lag of air temperature.

Rooke, & Elissa (1993) studied the transient behaviour of finned coil cross-flow heat exchangers. Firstly, previous applications available with analytical and numerical solutions were discussed. Water-to-air type cross-flow finned tube heat exchangers were investigated via the simplified governing equations and an up-wind finite difference scheme. Energy balances under some simplifications on an elemental unit of fin/tube, water, and air yielded the governing equations. The boundary and initial conditions were defined. A parametric study was presented as a result of this study. This research contributed further insight into Modelling requirements and insight into design of heat exchangers with considerations of transients.

In all these mentioned literature review, different type of heat exchangers under different operating modes have been modeled. However, the simultaneous coupling of two separate heat exchangers working in the real working conditions of an entire system, i.e. a water heater or a combi appliance, is missing. In this work our target is

to create this missing link between the comprehensive academic studies and the real-life industrial problems for the end-user benefit.

To sum up, in our study, the coupled heat cell and plate heat exchanger have been modeled for the standard combi boiler concept and only heat cell has been modeled for the primary DHW appliance concept.

CHAPTER FOUR
MATHEMATICAL MODELS FOR THE APPLIANCE CONCEPTS

1-D transient energy equations have been constructed to calculate the temperature profiles of the included media of the appliance concepts. For the standard combi boiler, energy equations have been constructed for the flue gas, CH water, and DHW, whereas for the primary DHW concept energy equations have been established only for the flue gas and DHW. For both of the models, heat transfer through the heat cell wall has been considered; hence they all include also the energy equation of the heat cell wall. The equations of each system have been solved simultaneously in Matlab. Cantera (Goodwin, 2002), an open source software, has been used in order to obtain thermodynamic properties of flue gas mixture and water.

4.1 Theoretical Model of the Heat Cell

Heat cell is one of the basic components including combustion inside. Combustion is exothermic conversion of chemical energy to thermal energy (Turns, 2012). The chemical equation of the combustion is given as follows:

$$\underbrace{C_n H_m}_{\text{Fuel}} + (n + \frac{m}{4})\underbrace{(O_2 + 3.76N_2)}_{\text{Oxidizer}} \rightarrow nCO_2 + \frac{m}{2} H_2O + 3.76(n + \frac{m}{4})N_2 \qquad (4.1a)$$

For the combustion in the combi boiler type heating appliances, fuel is natural gas and the oxidizer is air. Natural gas is composed of mainly CH_4 (methane) and other compounds (C_2H_6, C_3H_8, C_4H_{10}, etc.) having negligible percentages. Since methane is the basic compound in the natural gas, throughout this study, natural gas has been counted as CH_4. Furthermore, it is also assumed that the composition for air is 21 percent O_2 and 79 percent N_2 by volume, i.e., that for each mole of O_2 in air, there are 3.76 moles of N_2 (Turns, 2012).

After the simplifications about the fuel and the oxidizer of the combustion, the governing chemical equation specific to the heat cells under question is given below.

$$CH_4 + 2(O_2 + 3.76N_2) \rightarrow CO_2 + 2H_2O + 7.52N_2 \quad (4.1b)$$

The aforementioned combustion equation of the methane represents stoichiometric fuel-air mixtures. The stoichiometric quantity of the oxidizer is just that amount needed for complete burning of the fuel. If more than a stoichiometric quantity of oxidizer is supplied, the mixture is said to be fuel lean, or just lean, whereas if the supplied oxidizer is less than the stoichiometric amount, the mixture is called as fuel-rich, or just rich (Turns, 2012). In the combustion process that occurs in the heat cell, the air-fuel mixture is fuel lean, thus the last version of the combustion equation is given below with the introduction of excess air coefficient, λ.

$$CH_4 + 2\lambda(O_2 + 3.76N_2) \rightarrow CO_2 + 2H_2O + 2(\lambda - 1)O_2 + 7.52\lambda N_2 \quad (4.1c)$$

In the established mathematical model, the excess air coefficient in the chemical equation is calculated according the required CO_2 level of the appliance. In other words, CO_2 level is an input for the calculation algorithm of the mathematical model and excess air coefficient is defined according to it. CO_2 percentage is calculated using Equation 4.2a as CO_2 mole percentage and λ is calculated as given in Equation 4.2b. However, while calculating mole percantage of CO_2, the moles of H_2O are not considered since the gas analyzers from where CO_2 percentages are measured condensate H_2O at the time of measurement. Then, CO_2 levels are declared in the combi boiler catalogues according to the measurements from the gas analyzers and excess air coefficient is calculated with the above-mentioned logic.

$$CO_2\% = \frac{100}{1 + 2(\lambda - 1) + 7.52\lambda} \quad (4.2a)$$

$$\lambda = \frac{100 + CO_2\%}{9.52CO_2\%} \quad (4.2b)$$

While verifying the numerical results with the experiments, same working conditions have been created in the calculation algorithm. Therefore, the CO_2 levels

measured from the gas analyzers and put as the input in the calculations and λ is defined according to CO_2 level.

The energy arisen as a result of the combustion process is transferred to the CH water in the standard combi boiler concept. However, in the model of the primary DHW concept, the energy under question is transferred directly to the DCW. There are two heat cell concepts studied in this research. For the heat cells, general equation set is obtained and subsequently for experimental verification of the standard combi boiler concept, two heat cell models are chosen as conical and rectangular heat cell. The CH water in the standard combi boiler concept (or DCW in the primary DHW concept) flows around the conical heat cell, as modeled in Figure 4.1. As it is obvious, the conical heat cell has been approximated as a cylindrical model.

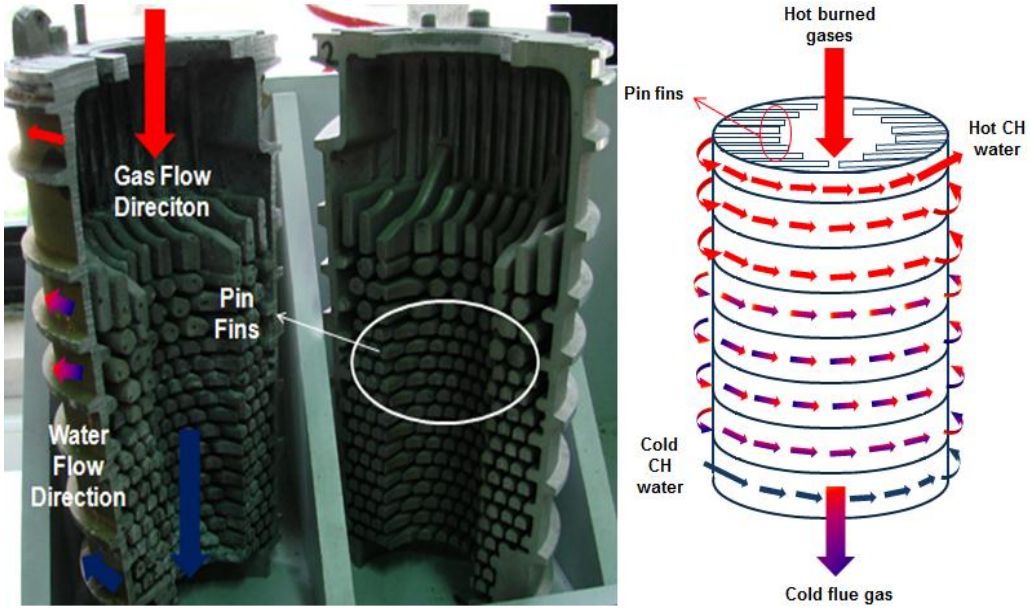

Figure 4.1 Cross-sectional view and the cylindrical model of the conical heat cell.

Heat transfer area of the HC between the hot combustion products and the cold water is enlarged with numerous number of pin fins for maximum heat transfer. In addition to fins, cross-flow arrangement of HC is also an important aspect for maximum heat transfer.

The basic working principle of the rectangular heat cell is similar to the conical heat cell; but the water (CH water of DCW) flows through the channels located inside of the heat cell as shown in Figure 4.2. There are annular fins around the water channels to increase heat transfer from hot combustion products to the water.

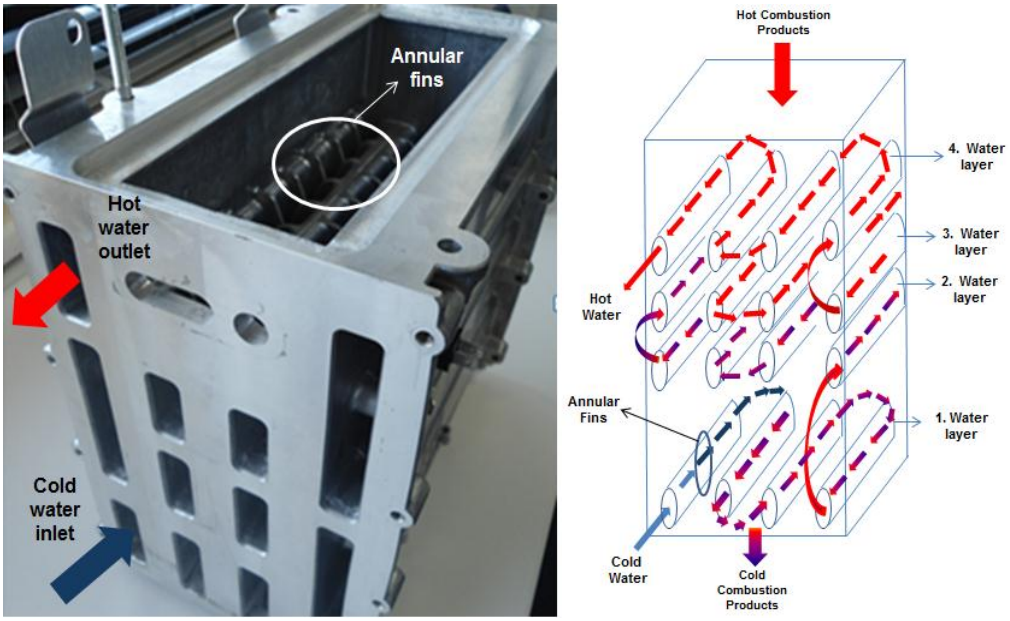

Figure 4.2 Designation of the working principle and numerical model of the rectangular heat cell.

For experimental verification of the standard combi boilers in eco and comfort working mode, both of the heat cells have been used; but for the subsequent comparisons and parametric studies conical heat cell has been taken as the reference model.

4.2 Theoretical Model of the Plate Heat Exchanger

A plate heat exchanger has layer by layer structure. The plates may have different forms depending on the heat transfer. As shown in Figure 4.3, a PHE has so compact sizes that it occupies very little volume in a combi boiler. The number of the plates is dependent upon the power of the heating appliance. Plate heat exchanger model has been included by only the standard combi boiler.

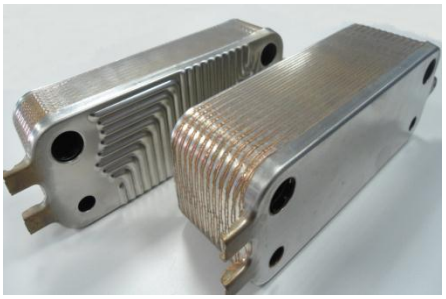

Figure 4.3 PHEs having different number of plates.

While hot CH water is passing through one layer of the PHE at the time of hot water demand, DCW (tapping water) passes through the subsequent layer; resulting in energy transfer from hot water to cold water in order to produce DHW. Schematic presentation of the working principle of the plate heat exchanger is summarized in Figure 4.4 by means of heat transfer units.

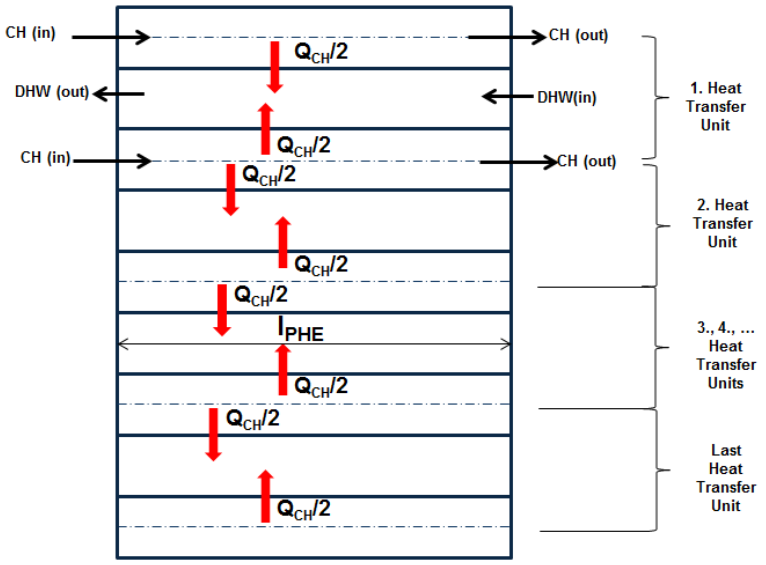

Figure 4.4 Schematic presentation of the heat transfer directions from hot CH water to DCW.

The plate heat exchangers under investigation are counter flow heat exchangers. A reference standard combi boiler with rectangular heat cell and 26-plate PHE, and another boiler with conical heat cell and 24-plate PHE have been used in the experiments. After the theoretical model has been verified with two separate different coupling of HC and PHE, each representing an appliance configuration, for the rest of the analyses conical heat cell and 24-plate PHE has been used for comparisons and parametric studies.

4.3 Common Assumptions of the Theoretical Analyses

There are basic assumptions and special considerations made while establishing the equations of the appliance concepts.

- The temperature of both fluids and the wall are functions of time and position.
  $T=f(x, t)$
- There are no thermal energy sources within the exchangers.
- Heat losses to the environment are taken into consideration for the HCs, whereas they are assumed negligible for the PHEs. Natural heat transfer coefficient of the surrounding air is used as 5 W/m^2K and the thermal resistance of the outer cover of the HCs is also ignored while considering the heat losses.
- The mass flow rates of both streams do not vary with time. Fluid passages are uniform in cross-sections.
- The velocity and temperature of each fluid at the inlet are uniform over the flow cross-section.
- The convective heat transfer coefficients on each side are constant.
- Thermal properties of the water are used as constant values although thermal properties of the flue gas and the wall changes with temperature.
- Longitudinal heat conduction within the fluids is neglected, but diffusion terms are added to the HC wall equations.
- The heat transfer surface area on each fluid side is uniformly distributed in the heat exchangers.
- The fouling resistance in PHEs is negligible.
- Temperature profiles of CH water and DHW are the same along each CH water channel and DHW channel, respectively.
- In PHEs, the thermal resistance of the plates is considered negligible, but in HCs, the wall resistance is evaluated.
- 80% of the inner and outer heat transfer area of the HC wall is assumed to be effective. For the other rectangular heat cell whole of the inner and outer surface areas have been used.

- Overall fin efficiency for the pin fins of the conical heat cell is calculated as 0.96 (Incropera, Dewitt, Bergman, & Lavine, 2007). For the annular fins, same efficiency value has been counted.
- Combustion in the HCs is completed.
- H_2O does not condensate during the combustion in the HCs.
- Radiation is considered negligible in the heat transfer analyses.

4.4 Mathematical Model of the Standard Combi Boiler

To sum up, when user demand is created, the CH water is heated in the HC, and then the hot CH water is sent through the channels of the PHE to transfers its energy to DCW tapped by the user. These phenomena, also shown in Figure 4.5 have been established with the mathematical equations of the heat exchangers, boundary, and the initial conditions. For the HC, energy equations of the flue gas, HC wall, and the CH water flowing around the HC have been constructed. Additionally, for heating DHW requested by the users, equations of the CH water and DCW flowing through the subsequent channels of the PHE have been established.

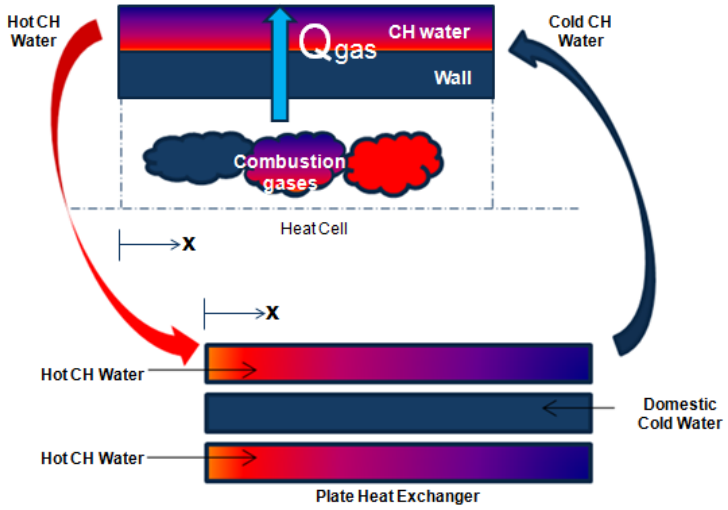

Figure 4.5 Schematic display of DHW supply function of a standard combi boiler.

Equations of the HC have been derived for the flue gas, HC wall, and the CH water of the HC while balancing the energy transfers on the control volumes (CVs) shown in Figure 4.6.

Schematic presentations have been prepared according to the conical heat cell since it easier. Since the working principle of the heat cells is the same, from this point of view, common energy equations are obtained and applied to the both of the systems only changing physical values of the parameters.

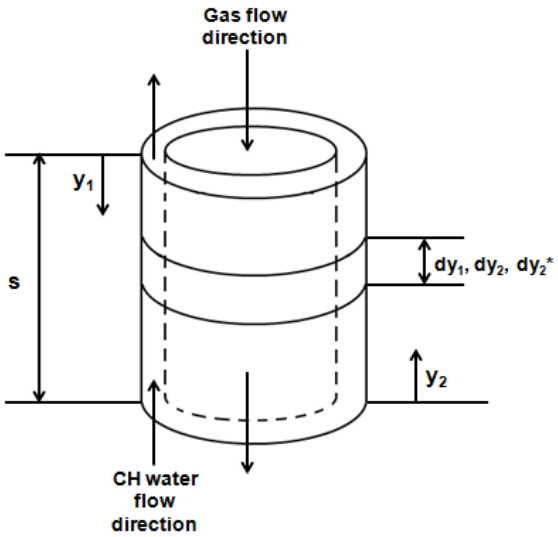

Figure 4.6 Control volumes (CVs) for the flue gas, HC wall, and the CH water in HC and flow directions.

Writing energy balances on the CVs of the PHE, energy equations of CH water and DCW in PHE also have been constructed. For the PHE model, control volumes and flow directions of the CH water and DHW are shown in Figure 4.7.

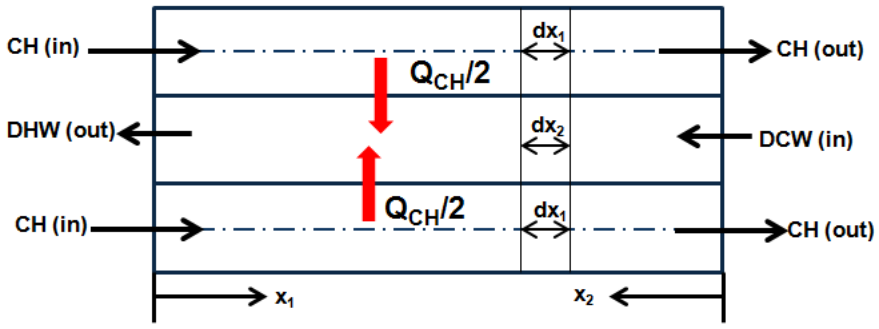

Figure 4.7 Control volumes of the PHE and flow directions.

In the investigated PHEs, there is one more excessive CH water channel when compared to the DCW channels. With reference to the heat transfer unit approach,

shown in Figure 4.4, energy transfer process is the same for every unit. Therefore, energy equations of one CH water and one DCW channel have been constructed and assumed to be same for all channels. However, when all heat transfer units have been grouped; totally one CH water channel (half of one CH water channel for the first heat transfer unit, and half for the last heat transfer unit) has been left as not being used also shown in Figure 4.4. As a result, to make heat transfer unit approach more realistic, CH water flow rate for one CH water channel of the PHE, which is necessary to be used directly in the mathematical model, has been defined dividing the total CH water flow rate by the numbers of DCW channels (not the numbers of the CH water channels). Consequently, the amount of one-channel CH water at least has been taken into consideration in the mathematical model.

Gas cools down since it gives its energy to CH water through the HC wall. The cooling of hot combustion gases in y_1 direction is expressed as

$$\rho_g A_{cs,g} c_{pg} \frac{\partial T_g}{\partial t} = -\dot{m}_g c_{pg} \frac{\partial T_g}{\partial y_1} - \frac{A_{sa,g} U_g}{s} (T_g - T_w) \tag{4.3}$$

Total thermal resistances are also modeled for CH water and gas domain, as shown in Figure 4.8.

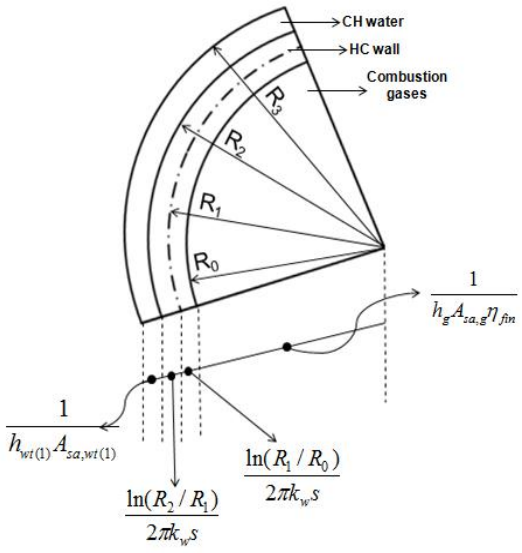

Figure 4.8 Modelling of the thermal resistances in the HC (Incropera et al., 2007).

The total thermal resistance between the HC wall and the combustion gases is calculated from

$$R_{t,g-w} = \frac{1}{U_g A_{sa,g}} = \frac{1}{h_g A_{sa,g} \eta_{fin}} + \frac{\ln(R_1 / R_0)}{2\pi k_w s} \tag{4.4}$$

The temperature of CH water around the HC increases while energy is transferred from the hot combustion gases to the CH water through HC wall. The heating of CH water in the HC along y_2 direction is given by

$$\rho_{wt} A_{cs,wt(hc)} c_{pwt} \frac{\partial T_{wt(1)}}{\partial t} = -\dot{m}_{wt(1)} c_{pwt} \frac{\partial T_{wt(1)}}{\partial y_2} + \frac{U_{wt(1)} A_{sa,wt(hc)}}{z} (T_w - T_{wt(1)}) - h_\infty \frac{A_o}{z} (T_{wt(1)} - T_\infty) \tag{4.5}$$

The total thermal resistance between the HC wall and CH water is as follows:

$$R_{t,wt(hc)-w} = \frac{1}{U_{wt(1)} A_{sa,wt(hc)}} = \frac{1}{h_{wt(1)} A_{sa,wt(hc)}} + \frac{\ln(R_2 / R_1)}{2\pi k_w s} \tag{4.6}$$

The temperature distribution of the HC wall along y_2 direction is explained by

$$\rho_w A_{cs,w} c_w \frac{\partial T_w}{\partial t} = k_w \frac{\partial^2 T_w}{\partial y_2^2} A_{cs,w} + \frac{U_g A_{sa,g}}{s} (T_g - T_w) - \frac{U_{wt(1)} A_{sa,wt(hc)}}{s} (T_w - T_{wt(1)}) \tag{4.7}$$

CH water in PHE gives its energy to DCW. The temperature distribution of CH water in PHE along x_1 direction is expressed as

$$\rho_{wt} \frac{V_{CHWC}}{l_{PHE}} c_{pwt} \frac{\partial T_{wt(2)}}{\partial t} = -\dot{m}_{wt(2)} c_{pwt} \frac{\partial T_{wt(2)}}{\partial x_1} - 2 \frac{U_{PHE} A_{PHE}}{l_{PHE}} (T_{wt(2)} - T_{wt(3)}) \tag{4.8}$$

The total thermal resistance in the PHE is written as follows:

$$R_{t,PHE} = \frac{1}{U_{PHE} A_{PHE}} = \frac{1}{h_{wt(2)} A_{PHE}} + \frac{1}{h_{wt(3)} A_{PHE}} \tag{4.9}$$

The heating of DCW in x_2 direction is calculated from

$$\rho_{wt} \frac{V_{DHWC}}{l_{PHE}} c_{pwt} \frac{\partial T_{wt(3)}}{\partial t} = -\dot{m}_{wt(3)} c_{pwt} \frac{\partial T_{wt(3)}}{\partial x_2} + 2 \frac{U_{PHE} A_{PHE}}{l_{PHE}} (T_{wt(2)} - T_{wt(3)}) \tag{4.10}$$

Finite Element Method is used to discretize the governing differential equations in order to solve them numerically. Implicit discretization of HC equations are made based on the control volume numbers shown in Figure 4.9.

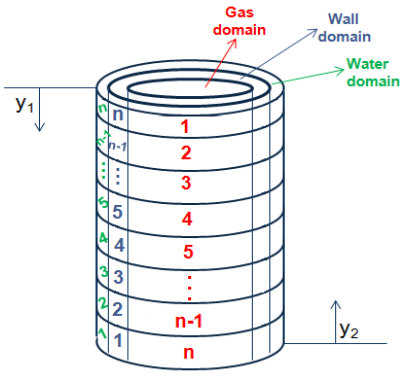

Figure 4.9 Display of control volume numbers for the combustion gases, the CH water, and HC wall.

For clear understanding, CV numbers that are used to discretize the equations of CH water and DHW domains are given in Figure 4.10.

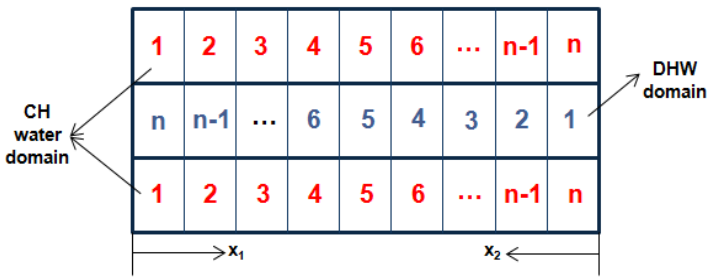

Figure 4.10 Display of the control volume numbers for the CH water and DHW channels of PHE.

Although both the HC wall and the CH water equations are written in y_2 direction, dy_2 and dy_2* are different from each other since the helical path of CH water around HC is longer than the HC length. In other words, in HC, to obtain same number of CVs for each domain, CV length for CH water is defined longer when compared to others $dy_1 = dy_2 \neq dy_2$*. As a result, same numbers of CVs for each domain provided ($s/dy_1 = s/dy_2^* = z/dy_2$). CV lengths chosen for CH water and DHW channels of PHE are equal to each other ($dx_1 = dx_2$).

The discretized form of Equation 4.3 is given by

$$\rho_g A_{cs,g} c_{pg} \left(\frac{T_{g(m)}^{p+1} - T_{g(m)}^{p}}{dt}\right) = -\dot{m}_g \, c_{pg} \left(\frac{T_{g(m)}^{p+1} - T_{g(m-1)}^{p+1}}{dy_1}\right) - \frac{A_{sa,g} U_g}{s} \left(T_{g(m)}^{p+1} - T_{w((s/dy_1)-m+1)}^{p+1}\right) \tag{4.11}$$

The discretised version of Equation 4.5 is as follows:

$$\rho_{wt} A_{cs,wt(hc)} c_{pwt} \left(\frac{T_{wt(1)(m)}^{p+1} - T_{wt(1)(m)}^{p}}{dt}\right) = -\dot{m}_{wt(1)} \, c_{pwt} \left(\frac{T_{wt(1)(m)}^{p+1} - T_{wt(1)(m-1)}^{p+1}}{dy_2}\right) + \frac{U_{wt(1)} A_{sa,wt(hc)}}{z} \left(T_{w(m)}^{p+1} - T_{wt(1)(m)}^{p+1}\right) - h_\infty \frac{A_o}{z} \left(\left(T_{wt(1)(m)}^{p+1} - T_\infty\right)\right) \tag{4.12}$$

Discretised form of Equation 4.7 is

$$\rho_w A_{cs,w} c_w \left(\frac{T_{w(m)}^{p+1} - T_{w(m)}^{p}}{dt}\right) = k_w A_{cs,w} \left(\frac{T_{w(m+1)}^{p+1} - 2T_{w(m)}^{p+1} + T_{w(m-1)}^{p+1}}{(dy_2^*)^2}\right) + \frac{U_g A_{sa,g}}{s} \left(T_{g((s/dy_1)-m+1)}^{p+1} - T_{w(m)}^{p+1}\right) - \frac{U_{wt(1)} A_{sa,wt(hc)}}{s} \left(T_{w(m)}^{p+1} - T_{wt(1)(m)}^{p+1}\right) \tag{4.13}$$

The discretization of Equation 4.8 is indicated by

$$\rho_{wt}\frac{V_{CHWC}}{l_{PHE}}c_{pwt}\left(\frac{T^{p+1}_{wt(2)(m)}-T^{p}_{wt(2)(m)}}{dt}\right)=-\dot{m}_{wt(2)}c_{pwt}\left(\frac{T^{p+1}_{wt(2)(m)}-T^{p+1}_{wt(2)(m-1)}}{dx_1}\right)-2\frac{U_{PHE}A_{PHE}}{l_{PHE}}\left(T^{p+1}_{wt(2)(m)}-T^{p+1}_{wt(3)((l_{PHE}/dx_1)-m+1)}\right) \quad (4.14)$$

The discretized form of Equation 4.10 is expressed by

$$\rho_{wt}\frac{V_{DHWC}}{l_{PHE}}c_{pwt}\left(\frac{T^{p+1}_{wt(3)(m)}-T^{p}_{wt(3)(m)}}{dt}\right)=-\dot{m}_{wt(3)}c_{pwt}\left(\frac{T^{p+1}_{wt(3)(m)}-T^{p+1}_{wt(3)(m-1)}}{dx_2}\right)+2\frac{U_{PHE}A_{PHE}}{l_{PHE}}\left(T^{p+1}_{wt(2)((l_{PHE}/dx_1)-m+1)}-T^{p+1}_{wt(3)}\right) \quad (4.15)$$

There are five energy equations as the mathematical model of the combi boiler. Flue gas, CH water in the HC, CH water in the PHE, and the DCW equations are first order partial differential equations, whereas the HC wall equation is second order partial differential equations because of the heat diffusion (conduction) term within the wall. Numerical results are obtained after solving these five equations simultaneously.

After discretization of these equations, boundary conditions (BCs) and initial conditions (ICs) of all domains are needed for the numerical solution. Except for the HC wall domain requiring two BCs since it is second order differential equation, only one BC is enough for solving the equations of first order.

Initial conditions for the HC wall, the CH water in HC and PHE, the flue gas and DHW are given below with Equations 4.16 and 4.17. They are defined according to the test conditions.

$$T_{g,wt(1),w}(y_{1,2},0)=10\ ^{\circ}C \quad (4.16)$$

$$T_{wt(2),wt(3)}(x_{1,2},0)=10\ ^{\circ}C \quad (4.17)$$

The BCs of the CH water in the HC and in the PHE are interconnected and dependent on time as given in Equations 4.18 and 4.19. The outlet temperature of the CH water from the HC is the BC of the CH water in the PHE and similarly, the outlet temperature of the CH water from the PHE is the BC of the CH water in the HC.

$$T_{wt(1)}(0,t) = T_{wt(2)}((l_{PHE} / dx_1), t) \tag{4.18}$$

$$T_{wt(2)}(0,t) = T_{wt(1)}((z / dy_2), t) \tag{4.19}$$

The BCs of DCW and the flue gas is used as constant values as given with Equations 4.20 and 4.21. For the combustion gases, adiabatic flame temperature assumption is used.

$$T_{wt(3)}(0,t) = 10\ ^{\circ}C \tag{4.20}$$

$$T_g(0,t) = T_{adia} \tag{4.21}$$

For the BCs of the HC wall equation, convection surface condition (Incropera et al., 2007) is used as given in Equations 4.22 and 4.23.

$$-k_w \frac{\partial T_w}{\partial y_2}\Big|_{y_2=0} = h_\infty (T_\infty - T_w(0,t)) \tag{4.22}$$

$$-k_w \frac{\partial T_w}{\partial y_2}\Big|_{y_2=(s/dy_1)} = h_\infty (T_\infty - T_w((s / dy_1), t)) \tag{4.23}$$

Numerical solutions have been obtained with the discretized versions of the equations with a calculation algorithm including simultaneous solution of these five equations under the aforementioned BCs and ICs.

4.5 Mathematical Model of the Primary DHW Concept

Primary DHW concept is similar to the standard combi boilers; but they differ in terms of DHW heating function since DCW is heated in the heat cell directly. Heat exchangers are in opposite working configuration when compared with the standard combi boilers. Since this study focuses on DHW supply function of the appliances, for primary DHW concept, only heat cell has been modeled. DHW supply function of the primary DHW concept has been summarized in the Figure 4.11.

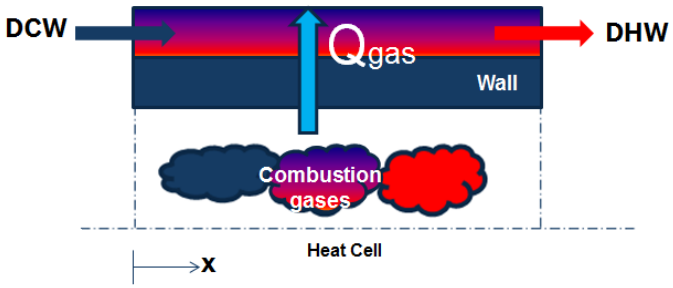

Figure 4.11 Schematic display of DHW supply function of a primary DHW concept.

The mathematical model is similar to the standard combi boiler's; but energy equation of the DCW has been written in the HC instead of CH water of the HC. This time, there are three equations that are needed to be solved simultaneously.

Control volumes, flow directions, and discretization numbers are defined in the same way shown in Figure 4.6.

Equation 4.24 is identical to the Equation 4.3 and expresses cooling of the hot combustion gases in y_1 direction.

$$\rho_g A_{cs,g} c_{pg} \frac{\partial T_g}{\partial t} = -\dot{m}_g c_{pg} \frac{\partial T_g}{\partial y_1} - \frac{A_{sa,g} U_g}{s} (T_g - T_w) \tag{4.24}$$

Total thermal resistance between the HC wall and the combustion gases have been calculated with Equation 4.4. Temperature distribution of the HC wall along y_2 direction is calculated from

$$\rho_w A_{cs,w} c_w \frac{\partial T_w}{\partial t} = k_w \frac{\partial^2 T_w}{\partial y_2^2} A_{cs,w} + \frac{U_g A_{sa,g}}{s}(T_g - T_w) - \frac{U_{dcw-w} A_{sa,wt(hc)}}{s}(T_w - T_{dcw}) \tag{4.25}$$

The heating of DCW in the HC along y_2 direction is given by

$$\rho_{wt} A_{cs,wt(hc)} c_{pwt} \frac{\partial T_{dcw}}{\partial t} = -\dot{m}_{dcw} c_{pwt} \frac{\partial T_{dcw}}{\partial y_2} + \frac{U_{dcw-w} A_{sa,wt(hc)}}{z}(T_w - T_{dcw}) - h_\infty \frac{A_o}{z}(T_{dcw} - T_\infty) \tag{4.26}$$

The total thermal resistance between the DCW around the HC and the HC wall is written as

$$R_{t,wt(hc)-w} = \frac{1}{U_{dcw-w} A_{sa,wt(hc)}} = \frac{1}{h_{dcw} A_{sa,wt(hc)}} + \frac{\ln(R_2 / R_1)}{2\pi k_w s} \tag{4.27}$$

The above-given three equations have been constructed as the mathematical model of the primary DHW concept. Gas equation is the same as the standard combi boilers' and the heat cell wall and the DCW heating equation are very similar to the equations of the previous system. After discretization of these equations, the calculation algorithm of the standard combi boilers has been used to solve them simultaneously in Matlab under the ICs and BCs.

For the discretized version of Equation 4.24, Equation 4.11 has been used, and as the discretized version of Equations 4.25 and 4.26, Equations 4.28 and 4.29 are given, respectively.

$$\rho_w A_{cs,w} c_w \left(\frac{T_{w(m)}^{p+1} - T_{w(m)}^{p}}{dt}\right) = k_w A_{cs,w} \left(\frac{T_{w(m+1)}^{p+1} - 2T_{w(m)}^{p+1} + T_{w(m-1)}^{p+1}}{(dy_2^*)^2}\right) + \frac{U_g A_{sa,g}}{s} \left(T_{g((s/dy_1)-m+1)}^{p+1} - T_{w(m)}^{p+1}\right) - \frac{U_{dcw-w} A_{sa,wt(hc)}}{s} \left(T_{w(m)}^{p+1} - T_{dcw(m)}^{p+1}\right) \quad (4.28)$$

$$\rho_{wt} A_{cs,wt(hc)} c_{pwt} \left(\frac{T_{dcw(m)}^{p+1} - T_{dcw(m)}^{p}}{dt}\right) = -\dot{m}_{dcw} c_{pwt} \left(\frac{T_{dcw(m)}^{p+1} - T_{dcw(m-1)}^{p+1}}{dy_2}\right) + \frac{U_{dcw-w} A_{sa,wt(hc)}}{z} \left(T_{w(m)}^{p+1} - T_{dcw(m)}^{p+1}\right) - h_\infty \frac{A_o}{z} \left(\left(T_{dcw(m)}^{p+1} - T_\infty\right)\right) \quad (4.29)$$

The ICs of these three equations are given by

$$T_{g,dcw,w}(y_{1,2}, 0) = 10\ ^\circ C \quad (4.30)$$

BCs of the gas and the HC wall equations are the same as the Equations 4.21-4.23. The boundary condition of DCW equation given in Equation 4.31 is the same as the BC of tapped water of the standard combi boiler.

$$T_{dcw}(0, t) = 10\ ^\circ C \quad (4.31)$$

4.6 Solution Algorithm of the Equation Sets

Implicit finite-difference scheme is used for the solution of these 5 equations governing the working principle of a combi boiler.

Implicit method evaluates the temperatures at the new (p+1) time, instead of previous (p) time. There are 5 equations to be solved in our case. All of the equations include also new (p+1) time values of some of the other unknowns, in addition to the main unknown of the equation which is intended to be solved. For solving the main

unknown, some assumptions are made on the other unknowns. Therefore, each time step will be solved iteratively. For example, HC wall equation includes (p+1) time values of HC water and combustion gases, as well. To find the main unknown of an equation, for the first iteration, previous time values are assigned to (p+1) values of the auxiliary unknowns. After the first calculation, (p+1) time results of the all unknowns are obtained. Since this approach is based on the assumptions, further iterations are necessary since the first calculated values may not be the exact results. It can be understood with the further iterations. Each iteration uses previous iteration's (p+1) time values for the unknowns which are necessary to be assumed to solve the equation under study. The same calculation procedure is repeated for each time step. The iteration phase of each time step goes on till the previous and current iteration values converge to each other within an acceptable error limit. The solution algorithm is summarized in Figure 4.12.

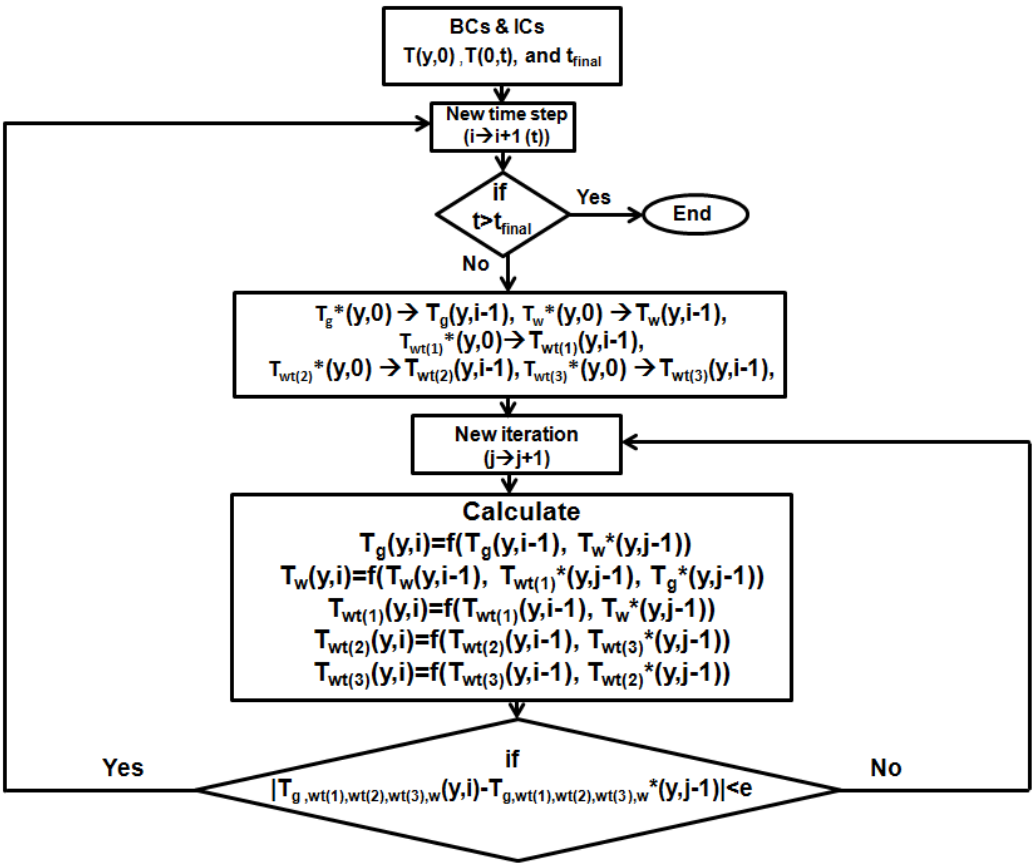

Figure 4.12 Steps of the solution algorithm.

In the above-given solution algorithm, the second independent variable (i) of T(y,i) shows the time steps, whereas second independent variable (j) of T*(y,j) displays the iteration numbers.

The solution algorithm has been shown for the equations of the standard combi boiler concept since it is more complicated. The same algorithm has been used for the primary DHW concept just changing the physical values of the parameters.

CO_2 percentage of the combustion process defined as a design criterion of the combi boiler, power of the appliance (as heat input rate), and domestic hot water flow rate requested by the users are the inputs of the calculation algorithm. According to these data, temperature distribution of the HC wall, flue gas, CH water in the HC and PHE, and DHW could be calculated under different operating conditions of the standard combi boilers. In similar way, for primary DHW concept, temperature profiles of the HC wall, flue gas, and the DCW in the HC could also be obtained as the outputs. Moreover, changes of energies with respect to time in all domains could be investigated.

The model has been solved for 1 second time steps and 0.00025 m CV length for each node, i.e., 1200 nodes for the HC. Nodal analyses have been given in Figure 4.13. The results are not dependent upon the number of the nodes for 300, 600, 1000, and 1200 node numbers. However, for 100 and 30 node numbers, the results start to shift upward from the exact values. Then, 1200 node number has been chosen for all numerical analyses conducted during the study.

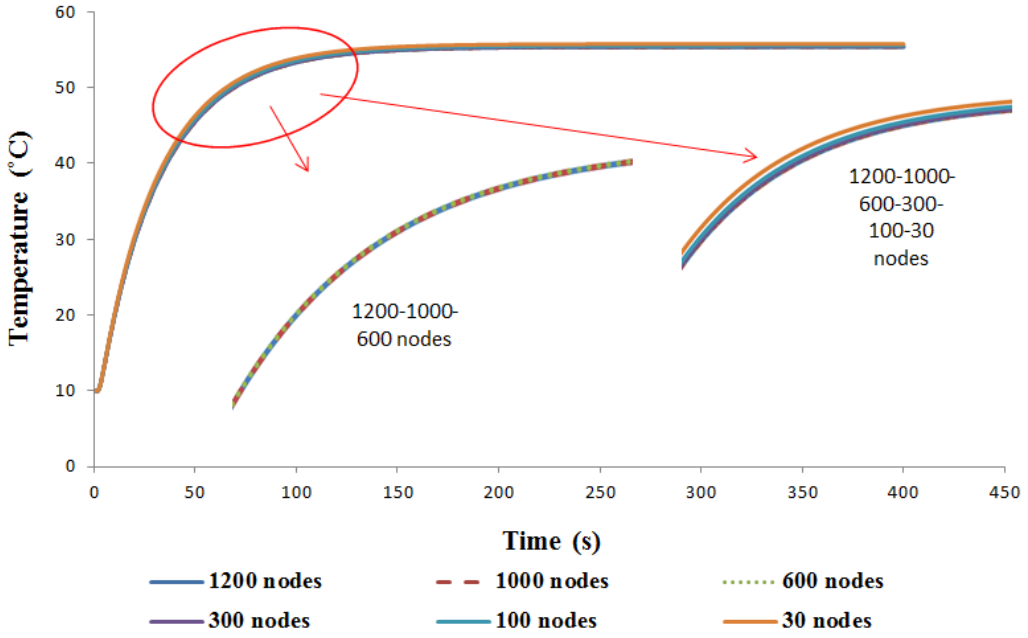

Figure 4.13 Nodal sensitivity of the results.

4.7 Adiabatic Flame Temperature

As the boundary condition of the flue gas part, adiabatic flame temperature assumption is made. There are two kinds of adiabatic flame temperatures for constant-pressure combustion and for constant-volume combustion.

In an adiabatic constant-pressure combustion of the fuel-air mixture, the standardized enthalpy of the reactants at the initial state (i.e., T=298 K, P= 1atm) equals the standardized enthalpy of the products at the final state ($T=T_{adia}$, P= 1 atm). Originating from the first law of thermodynamics, Equations 4.32 and 4.33 designate constant-pressure combustion in a more general form and on a per-mass-of-mixture basis, respectively (Turns, 2012).

$$H_{reac}(T_{is}, P) = H_{prod}(T_{adia}, P) \tag{4.32}$$

$$h_{reac}(T_{is}, P) = h_{prod}(T_{adia}, P) \tag{4.33}$$

From Equations 4.32 and 4.33, a constant-pressure adiabatic flame temperature could be calculated with the knowledge of the composition of the combustion products. The definition of Equations 4.32 and 4.33 is graphically shown in Figure 4.14 on the enthalpy versus temperature graph of the reactants and the products. At typical flame temperatures, which are typically several thousand Kelvins, the products dissociate and at that time the mixture is composed of many species.

In some kinds of analyses such as ideal Otto-cycle, a constant-volume adiabatic flame temperature is used. Similar to constant-pressure combustion, internal energy of the products is equal to the internal energy of the reactants and from the same point of view, the first law of thermodynamics yields adiabatic flame temperature at constant-volume as follows:

$$U_{reac}(T_{is}, P_{is}) = U_{prod}(T_{adia}, P_{fs}) \tag{4.34}$$

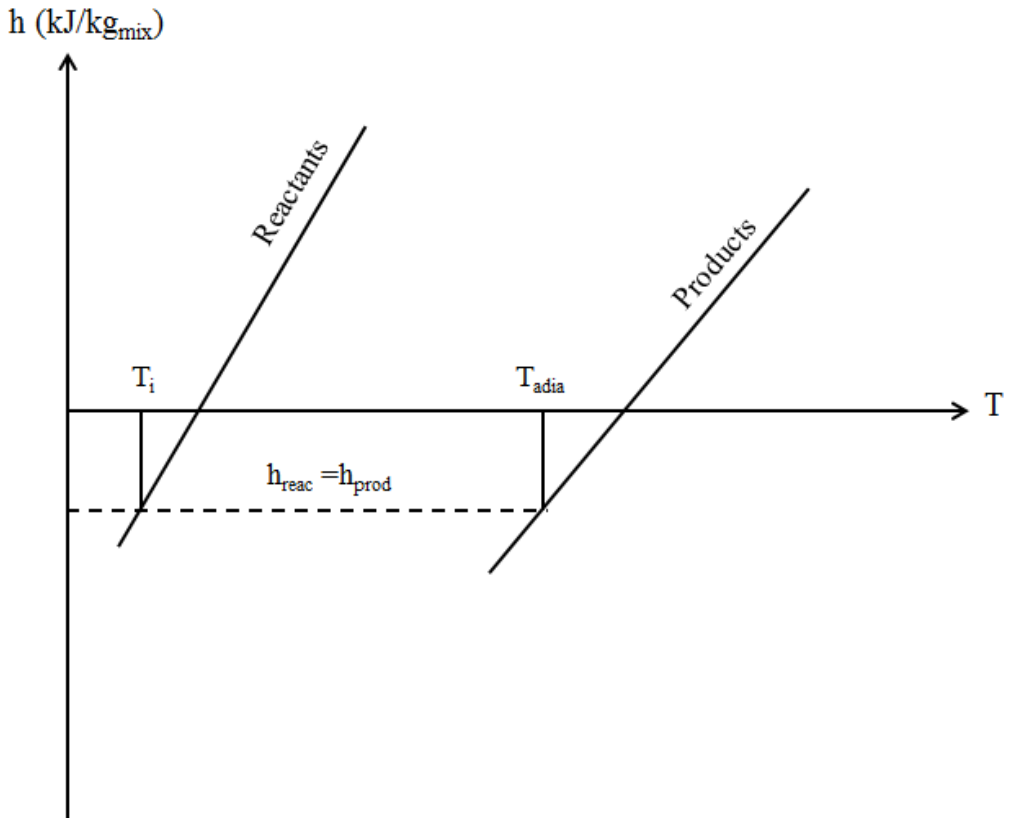

Figure 4.14 Illustration of constant-pressure adiabatic flame temperature on h-T diagram (Turns, 2012).

In a closed system, like an Otto engine, since combustion is assumed to be at a constant volume, Equation 4.34 is used to calculate the adiabatic flame temperature. However, in open systems, like the modeled heat cells of this study, constant pressure adiabatic flame temperature is calculated. Therefore, the constant-pressure adiabatic flame temperature calculation is given by equating the enthalpy of the products and the enthalpy of the products for a lean fuel (CH_4)-air mixture.

Equations 4.35 and 4.36 are used to calculate the enthalpy of the reactants (Turns, 2012). In this case pressure is 1 atm and the initial reactant temperature is 298 K.

$$H_{reac} = \sum_{reac} N_i \overline{h_i} \tag{4.35}$$

$$H_{reac} = N_{CH_4} \overline{h}^0_{f,CH_4} + N_{O_2} \overline{h}^0_{f,O_2} + N_{N_2} \overline{h}^0_{f,N_2} \tag{4.36}$$

Equations 4.37 and 4.38 are used for the enthalpy of the products (Turns, 2012). The product mixture enthalpy is estimated under constant specific heat assumption. For the evaluation of the specific heats, the mean value of the initial temperature of the reactants and the estimated adiabatic flame temperature (2000 K), T_{adia} of the products is used.

$$H_{prod} = \sum_{prod} N_i \overline{h_i} \tag{4.37}$$

$$\begin{aligned} H_{prod} = {} & N_{CO_2}[\overline{h}^0_{f,CO_2} + \overline{c}_{p,CO_2}(T_{adia} - 298)] + N_{O_2}[\overline{h}^0_{f,O_2} + \overline{c}_{p,O_2}(T_{adia} - 298)] \\ & + N_{N_2}[\overline{h}^0_{f,N_2} + \overline{c}_{p,N_2}(T_{adia} - 298)] \end{aligned} \tag{4.38}$$

Enthalpy of formation, $\overline{h}^0_{f,i}$ at 298 K is used for all species in order to calculate the enthalpy of the reactants and the products in Equations 4.35-4.38 (Turns, 2012).

As a result, equating H_{reac} to H_{prod} and solving for T_{adia} yields a value around 2000 K for the boundary condition of the flue gas cooling equation.

4.8 Convective Heat Transfer Coefficient of the Flue Gas in the Heat Cell

For the convective heat transfer coefficient of the flue gas, the gas flow channels of the modeled HCs have been primarily investigated to decide on the characteristics of the flow. Constant heat transfer coefficient assumption is made throughout the HCs (Bunce, & Kandlikar, 1995).

The conical heat cell has a very condense pin fins arrangement, as shown in Figure 2.8. The flow channels in the conical heat cell are shown in the technical drawing of the cross-sectional view from the top side (Figure 4.15).

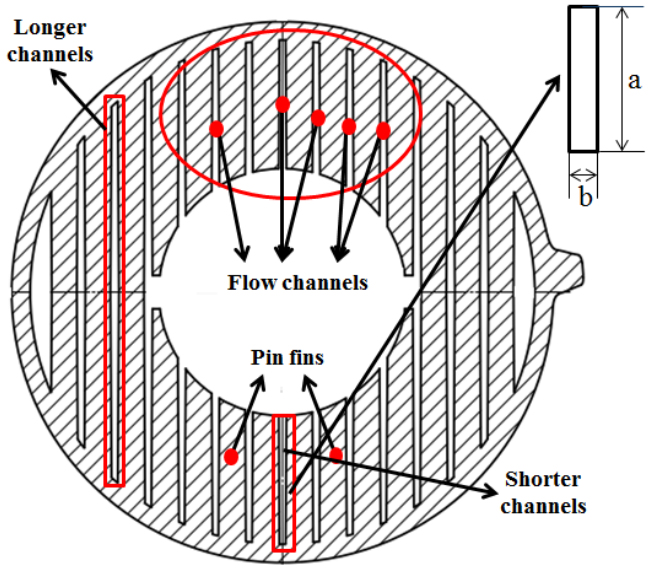

Figure 4.15 One of the cross-sectional view of the pin fin arrangements in the HC (schematically).

There are different flow configurations throughout the heat cell, but as the flow model, it is needed to prepare a reference model tends to simulate all system behavior. Therefore, the signed pin fins (with red dot in Figure 4.15) and the flow channels have been used as the reference cross-sectional area of the flow since there are more shorter channels when compared to the longer channels.

While using the dimensions of the shorter flow channels (a,b) for the hydraulic diameter calculation given in Equations 4.39 and 4.40 (Incropera et al., 2007), the mass flow rate of the flue gas per channel (for 28.5 kW heat input, since it is the

maximum for the arranged appliance configuration with the conical heat cell), and the physical properties of the flue gas, Reynolds Number (Re) has been calculated as follows (Incropera et al., 2007):

$$D_h = \frac{4A_c}{P_h} \tag{4.39}$$

$$D_h = \frac{4ab}{2(a+b)} \tag{4.40}$$

$$\mathrm{Re}_D = \frac{4\dot{m}}{\pi D_h \mu} \tag{4.41}$$

The flow has been concluded to be laminar (Incropera et al., 2007) at those working conditions.

According to the chosen fin profile in the HC, the inside part in contact with the flue gas has been modeled, enabling to simulate all system characteristics. Under these approaches, there are 400 hundred pin fins having 11 mm diameter and 50 mm length, and the number of the rows of the pin fins is 18 along the HC, and hence flow channels have been arranged as 3 mm width and 50 mm length as the dimensions they have.

Using the maximum gas flow rate per channel, Reynolds Number within one of the channels, Re_D has been calculated as 2214, resulting in laminar flow since it is lower than 2300 (Incropera et al., 2007). After chosing a suitable Nusselt Number according to the laminar flow conditions and the channel geometry (Incropera et al., 2007), convective heat transfer coefficient, h for flue gas has been calculated as 113 W/m^2K using Equation 4.42 (Incropera et al., 2007).

$$h = \frac{Nu_D k}{D_h} \tag{4.42}$$

For the second rectangular heat cell model investigated in this study, similar approaches have been used. Flue gas channels are approximated to rectangular channels, as given in Figure 4.16.

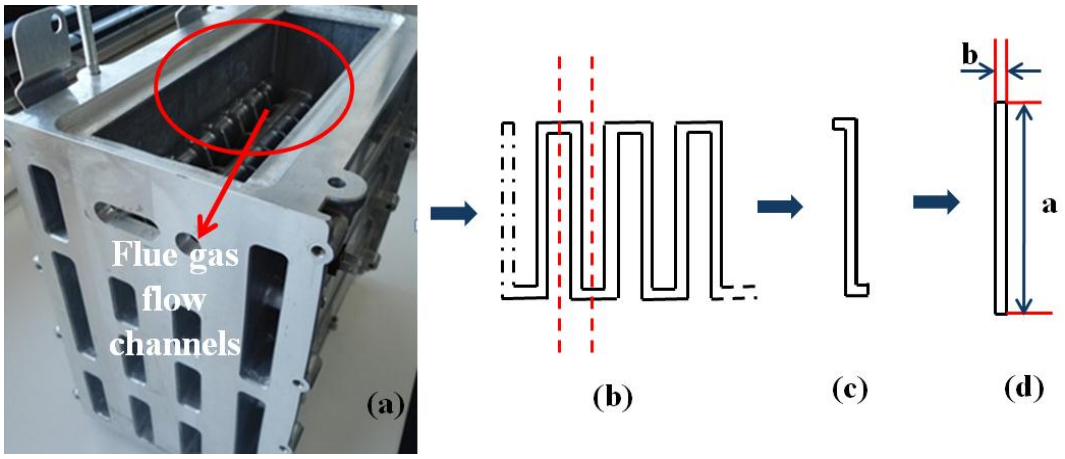

Figure 4.16 (a) Condense arrangement of annular fins, (b) Schematic view of the flow channels of the flue gas, (c) Initial model of the flow channel, (d) Final model of the flow channel.

Firstly, flow through the annular fins has been sketched, as shown in Figure 4.16 (a), then regular flow pattern has been discovered, as shown in Figure 4.16 (b). Finally the pattern in (c) has been thought as the rectangular flow-cross section in (d). The rest is the same as the conical heat cell. Equations 4.39 and 4.40 have been used for the hydraulic diameter calculated as 2 mm with the modeled dimensions of the rectangular flow area (20.7 mm length and 4.5 mm width). While using Equation 4.41, Re_D has been decided and the flow has been concluded as laminar since Re_D is 1349 according to the maximum gas flow rate of the appliance configuration of the rectangular heat cell, 36 kW. Consequently, convective heat transfer coefficient of the flue gas in the rectangular heat cell with the same Nusselt Number of the conical heat cell has been calculated as 320 W/m^2K using Equation 4.42.

4.9 Convective Heat Transfer Coefficient of the Water around/inside the Heat Cell

First, hydraulic diameter of the water channels around/inside the HC, then Re_D, Nu_D, and finally convective heat transfer coefficient of the water (CH water for the

standard combi boiler and DCW for the primary DHW concept) have been calculated. For the rectangular heat cell, the convective heat transfer coefficient of the water in the channels inside the HC; and for the conical heat cell the coefficient of the water in the channels around the HC have been calculated with the same correlation.

According to the all possible flow rates of the different operating conditions, the flow inside/around the heat cell has been calculated as turbulent using Equations 4.40 and 4.41.

The *Dittus-Boelter equation* for heating applications is given by (Incropera et al., 2007).

$$Nu_D = 0.023 \mathrm{Re}_D^{4/5} \mathrm{Pr}^{0.4} \tag{4.43a}$$

Equation 4.43a has been confirmed experimentally for the following conditions (Incropera et al., 2007).

$$\begin{aligned} &0.6 \le \mathrm{Pr} \le 160 \\ &\mathrm{Re}_D \ge 10.000 \\ &\frac{L}{D_h} \ge 10 \end{aligned} \tag{4.43b}$$

Pr is the Prandtl number, which is the ratio of the momentum and thermal diffusivities while it is calculated from (Incropera et al., 2007)

$$\mathrm{Pr} = \frac{c_p \mu}{k} \tag{4.44}$$

From the calculated Nusselt number and the thermal properties of the water around the HC, the convective heat transfer coefficient of the water has been calculated using Equation 4.42.

4.10 Mass Flow Rate of the Flue Gas

Mass flow rate of the flue gas is calculated from the power of the appliance. If a combi boiler is tested and the heat input rate (power) of the appliance, $\dot{Q}_i$ (kW) is desired to be calculated from the volume flow rate of the fuel consumed by the appliance, the following heat input formula given by Equation 4.45 (BS EN 483:1999+A4:2007, 2007) is used. While verifying the numerical results with the experimental results, the power input of the numerical code has been calculated with the volume flow rate of the fuel using the above-mentioned formula. The volume flow rate of the fuel has been measured with the gas meter of a special test rig, which will be mentioned in detail in the succeeding chapters.

There is an additional correction factor, C_f in Equation 4.45 as being different from the original formula given in the related standard (BS EN 483:1999+A4:2007, 2007) since the error of the gas meter is compensated with that calibration factor read from the calibration curve of the gas meter of the test rig (see Appendix C).

$$\dot{Q}_i = \frac{V(LHV)C_f(p_a + p_g)(288.15)}{3.6(1013.25)(273.15 + t_g)} \tag{4.45}$$

For theoretical calculations, any required power value could be used as the input in the calculation algorithm; but for experimental verifications, power will be defined according the volumetric flow rate of the appliance. After power is decided directly or from the volumetric flow rate of the fuel read from the gas meter, the mass flow rate of the flue gas can be calculated with the following Equations.

Mass flow rate of the flue gas is equal to the sum of the mass flow rate of the fuel and air, as shown in Equation 4.46.

$$\dot{m}_g = \dot{m}_f + \dot{m}_a \tag{4.46}$$

Mass flow rate of the fuel is calculated as follows (dividing the power of the appliance by lower heating value (LHV) of the fuel (methane)):

$$\dot{m}_f = \frac{Power(\dot{Q}_i)}{LHV} \tag{4.47}$$

Mass flow rate of the fuel is converted to molar flow rate of the fuel with Equation 4.48. Mass flow rate of the fuel is divided by the molar mass of the fuel, W_f.

$$\dot{n}_f = \frac{\dot{m}_f}{W_f} \tag{4.48}$$

From molar flow rate of the fuel, molar flow rate of the air (O_2 and N_2) is calculated with Equations 4.49, and 4.50.

$$\dot{n}_{O_2} = \frac{\dot{m}_f}{W_f}(2\lambda) \tag{4.49}$$

$$\dot{n}_{N_2} = \frac{\dot{m}_f}{W_f}(7.52\lambda) \tag{4.50}$$

From molar flow rate of the O_2 and N_2, mass flow rate of the air is calculated with Equation 4.51.

$$\dot{m}_a = \dot{n}_{O_2} W_{O_2} + \dot{n}_{N_2} W_{N_2} \tag{4.51}$$

Then, turning back to Equation 4.46, mass flow rate can be calculated with the summation of the mass flow rate of the fuel and the air, after they are calculated separately, as shown in Equations 4.47-4.51.

4.11 Convective Heat Transfer Coefficients of the Hot and Cold Sides of the PHE

It is one of the hardest point to calculate convective heat transfer coefficients of the fluids in the hot side and the cold side of PHE due to the complex plate geometry. In theory, it is possible to calculate these coefficients (Kakaç, & Liu, 2012) under some conditions. Therefore, application area of these correlations is limited because of the specific conditions. Moreover, theoretical calculations cannot give the exact results; when compared to experimental results they are less reliable.

Convective heat transfer coefficients are calculated separately to yield the overall heat transfer coefficient of the PHE. However, there are two other ways to decide on the overall heat transfer coefficient of the PHE experimentally. These two experimental set-ups will be mentioned in the next chapter. The following equations are for just theoretical calculations of the overall heat transfer coefficient of the PHE.

Actually, in the numerical calculations experimental overall heat transfer coefficients have been used. Even so, theoretical procedure will be mentioned in case there is no experimental set-up and finding this coefficient is an urgent topic. Correlations with their specifications give reasonable results to evaluate them in the place of necessity.

The example theoretical calculation of the coefficient in this study is made only 24-plate PHE having chevron plates with angle of 60˚, as shown in Figure 4.17.

Figure 4.17 An example of chevron plate.

In the following example calculation, 8.7 l/min and 60 ˚C hot usage water is requested from an appliance having maximum 28.5 kW power capacity; thereby resulting 0.029 kg/s water for each hot water channel and 0.013 kg/s water for each cold water channel. On this reference PHE, all plate configurations are same.

According to Kakaç, & Liu, (2002), the projected plate area, A_{1p} of a plate is calculated from the projected plate length, L_p and the plate width inside gasket, L_w as shown in Equation 4.52. These dimensions are shown on th schematic diagram of one plate in Figure 4.18.

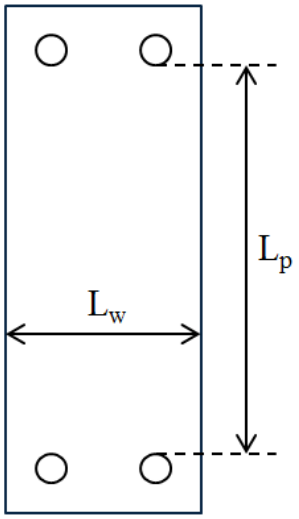

Figure 4.18 Projected plate length and plate width inside gasket shown on the sketch of the plate.

$$A_{1p} = L_p L_w \tag{4.52}$$

The mean channel flow gap, b_m is calculated from Equation 4.53 by using plate pitch p_p, and the plate thickness t_p, as shown in Figure 4.19.

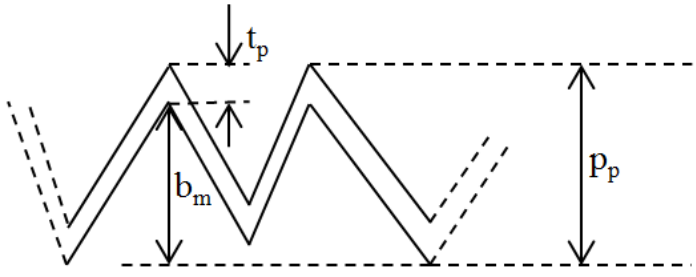

Figure 4.19 Mean channel flow gap on the channel configuration.

$$b_m = p_p - t_p \tag{4.53}$$

The enlargement factor is calculated dividing the single-plate heat transfer area, A_1 by the projected plate area as follows:

$$\phi = \frac{A_1}{A_{1p}} \tag{4.54}$$

The channel hydraulic / equivalent diameter is calculated from

$$D_{hp} = \frac{2b_m}{\phi} \tag{4.55}$$

$\dot{m}_{wt(2)}$ and $\dot{m}_{wt(3)}$ have been defined already. There are 24 plates in the content of the PHE; 11 of them are cold water channels, 12 of them are hot water channels.

The mass velocity, G_h for hot water and G_c for cold water is calculated dividing the mass flow rate per channel by one channel flow area as follows:

$$G_h = \frac{\dot{m}_{wt(2)}}{A_{ch}} \tag{4.56}$$

$$G_c = \frac{\dot{m}_{wt(3)}}{A_{ch}} \tag{4.57}$$

One channel flow area, A_{ch} is calculated from

$$A_{ch} = b_m L_w \tag{4.58}$$

Hot fluid Reynolds number, Re_h and cold fluid Reynolds number, Re_c are

$$\mathrm{Re}_h = \frac{G_h D_h}{\mu_h} \tag{4.59}$$

$$\mathrm{Re}_c = \frac{G_c D_c}{\mu_c} \tag{4.60}$$

Resultantly, for hot side $\mathrm{Re_h}$ has been calculated as 842, and for cold side $\mathrm{Re_c}$ has been calculated as 380. Then, it is necessary to find suitable correlations covering this Reynolds number range.

Nusselt numbers, $\mathrm{Nu_h}$ and $\mathrm{Nu_c}$ for the flow in the hot and cold water channels have been calculated using the following correlations and conditions given by (Kakaç, & Liu, 2002)

$$Nu_h = 0.1096\,\mathrm{Re}_h^{0,78}\,\mathrm{Pr}^{1/3}(\mu/\mu_w)^{0.14} \qquad \mathrm{Re}_h \geq 800 \tag{4.61}$$

$$Nu_c = 0.2\,\mathrm{Re}_c^{0.75}\,\mathrm{Pr}^{0.4} \qquad 10 \leq \mathrm{Re}_c \leq 720 \tag{4.62}$$

$\mathrm{h_{wt(2)}}$ and $\mathrm{h_{wt(3)}}$ are calculated from

$$h_{wt(2)} = \frac{Nu_h k}{D_{hp}} \tag{4.63}$$

$$h_{wt(3)} = \frac{Nu_c k}{D_{hp}} \tag{4.64}$$

Using Equation 4.9, multiplication of overall heat transfer coefficient and heat transfer area of one plate "$U_{PHE}A_{PHE}$" has been calculated as 53.9 W/K for the 24-plate PHE.

4.12 Overall Surface Efficiency

Overall surface efficiency has been calculated for the pin fin arrangement and as stated in the assumptions, this value has been used for both of the heat exchangers modeled in this study. As the physical meaning, the overall surface efficiency, η_{fin} characterizes the performance of an array of fins and the base surface to which they are attached.

If there are Z fins in an array, the total area, A_{total} is calculated by

$$A_{total} = ZA_f + A_b \tag{4.65}$$

where A_f is surface area of a single fin, and A_b is the area of the prime surface. For a pin fin given in Figure 4.20, A_f is calculated from

$$A_f = \pi D_{fin} L_c \tag{4.66}$$

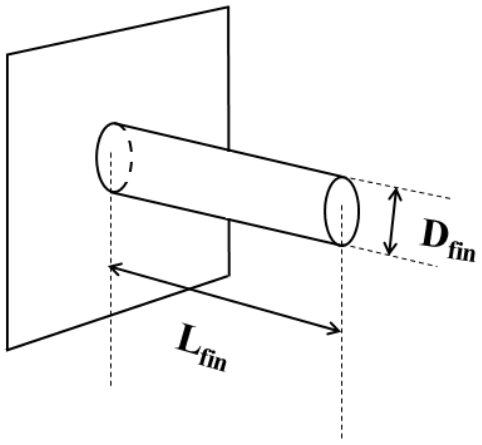

Figure 4.20 Reference pin fin and its dimensions.

Corrected fin length, L_c is given by

$$L_c = L_{fin} + \frac{D_{fin}}{4} \tag{4.67}$$

Resultantly, the overall surface efficiency is formulated as

$$\eta_{fin} = 1 - \frac{ZA_f}{A_{total}}(1 - \eta_{fs}) \tag{4.68}$$

η_{fs} is the single fin efficiency and calculated by

$$\eta_{fs} = \frac{\tanh mL_c}{mL_c} \tag{4.69}$$

where m is defined as

$$m = \sqrt{\frac{4h_g}{k_{ff} D_{fin}}} \tag{4.70}$$

CHAPTER FIVE
COMFORT-EFFICIENCY TESTS OF COMBI BOILERS & EXPERIMENTAL SET-UPS

Comfort and efficiency tests of the combi boilers are defined by the International Standards. Comfort tests are investigated in the standard called as "Assessment of performance of hot water deliveries" (BS EN 13203-1:2006, 2006). There are six different tests in the content. Efficiency test standard is called "Assessment of energy consumption" (BS EN 13203-2:2006, 2006).

5.1 Comfort Tests of the Combi Boilers (BS EN 13203-1:2006, 2006)

The international test instruction is established in order to create a common decision mechanism about the comfort level of the gas-fired domestic appliances producing hot water (not exceeding 70 kW heat input and 300 l water storage capacity).

There are 6 different tests for measuring the comfort level of a combi boiler type appliance named as waiting time, temperature variation according to water rate, temperature fluctuation at constant water rate, temperature stabilization time on variation of the water rate, minimum nominal water rate, and temperature fluctuation between successive deliveries. Each test has its own point scale; the appliance gets a grade from each test according to its performance. Each test also has a coefficient factor according to its importance. The test scores are multiplied by their own coefficients factors. All six evaluated results are summed in the end; therefore the appliance gets *, **, and *** as the comfort level (BS EN 13203-1:2006, 2006). In the market, combi boiler type heating appliances are categorized according to the number of stars in terms of their comfort level.

In waiting time test, DHW outlet temperature profile is investigated if a hot water demand is created after an appliance gets out of the comfort cycles where CH water is periodically heated in case of possible user requests. According to the minimum

and maximum points of DHW outlet temperature and the time duration between these points, the appliance gets a score. Hence, the most important points of this test are the minimum and maximum points of DHW outlet temperature and the elapsed time between these maximum and minimum peaks.

Temperature variation according to water rate test investigates the steady-state temperature differences between the user requests at various flow rates defined according to the power of the appliance.

In temperature fluctuation at constant water rate test, similar to previously defined tests, various flow rates are defined according to the power of the appliance. At each user demand, DHW outlet temperature is analyzed when it starts to be stabilized. The appliance gets a performance point from this test related to the maximum and minimum DHW outlet temperature difference at the time of stabilization.

Temperature stabilization time on variation of the water rate analyzes the temperature fluctuations at successive tappings of various flow rates defined regarding the power of the appliance. The grade is evaluated in accordance with the maximum and minimum DHW outlet temperature between which fluctuations occurs for each flow rate.

Minimum nominal water rate test investigates the behavior of the appliance at possible minimum DHW flow rates. User requests are created at the possible minimum flow rates defined according to the standard at issue one by one. At the minimum flow rate that the appliance could work, temperature fluctuations are investigated after specific time duration decided by the standard. Regarding this fluctuation, the appliance gets a performance point.

Lastly, in temperature fluctuation between successive deliveries test, the tapping is regularly stopped at the same and constant flow rate and re-started again. The pause time is increased at each stop, and the peaks in the DHW outlet temperature are observed. The test continues until the difference between the overshoot of the

current tap and the overshoot of the previous tap is within a defined interval by the standard.

Only waiting time test has been modeled with the simulation of comfort working mode throughout this study.

5.2 Efficiency Tests of the Combi Boilers (BS EN 13203-2:2006, 2006)

Similar to the comfort tests, the procedure of the efficiency test is also defined by a common standard for the gas-fired domestic appliances producing hot water (not exceeding 70 kW heat input and 300 l water storage capacity).

During this test, there are successive deliveries and these deliveries compose the tapping cycles simulating the users' consumption profile. With these tapping cycles, the daily energy consumption is determined. There are four different tapping cycles depending on the use. Table 5.1 is an example of the tapping cycles.

Table 5.1 An example tapping cycle.

Start (h.min)	Type of delivery	ΔT desired (K), to be achieved during tapping	Min. ΔT (K), =start of counting useful energy
07:00	Small		15
07:30	Small		15
08:30	Small		15
09:30	Small		15
11:30	Small		15
11:45	Small		15
12:45	Dish washing	45	0
18:00	Small		15
18:15	Household cleaning		30
20:30	Dish washing	45	0
21:30	Large		30

Each type of flow rate corresponds to a specific value as shown in Table 5.2.

The daily energy requirement is determined with the measurement of the energy recovered by the useful water, calculation of the gas energy, calculation of the

electrical energy, measurement of stand-by mode energy consumption, and measurement of auxiliary energy consumption with the off mode, etc. and all of these specific energy consumption investigation points are defined and formulated by the same standard.

Table 5.2 Tapping flow rates.

Type of tapping	**Hot water flow rates corresponding to a temperature rise of 45 K (l/min)**
Household cleaning	3±0,5
Small	3±0,5
Floor cleaning	3±0,5
Dish washing	4±0,5
Large	4±0,5

Useful energy is consumed by the quantity of the water delivered for which the temperature increase is in accordance with the fixed requirement for each individual delivery of the tapping cycles. On the other hand, if the temperature increase cannot reach to the level of the fixed requirement for that flow rate, this time the amount of energy consumed by the delivered water is called as wasted energy.

Modelling the DHW efficiency test with all details is not included by this study. It only compares theoretical wasted energy/useful energy ratio for 8.7 l/min user demand and 30 K inlet and outlet temperature difference after which the consumed energy is counted as useful. The flow rate and the critical temperature difference is defined randomly according to the available data at hand just for comparing two appliance concept (the primary DHW concept and the standard combi boiler) in a similar way that the standard does.

Actually, comparing the appliance concepts from the normal efficiency view (output/input) is enough to see the difference between them basically since this study is just a kind of broad investigation.

5.3 Experimental Set-ups

There are two experimental set-ups used in this study. One of them is used to measure CH water temperature from the inlet and outlet of the HC, flue gas temperature, and the DHW outlet temperature.

With this special test rig just mentioned, all these six comfort tests and efficiency test measurements are made automatically. The view of the above-mentioned experimental set-up is given in Figure 5.1. In the below given figure, a standard combi boiler is installed to the test rig with all pipe connections. Tests are controlled from the screen of the test rig.

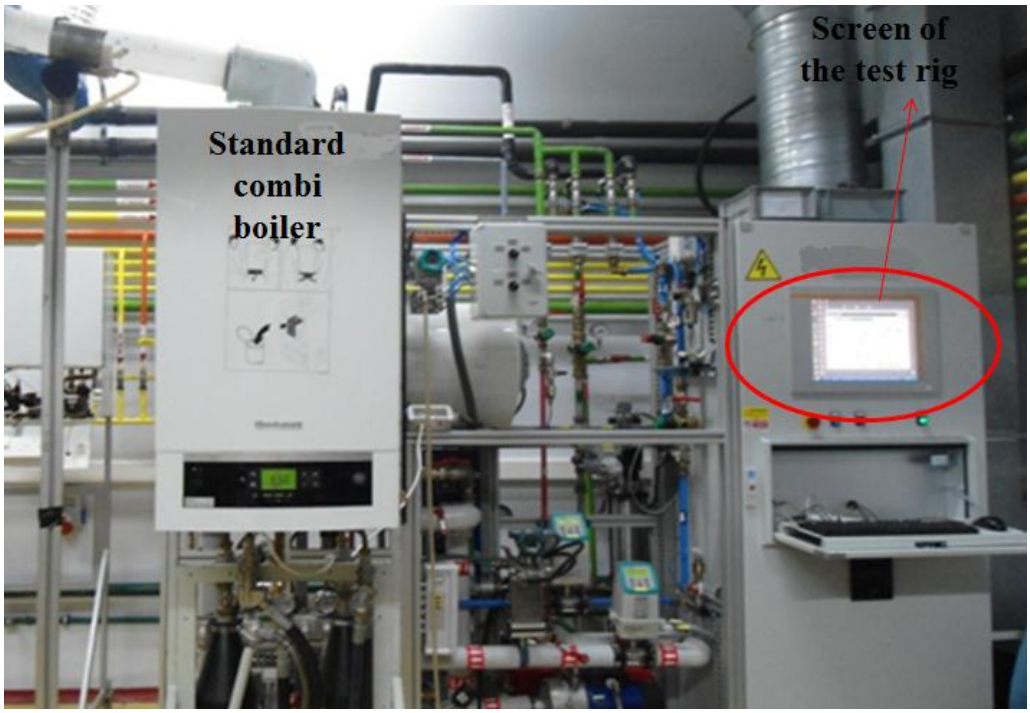

Figure 5.1 Special test rig for the comfort/efficiency tests of the combi boilers.

DHW outlet temperatures have been directly measured from this set-up by only adjusting the required DHW flow rate as the input to the test rig. Before starting tests, CO_2 levels of the appliances are checked with a gas analyser as shown in Figure 5.2 to check the excess air coefficient.

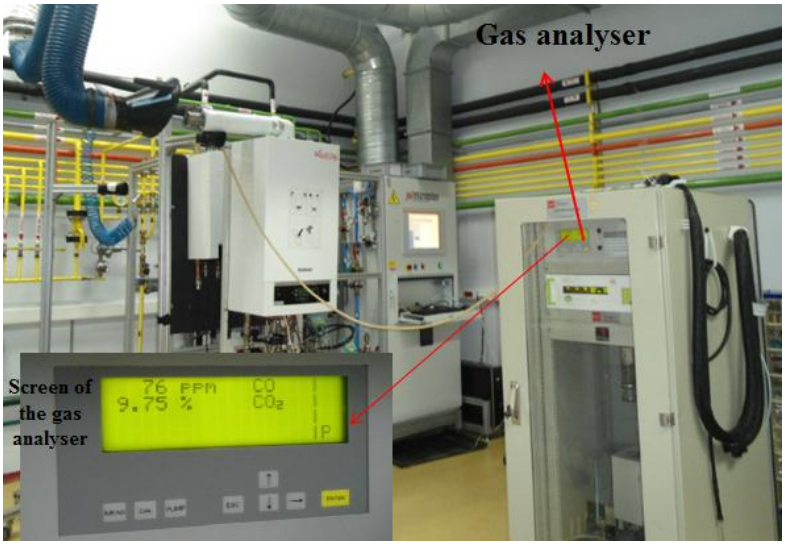

Figure 5.2 Gas analyzer checking the CO and CO_2 level of the appliance.

The uncertainty of this set-up is ±1 ˚C for the temperature and ±1 % of the measured flow rate. While measuring DHW outlet temperature there is an important issue needed to be considered: type of thermocouple used for DHW outlet temperature measurement. In these kinds of test rigs there are generally 2 thermocouple options as single thermocouple and triple thermocouple system as shown in Figure 5.3.

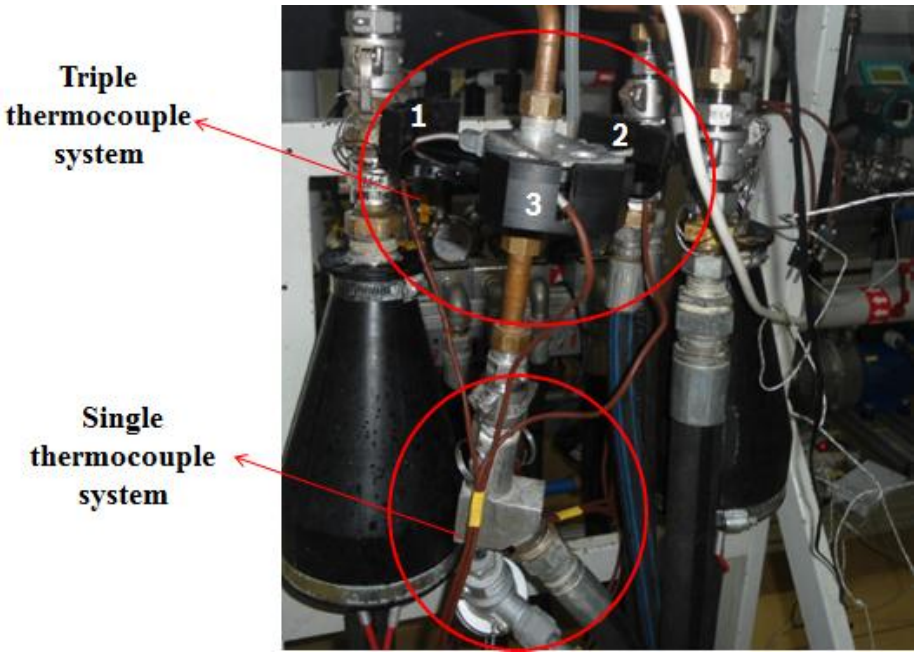

Figure 5.3 Single and triple thermocouple system on the water line.

Triple thermocouple system response is faster when compared to the single thermocouple. It takes measurements from three different points on the water pipe as shown in Figure 5.4; thereby taking more reliable measurement.

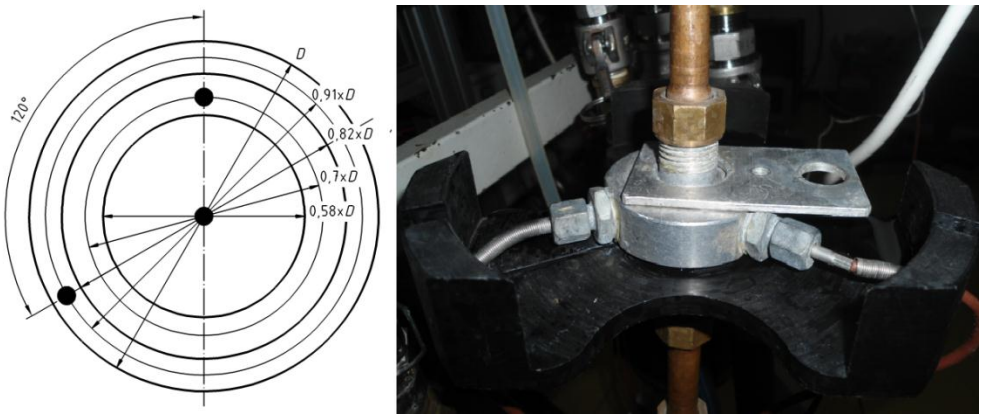

Figure 5.4 An example of position of triple thermocouples (D:diameter) and enlarged view.

If one thermocouple system is used instead of the triple system, sudden temperature peaks cannot be observed since their response is slow when compared to the triple thermocouple systems. The comparison of these two thermocouples in economic mode is given in Figure 5.5.

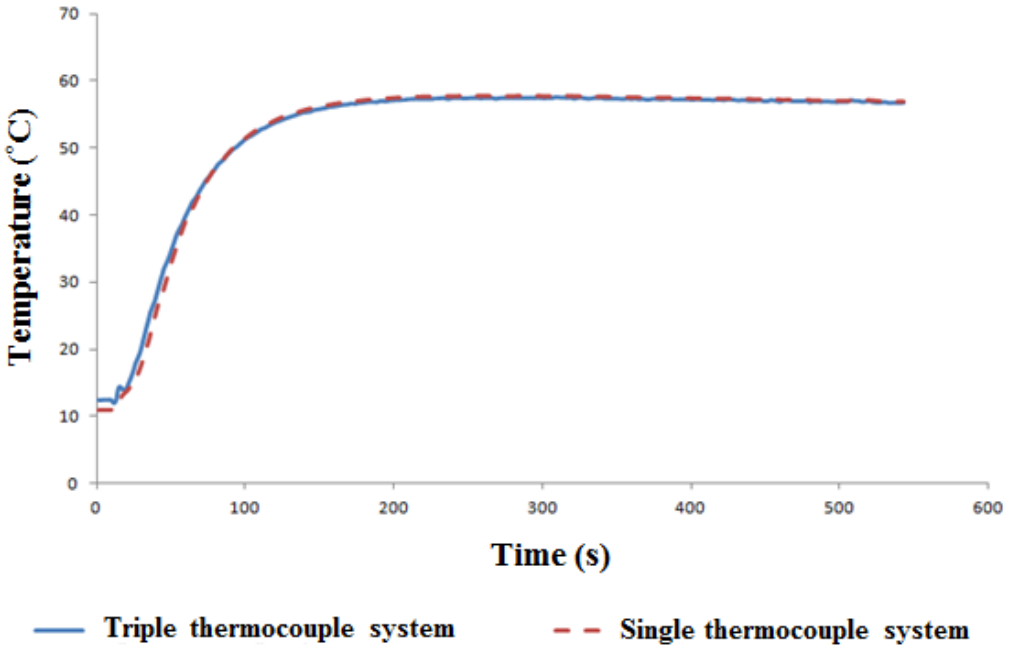

Figure 5.5 Comparison of the triple thermocouple and single thermocouple system in eco mode.

In economic working mode, slow response of the single thermocouple system does not cause any noticeable difference as it is obvious from Figure 5.5. However, the dramatic temperature increase at the time of tapping just after the comfort cycle cannot be observed as shown in Figure 5.6.

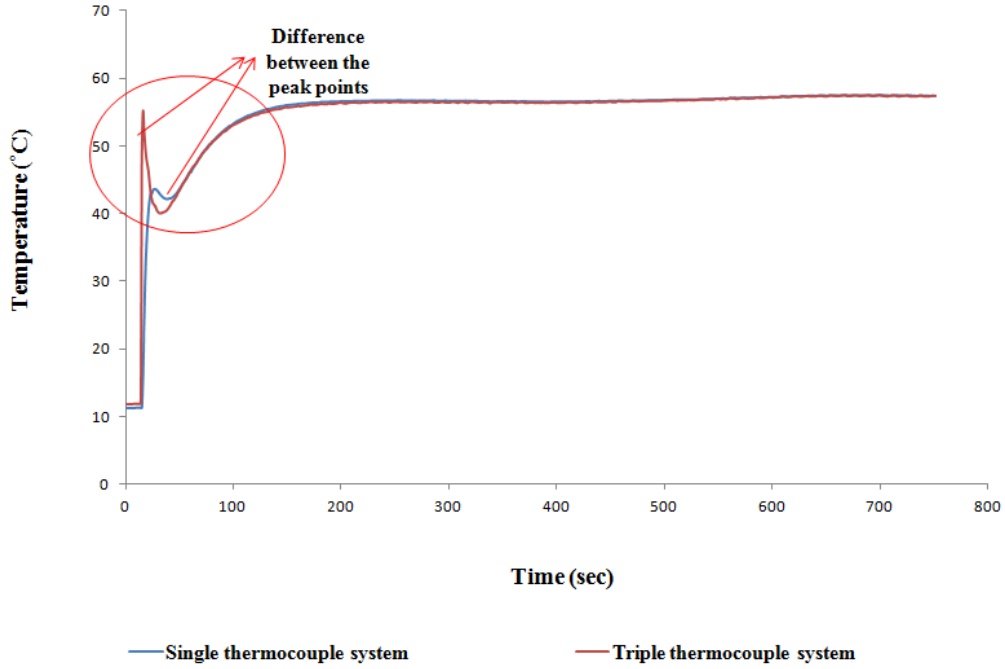

Figure 5.6 Comparison of the triple thermocouple and single thermocouple system in comfort mode.

As a result, measurements recorded by only single thermocouple system may be misleading; then it is a must to use triple thermocouple systems in such kind of measurements including overshoots.

Although comfort and efficiency tests are automatic and DHW outlet temperature can be directly measured with the test rig, HC inlet and outlet temperatures of the CH water, and the flue gas temperature measurement options are not included by the test rig in DHW mode. Then, thermocouples have been attached to these points (HC inlet, HC outlet, and inlet of the flue gas pipe) as shown schematically in Figure 5.7. Figure 5.8 is the view of the measurement points on the real appliance.

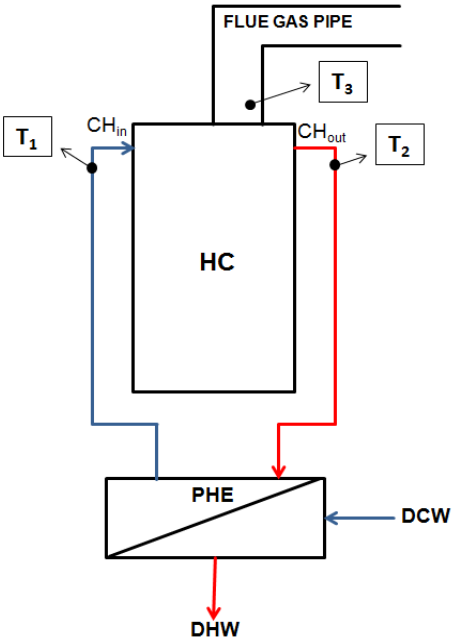

Figure 5.7 Schematic view of the additional thermocouple attachment points.

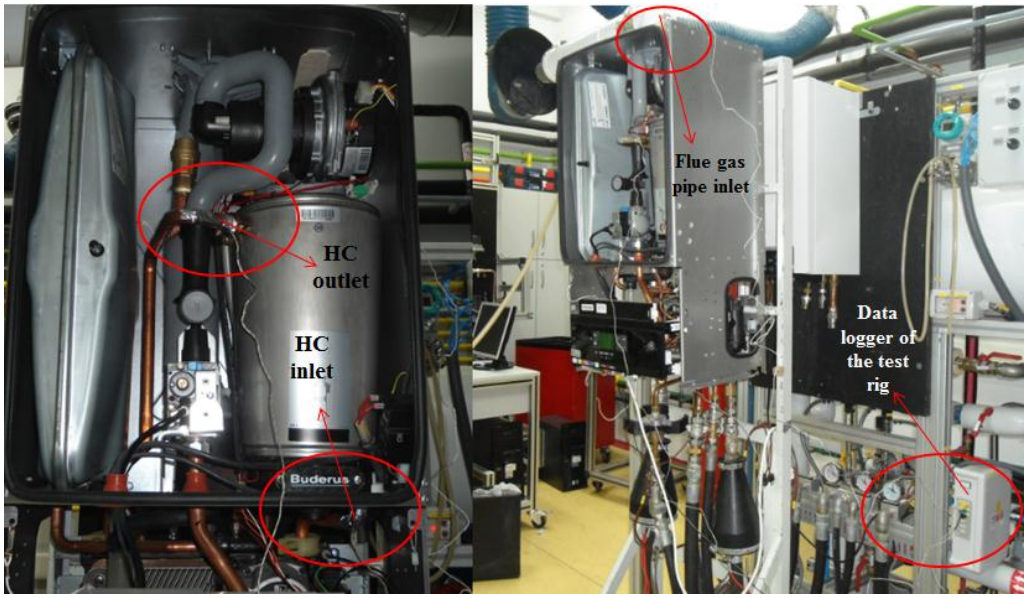

Figure 5.8 Thermocouple attachment points on the real appliance and their connection to the test rig.

The second measurement set-up used in this study is related to the plate heat exchangers. Performance of the plate heat exchangers are tested with this set-up shown in Figure 5.9, i.e., pressure drop, and DHW outlet temperature. CH water inlet and outlet temperatures and DHW inlet and outlet temperatures has been measured by this test rig to calculate multiplication of overall heat transfer coefficient and heat

transfer area of one plate "$U_{PHE}A_{PHE}$" to use later in the numerical algorithm. This test-rig has been proposed as the second way of calculating "$U_{PHE}A_{PHE}$" in addition to theoretical calculation.

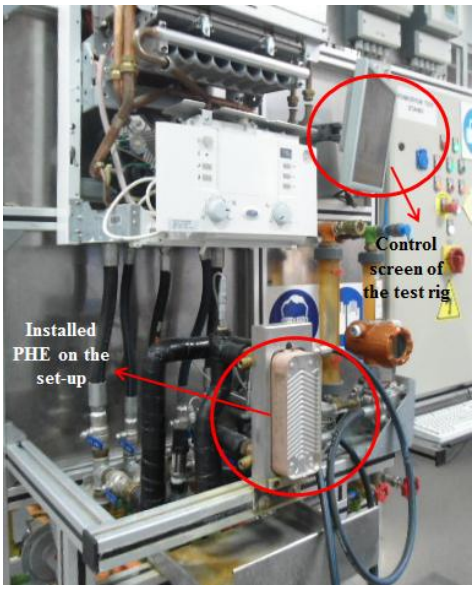

Figure 5.9 A test rig for the performance measurements of the PHEs.

Schematic view of the PHE performance test rig is given in Figure 5.10.

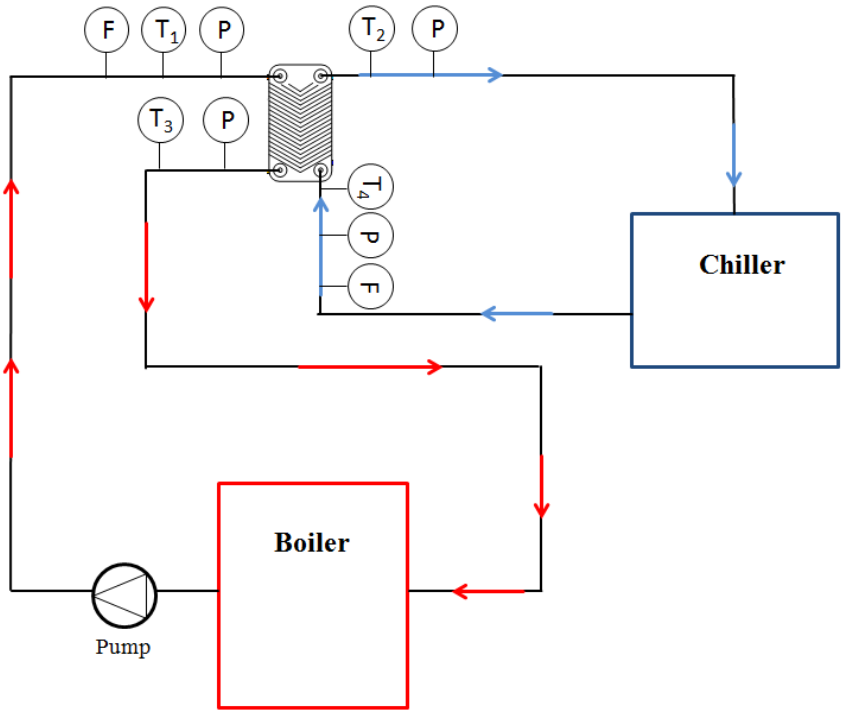

Figure 5.10. Schematic view of the PHE performance test rig

Boiler supplies hot water continuously to the plate heat exchanger installed on the test rig; thereby simulating a combi boiler working in DHW supply mode at a specific hot water flow rate as the user demand. The hot water cooled in the PHE turns back to the boiler to be heated up again to a desired CH water temperature. The cold user tapping water is supplied by the chiller of the test-rig. As a result, the main components of the PHE performance test rig are the boiler and the chiller to configure out that PHE is working in a combi boiler at a specific DCW and CH flow rates and inlet temperatures. Inlet temperatures of both water media are supplied fixing the chiller and the boiler temperature to the desired set point. All inlet temperatures and flow rates are controlled from the screen of the test rig given in Figure 5.9. As given in the schematic view, CH inlet temperature T_1, CH outlet temperature T_3, DCW inlet temperature T_4, and DHW outlet temperature T_2 are measured by the thermocouples located at the regarding inlets and outlets of the PHE; pressures are measured by the pressure transducers shown as the symbol "P" in Figure 5.10 at each inlet and outlet. Finally, CH flow rate and DHW flow rate is measured by the flow meters shown as the symbol "F" in Figure 5.10 on CH line and DCW line, respectively.

While calculating "$U_{PHE}A_{PHE}$" multiplication with this test rig in addition to the theoretical way, T_1, T_2, T_3, T_4, flow rates of DCW and DHW are necessary to measure. First of all, the rate of energy transfer from one hot water channel to one cold water channel, Q_{CH}, also shown schematically in Figure 4.4, is calculated. Then, logarithmic mean temperature difference ΔT_{lm} of PHE is calculated with Equation 5.1. As a result, dividing $\dot{Q}_{CH}$ by ΔT_{lm}, "$U_{PHE}A_{PHE}$" multiplication is obtained with Equation 5.2.

$$\Delta T_{lm} = \frac{(T_1 - T_2) - (T_3 - T_4)}{\ln((T_1 - T_2)/(T_3 - T_4))} \tag{5.1}$$

$$U_{PHE} A_{PHE} = \frac{\dot{Q}_{CH}}{\Delta T_{lm}} \tag{5.2}$$

As a result, PHE performance test rig is the second way of calculating the rough value of "$U_{PHE}A_{PHE}$" multiplication. The third way is collecting required measurement data to calculate the multiplication under question from the appliance while working in the DHW supply mode. As it is shown in Figure 5.7, with thermocouples attachment, CH water outlet and inlet temperatures can be measured from the inlet and outlet of the HC. CH water outlet temperature from the HC is used as CH water inlet temperature to the PHE, and CH water inlet temperature to the HC is used as CH water outlet temperature from the PHE. DHW inlet and outlet temperatures are recorded automatically by the test rig; hence there is no need to add any thermocouples.

Finally, there are three proposed ways for calculating "$U_{PHE}A_{PHE}$" as (i) theoretical approach, (ii) collecting required data PHE performance test rig, and (iii) collecting required data from the appliance working in DHW mode at the required test conditions. The reliability of these three ways will be discussed in the next chapter.

CHAPTER SIX
RESULTS AND DISCUSSION

The numerical results have been validated with the experimental results in this chapter. First of all, theoretical convective heat transfer coefficient of the flue gas inside the heat cell and the theoretical convective heat transfer coefficient of the water have been corrected with experimental temperature measurements from the flue gas pipe inlet, HC water inlet, and HC water outlet. The second verification is for the physical value of "$U_{PHE}A_{PHE}$" multiplication which could be obtained in both experimental and theoretical ways discussed in the previous chapters. Thirdly, the theoretical model has been validated by using two standard combi boiler each has a different heat cell and plate heat exchanger combination. After the experimental verification, standard combi boiler concept and the primary DHW concept has been compared on the basis of prepared theoretical models. Later on, a parametric study has been conducted for each appliance concept separately to see the effects of common and critical parameters on both concepts. Lastly, general efficiency values and wasted energy/useful energy ratios of both concepts have been compared.

6.1 Experimental Verification of Convective Heat Transfer Coefficients of the Heat Cell

According to the mathematical model, it is necessary to calculate the convective heat transfer coefficients of the flue gas and the water around the HC separately; hence regarding correlations have been used. However, it is needed to validate these values in a way that they should be corrected experimentally. Then, the inlet and outlet of the CH water from the HC have been collected with the thermocouples attached as in Figure 5.7. Flue gas outlet temperature can be measured from the inlet of the flue gas pipe, but flue gas inlet temperature cannot be measured as soon as combustion occurs due to the lack of thermocouples at hand that can resist very high temperatures i.e., 1900, 2000 ˚C. Therefore, inlet temperature of the flue gas is assumes as adiabatic flame temperature. As a result, a semi-experimental overall heat transfer coefficient and average heat transfer area of the HC multiplication,

"$U_{HC}A_{HC}$" can be calculated. The overall multiplication "$U_{HC}A_{HC}$" is not used directly in the mathematical model. However, via the experimental verification of this multiplication, the theoretical correlations are validated.

First of all, "$U_{HC}A_{HC}$" multiplication is found theoretically with the theoretical heat transfer coefficients and related heat transfer areas as follows:

$$\frac{1}{U_{HC}A_{HC}} = \frac{1}{h_g A_{sa,g}\eta_{fin}} + \frac{1}{h_{wt(1)}A_{sa,wt(hc)}} \tag{6.1}$$

The result of above given equation is validated with the semi-experimental "$U_{HC}A_{HC}$" given in Equation 6.2. Required temperatures are shown in Figure 6.1 also to clarify the terms used in the following equations.

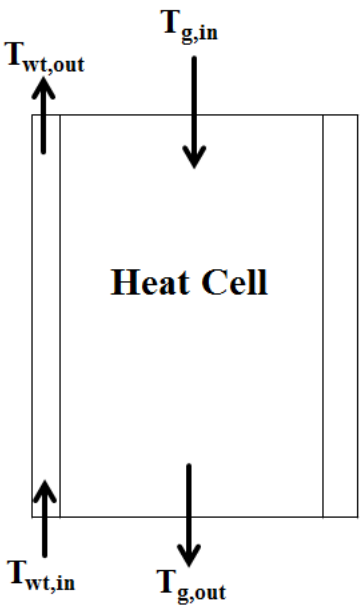

Figure 6.1 Schematic display of the temperatures of the fluids in and out of the HC.

$T_{g,in}$ and $T_{g,out}$ are the flue gas inlet and the outlet temperatures, respectively. In addition to the measured and assumed flue gas temperatures, HC water inlet temperature, $T_{wt,in}$ and outlet temperature, $T_{wt,out}$ are measured to calculate logarithmic mean temperature difference of the heat cell. After calculating the energy

transfer rate, $\dot{Q}_{gas}$ within the heat cell from gas to the water, the semi-experimental "$U_{HC}A_{HC}$" can be calculated as given in Equations 6.2 and 6.3.

$$\Delta T_{lm,HC} = \frac{(T_{g,in} - T_{wt,out}) - (T_{g,out} - T_{wt,in})}{\ln((T_{g,in} - T_{wt,out})/(T_{g,out} - T_{wt,in}))} \quad (6.2)$$

$$U_{HC}A_{HC} = \frac{\dot{Q}_{gas}}{\Delta T_{lm,HC}} \quad (6.3)$$

Resultantly, theoretical "$U_{HC}A_{HC}$" is calculated as 65.1 W/K, whereas it is 68.3 W/K according to the semi-experimental calculations for maximum 28.5 kW (as heat input rate) appliance and 8.7 l/min user demand of DHW. Therefore, the semi-experimental and theoretical results is found very close to each other and, correlations are used in the other model simulations.

6.2 Experimental Verification of Convective Heat Transfer Coefficients of the Plate Heat Exchanger

As mentioned in the previous fifth and fourth chapters, "$U_{PHE}A_{PHE}$" multiplication has been found in three ways for a plate heat exchanger. The theoretical "$U_{PHE}A_{PHE}$", for 24-plate PHE, 8.7 l/min user demand of DHW, and 21 l/min corresponding CH water, has been calculated as 53.9 W/K as mentioned before. According to the data collected from the PHE performance test rig, this multiplication has been calculated very close to the previous theoretical value, 52.5 W/K. However, with a similar calculation way of the PHE performance test rig, when the data is collected from the appliance having a 24-plate PHE and working at 8.7 l/min user demand, the "$U_{HC}A_{HC}$" multiplication is calculated as 45 W/K.

The third one is the most trustable one because it takes into consideration all resistances and components of the system. Actually, while testing an appliance at a

specific flow rate in DHW mode, CH flow rate cannot be known; only DHW flow rate can be measured and recorded. Then, even in the PHE performance test rig, a close value for CH flow rate has been assumed. Moreover, since the PHE performance test rig tests PHE alone and the system lacks other resistances thereby resulting in different flow characteristics for both DHW and CH water sides when compared to actual working conditions in the real appliance, theoretical results are less reliable. Therefore, after these comparisons, it has been decided to use "$U_{PHE}A_{PHE}$" multiplication calculated according to the data of the actual appliance. In this study mainly three flow rates have been used as 8.7, 7, and 5 l/min in the experimental verification section. All "$U_{PHE}A_{PHE}$" multiplications for the flow rates of 8.7, 7, and 5 l/min have been calculated as 45, 42, and 36.9 W/K, respectively, using the experimental data collected from the appliance working at those conditions.

In Figure 6.2, for 8.7 l/min DHW user demand in 28.5 kW (as maximum heat input rate) appliance, the effect of three "$U_{PHE}A_{PHE}$" multiplication methods on DHW outlet temperature profile has been discussed and compared with the experimental results.

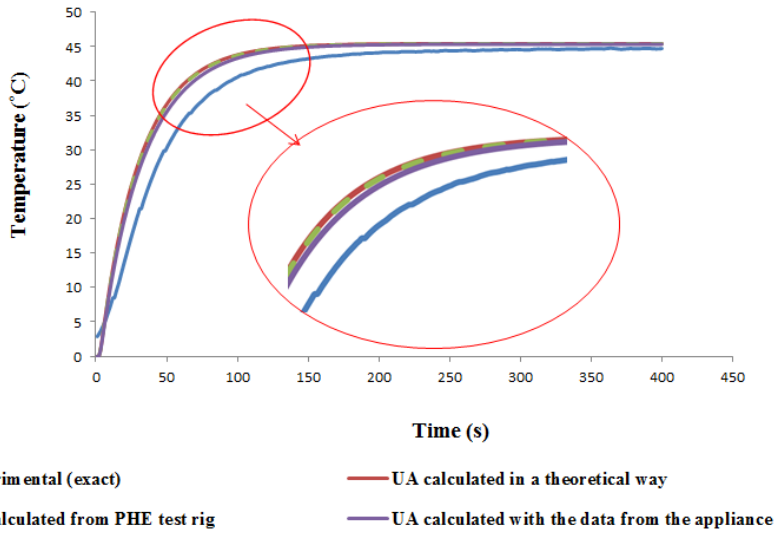

Figure 6.2 Effect of the physical value of the "$U_{PHE}A_{PHE}$" multiplication on the DHW outlet and inlet temperature difference.

As it is obvious from Figure 6.2, calculating "$U_{PHE}A_{PHE}$" multiplication in an experimental way is suggested although it is not enough to catch the system

behavior. Making the experiments in the real working conditions and in the system as a whole gives us closer results to the exact results. However, if there is a lack of experimental set-up or any necessary equipment, theoretical "$U_{PHE}A_{PHE}$" multiplication can be used to get rough results or broad idea about such a system modeled 1D energy equations.

6.3 Experimental Verification of the Mathematical Model

The numerical results have been validated with the experimental results. The first pair is the appliance concept having rectangular heat cell and 26-plate PHE with maximum 36.5 kW power and 10.4 l/min DHW user demand. Eco and comfort mode simulations of this appliance concept are the preliminary comparisons. The following simulation verifications for another appliance concept, 24-plate PHE and conical HC combination also used as the reference system in the parametric study part, include more detailed comparisons.

Figure 6.3 shows eco working mode simulation and experimental verification of the above-mentioned appliance at 10.4 l/min DHW demand in the eco mode.

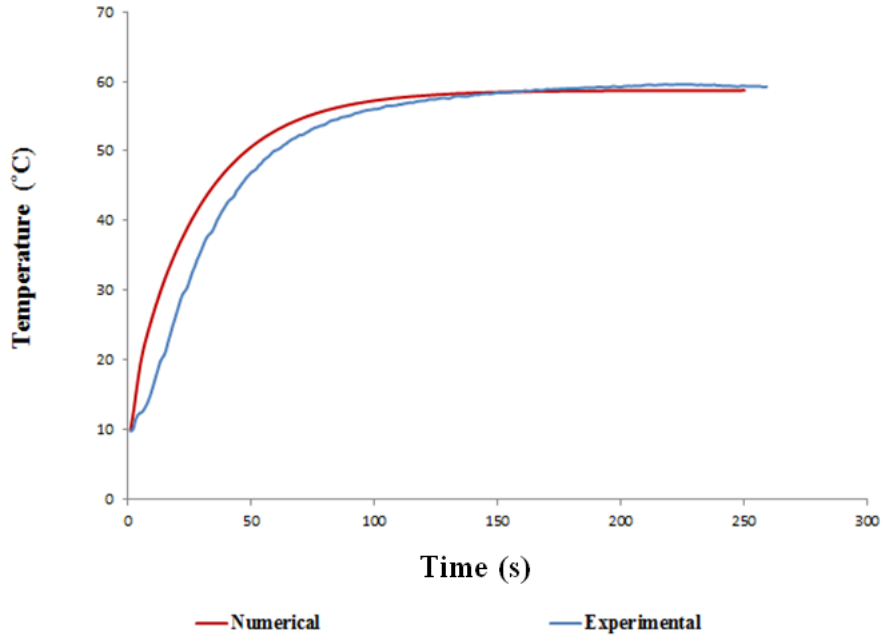

Figure 6.3 Comparison between the experimental and numerical DHW outlet temperature of the rectangular HC and 26-plate PHE combination in eco mode at 10.4 l/min DHW request.

Figure 6.4 shows the numerical and experimental DHW outlet and inlet temperature difference of 26-plate PHE and the rectangular HC combination in the comfort mode for the same flow rate of the previous simulation.

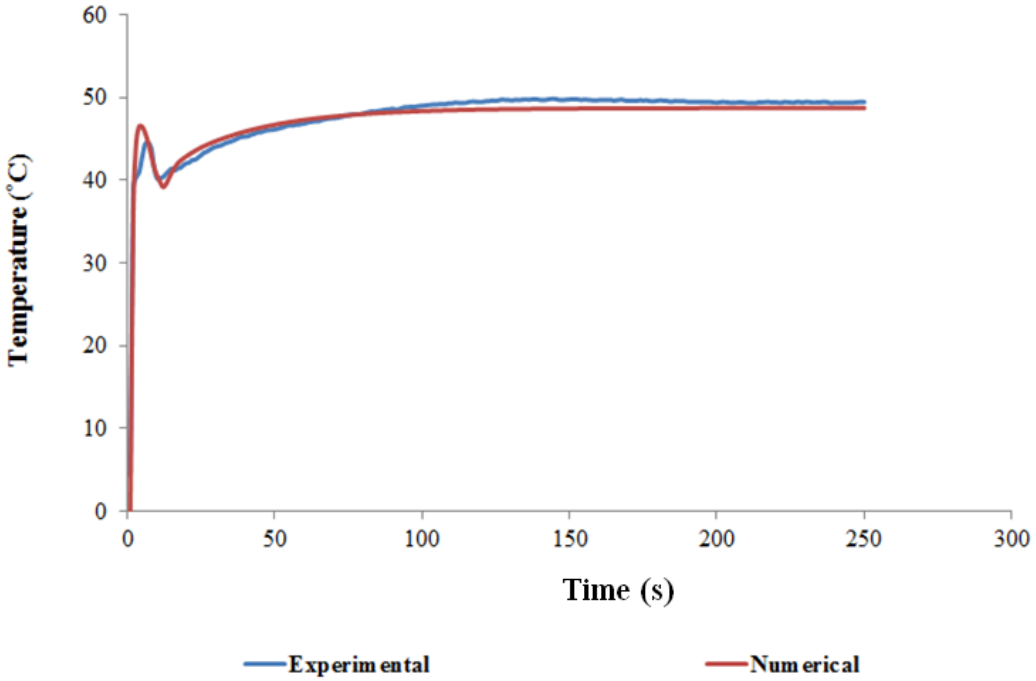

Figure 6.4 Comparison between the experimental and numerical DHW inlet and outlet temperature difference of the rectangular HC and 26-plate PHE combination in comfort mode at 10.4 l/min DHW request.

For this above-mentioned combination, the numerical algorithm has been corrected in terms of the conservation of the energy; meaning that the energy given by the combustion gases is equal to the energy gain of the CH water in the HC, and the energy given by the CH water is equal to the energy gain of the DCW in PHE, as shown in Figure 6.5.

Another correction of the system is about the rate of the energy storage with respect to time in all system elements of rectangular HC and 26-plate PHE combination. As it is shown in Figure 6.6, stored energy within the system goes zero as it reaches the steady-state conditions.

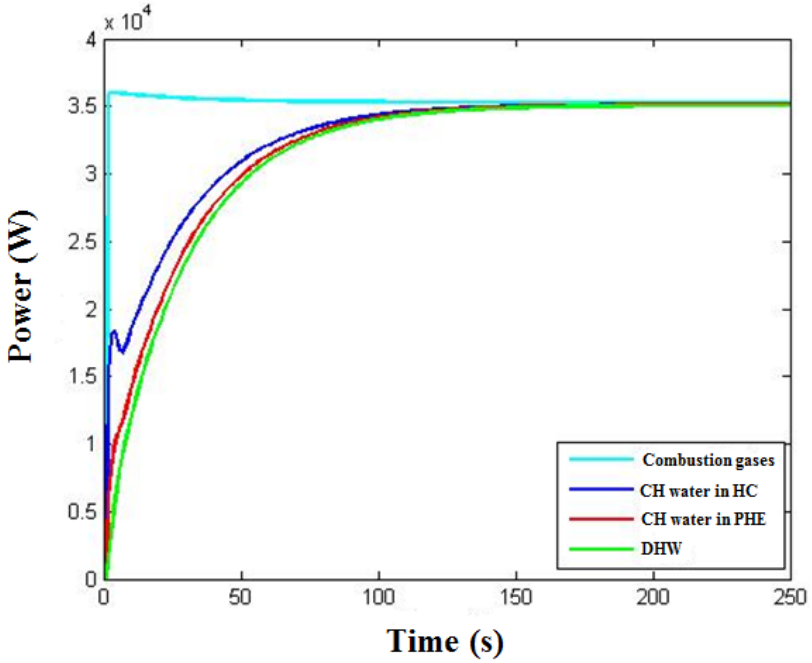

Figure 6.5 Energy transfer rate within the rectangular HC and 26-plate PHE combination.

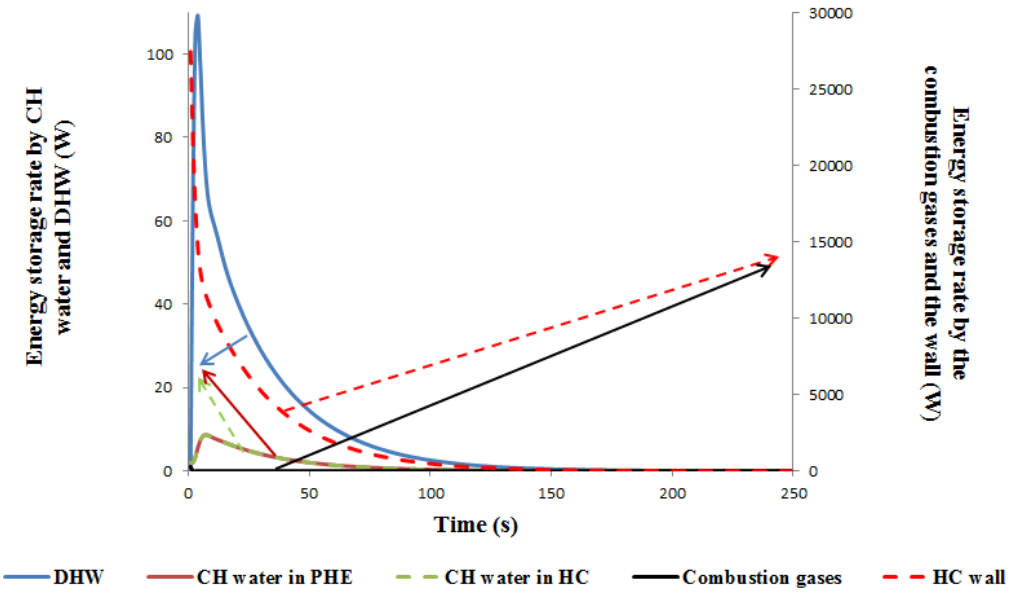

Figure 6.6 Energy storage rate in the components of the rectangular HC and 26-plate PHE combination.

Another combination, which is also the reference appliance concept is 24-plate PHE and the conical HC with maximum 28.5 kW heat input rate. The verifications are more detailed when compared to the previous combination. For three different flow rates of DHW, i.e., 8.7, 7, 5 l/min, the numerical and the experimental values of

CH water at the HC inlet, CH water at the HC outlet, flue gas, and DHW inlet and outlet temperature differences in eco mode have been compared. For the 5 l/min and 7 l/min, since there is power modulation in the software of the appliance, the same power modulation has also been added to the numerical algorithm. Also tapping after comfort cycle comparison in terms of DHW outlet and inlet temperature difference also has been given only for 8.7l/min.

Figure 6.7 shows the numerical and experimental flue gas outlet temperature in eco mode at 5 l/min DHW flow rate. The regions numbered as 1, 2, and 3 in the following figure show different power levels supplied to the appliance according to the software.

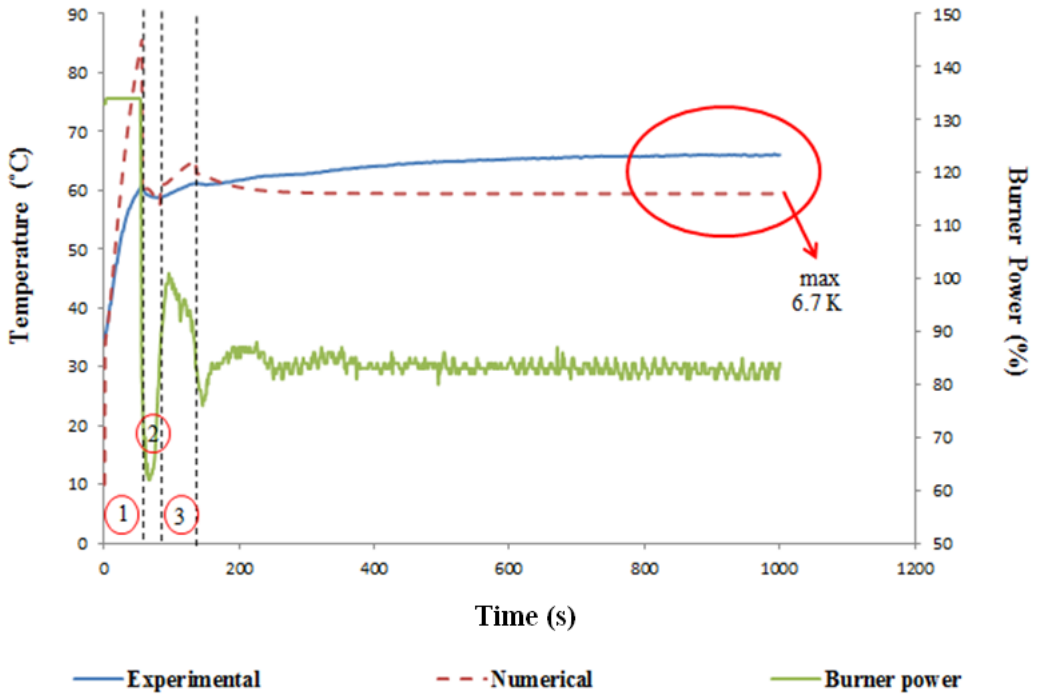

Figure 6.7 Comparison between the numerical and experimental flue gas outlet temperature of 24-plate PHE and the conical HC combination in eco mode at 5 l/min DHW flow rate.

Flue gas temperature in theoretical and experimental does not show a good agreement; but gas temperature is very hard to measure and calculate. It is in our scope of investigation; but not as the main target. However, the calculation algorithm can show us the steady-state temperature broadly, the peak points according to appliance modulation, and such kind of general things. For example, in region 2 on

the Figure 6.7, the power starts to increase, and then this effect is directly seen on the flue gas temperature in region 3. As a result, with this numerical algorithm, especially for lower DHW request, flue gas temperature characteristics could be broadly predicted.

Figure 6.8 shows the numerical and experimental CH water temperature of 24-plate PHE and the conical HC combination at the HC inlet in eco mode at 5 l/min DHW flow rate.

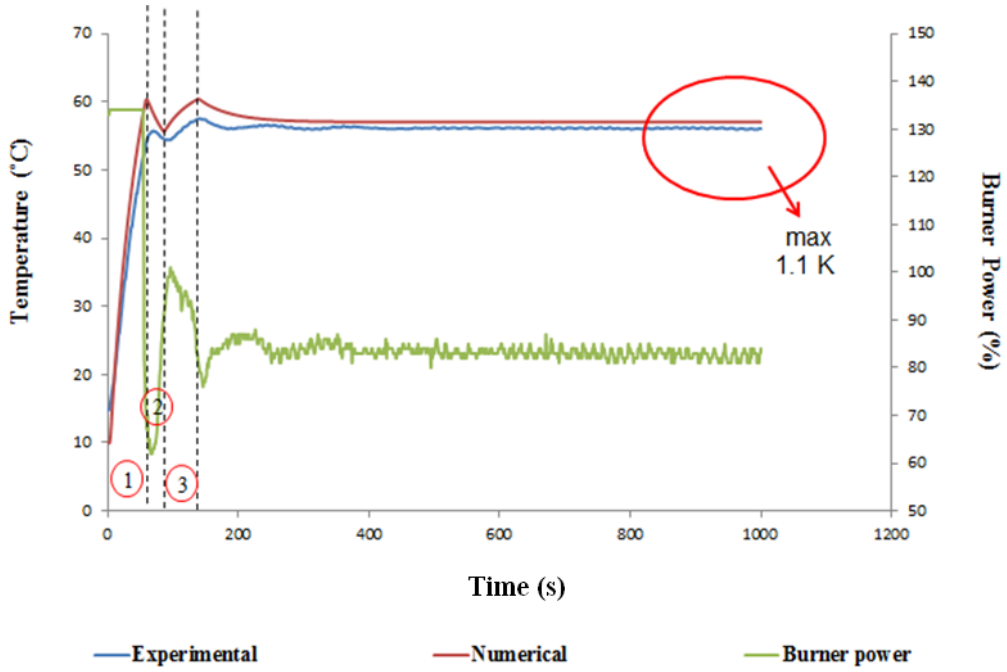

Figure 6.8 Comparison between the numerical and experimental CH water temperature of 24-plate PHE and the conical HC combination at the HC inlet in eco mode at 5 l/min DHW flow rate.

Figure 6.9 shows the numerical and experimental CH water temperature of 24-plate PHE and the conical HC combination at the HC outlet in eco mode at 5 l/min DHW flow rate.

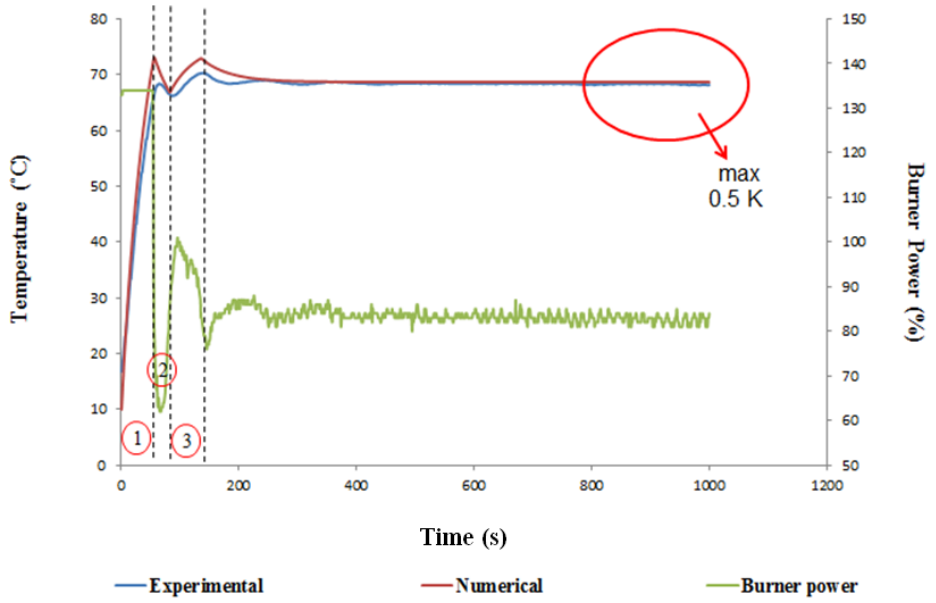

Figure 6.9 Comparison between the numerical and experimental CH water temperature of 24-plate PHE and the conical HC combination at the HC outlet in eco mode at 5 l/min DHW flow rate.

Figure 6.10 shows the numerical and experimental DHW outlet and inlet temperature difference of 24-plate PHE and the conical HC combination in eco mode at 5 l/min DHW flow rate.

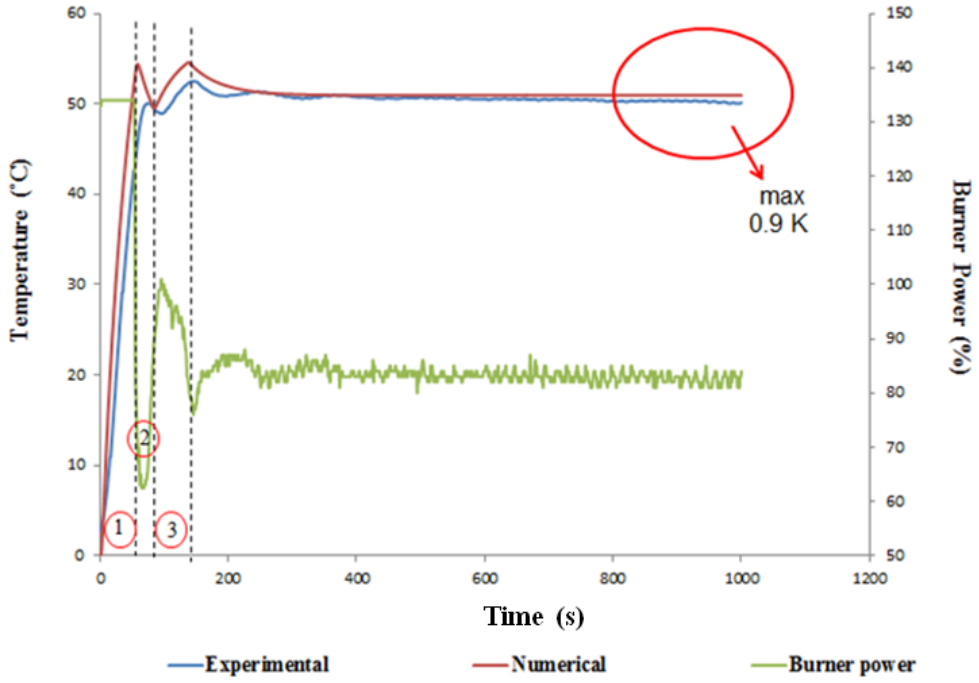

Figure 6.10 Experimental and numerical DHW inlet and outlet temperature difference of the 24-plate PHE and the conical HC combination in eco mode at 5 l/min.

Figure 6.11 shows the numerical and experimental flue gas outlet temperature in eco mode at 7 l/min DHW flow rate. The same comments could be made for 7 l/min as made for the flue gas outlet temperature at 5 l/min. However, this time numerical results are closer to the experimental data when compared to flow rate of 5 l/min. Moreover, the power of the appliance modulates also for this flow rate as shown in 1.,2., and 3. power region in the following figure. Consequently, not only general behavior has been simulated for the flue gas, but also closer results have been obtained i.e., steady-state temperature of the flue gas.

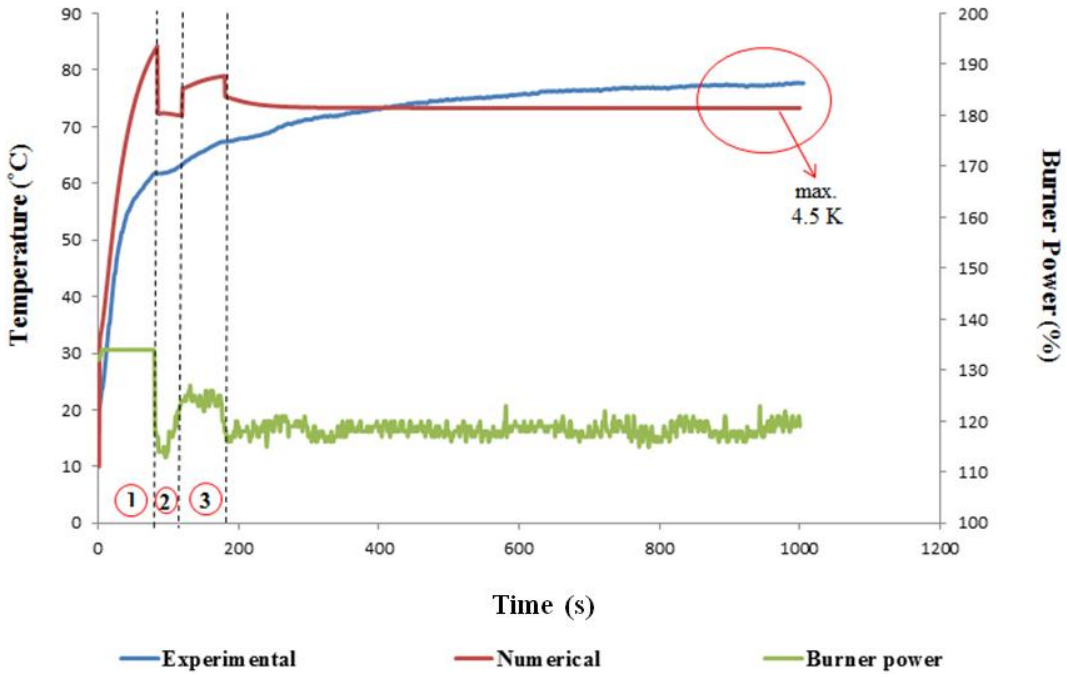

Figure 6.11 Comparison between the numerical and experimental flue gas outlet temperature of 24-plate PHE and the conical HC combination in eco mode at 7 l/min DHW flow rate.

Figure 6.12 shows the numerical and experimental CH water temperature of 24-plate PHE and the conical HC combination at the HC inlet in eco mode at 7 l/min DHW flow rate.

Figure 6.13 shows the numerical and experimental CH water temperature of 24-plate PHE and the conical HC combination at the HC outlet in eco mode at 7 l/min DHW flow rate.

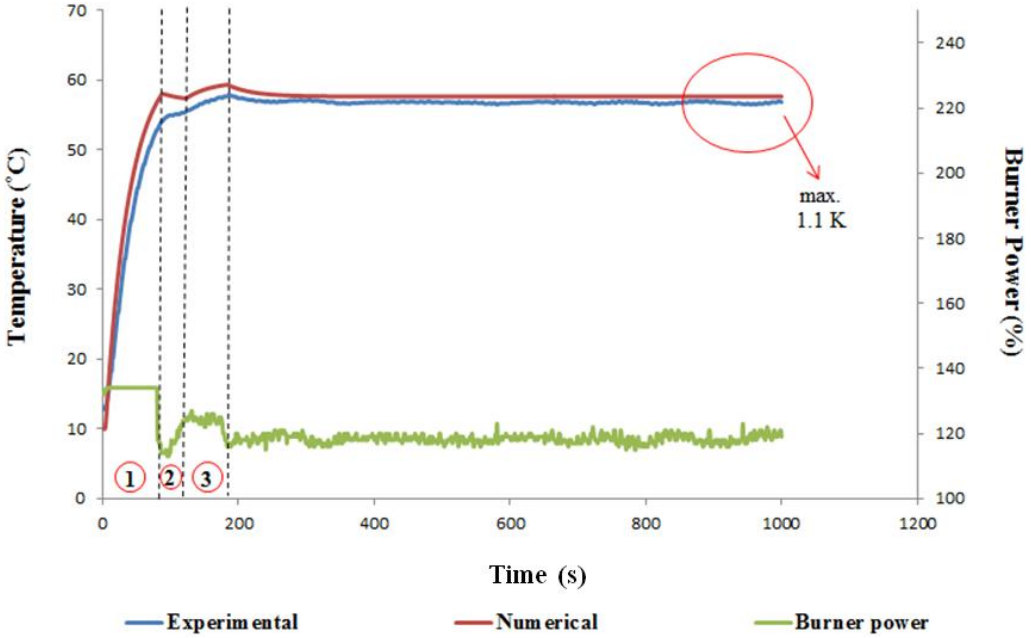

Figure 6.12 Comparison between the numerical and experimental CH water temperature of 24-plate PHE and the conical HC combination at the HC inlet in eco mode at 7 l/min DHW flow rate.

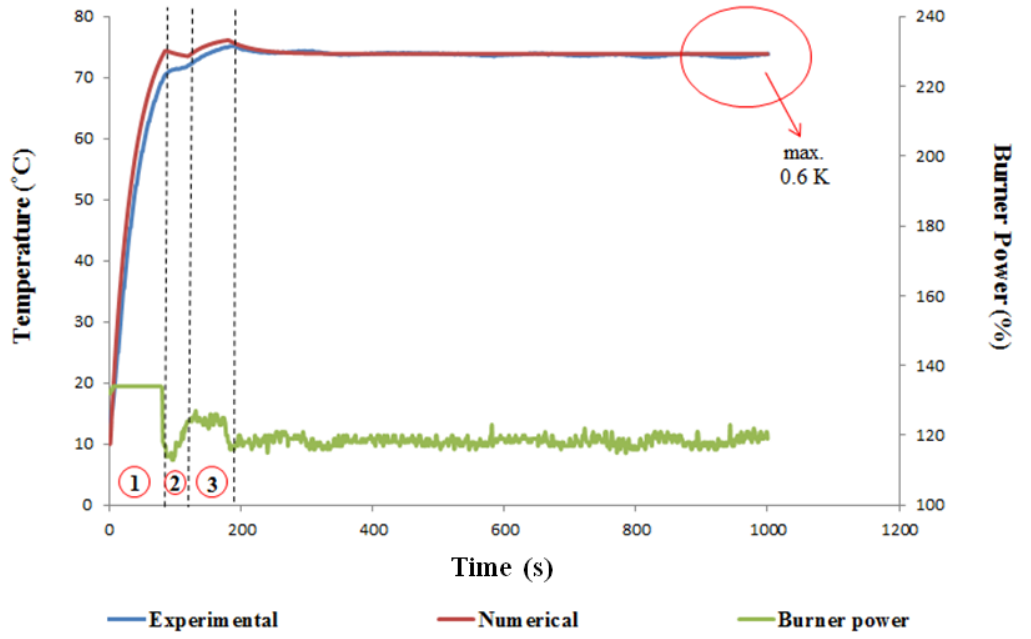

Figure 6.13 Comparison between the numerical and experimental CH water temperature of 24-plate PHE and the conical HC combination at the HC outlet in eco mode at 7 l/min DHW flow rate.

Effects of the power modulation are also observed on the HC inlet and outlet temperatures of the CH water (1.,2., and 3. power regions) as shown in Figure 6.12, and 6.13, respectively.

Figure 6.14 shows the numerical and experimental DHW outlet and inlet temperature difference of 24-plate PHE and the conical HC combination in eco mode at 7 l/min DHW flow rate.

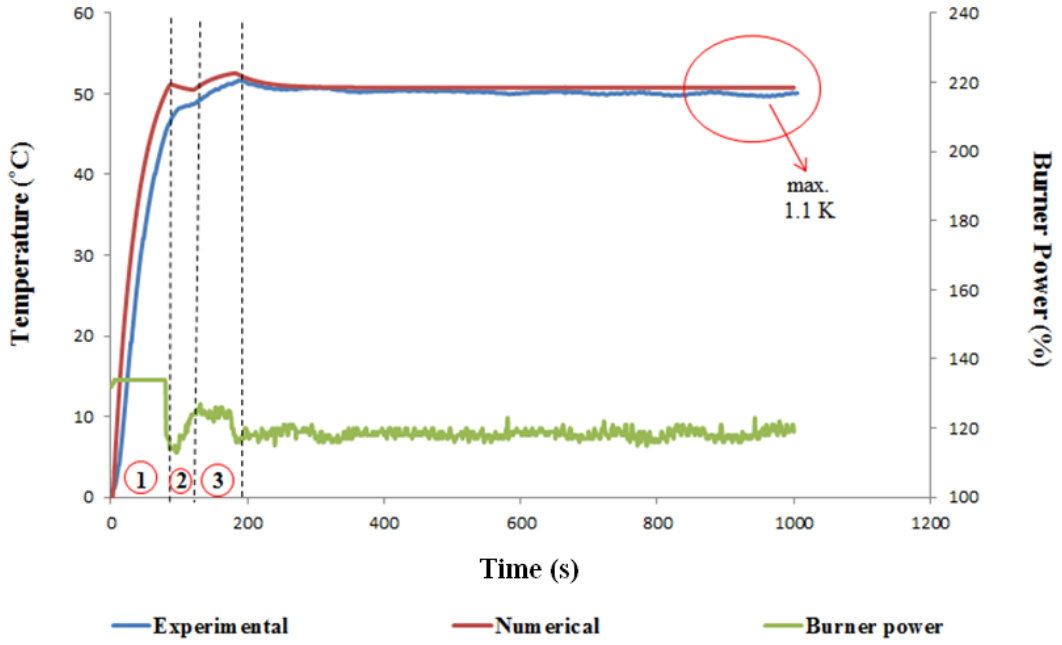

Figure 6.14 Experimental and numerical DHW inlet and outlet temperature difference of the 24-plate PHE and the conical HC combination in eco mode at 7 l/min.

Figure 6.15 shows the numerical and experimental flue gas outlet temperature in eco mode at 8.7 l/min DHW flow rate. In this simulation, there is no power modulation as shown in Figure 6.15. Since the DHW request is at a higher flow rate when compared to previous demands, the appliance operates at constant power. This behavior cannot be predicted actually; they depend on the software of the appliance. In this study, the power of the appliance with respect to time has also been recorded and using these data, simulations have been prepared. Resultantly, it is seen that the numerical calculation algorithm for a standard combi boiler is working properly and gives reasonable results.

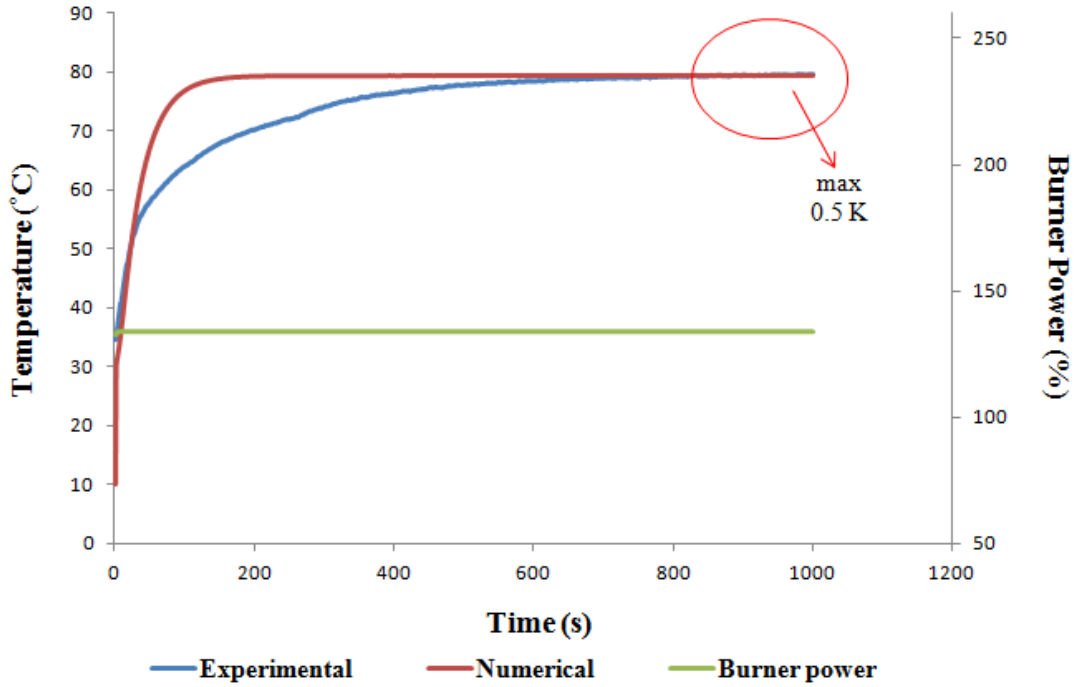

Figure 6.15 Comparison between the numerical and experimental flue gas outlet temperature of 24-plate PHE and the conical HC combination in eco mode at 8.7 l/min DHW flow rate.

As it is shown in Figure 6.15, the closest results to the experimental data for the flue gas outlet temperature have been obtained for this flow rate value. Then, it can be concluded that flue gas outlet temperature could be calculated resulting with more trustable values for higher flow rates of DHW request.

Figure 6.16 shows the numerical and experimental CH water temperature of 24-plate PHE and the conical HC combination at the HC inlet in eco mode at 8.7 l/min DHW flow rate.

Figure 6.17 shows the numerical and experimental CH water temperature of 24-plate PHE and the conical HC combination at the HC outlet in eco mode at 8.7 l/min DHW flow rate.

Figure 6.18 shows the numerical and experimental DHW outlet and inlet temperature difference of 24-plate PHE and the conical HC combination in eco mode at 8.7 l/min DHW flow rate.

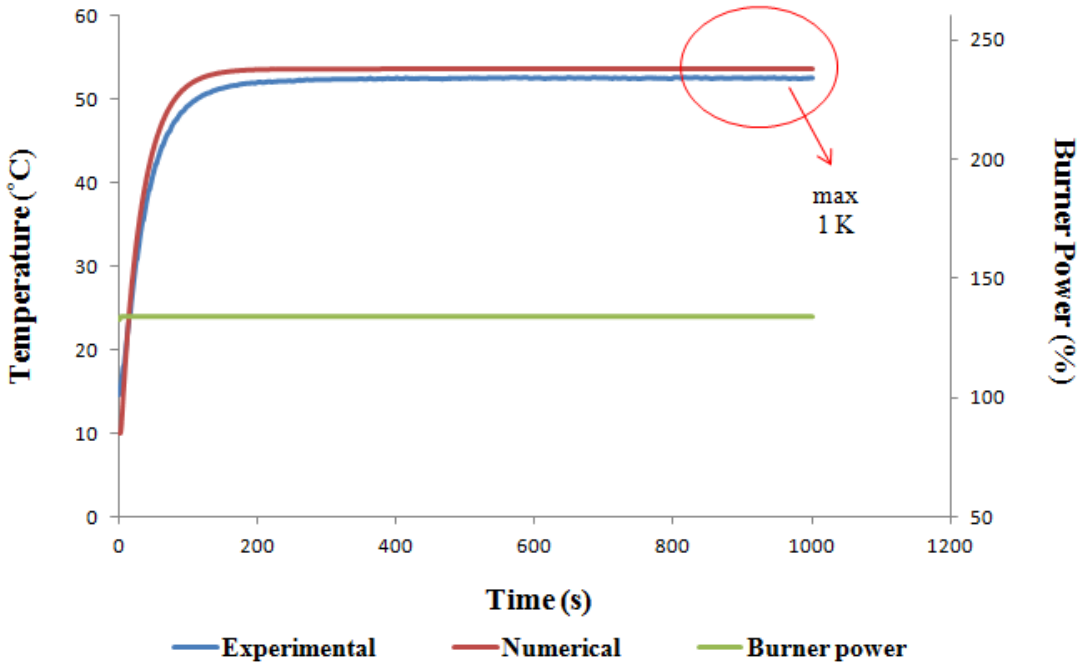

Figure 6.16 Comparison between the numerical and experimental CH water temperature of 24-plate PHE and the conical HC combination at the HC inlet in eco mode at 8.7 l/min DHW flow rate.

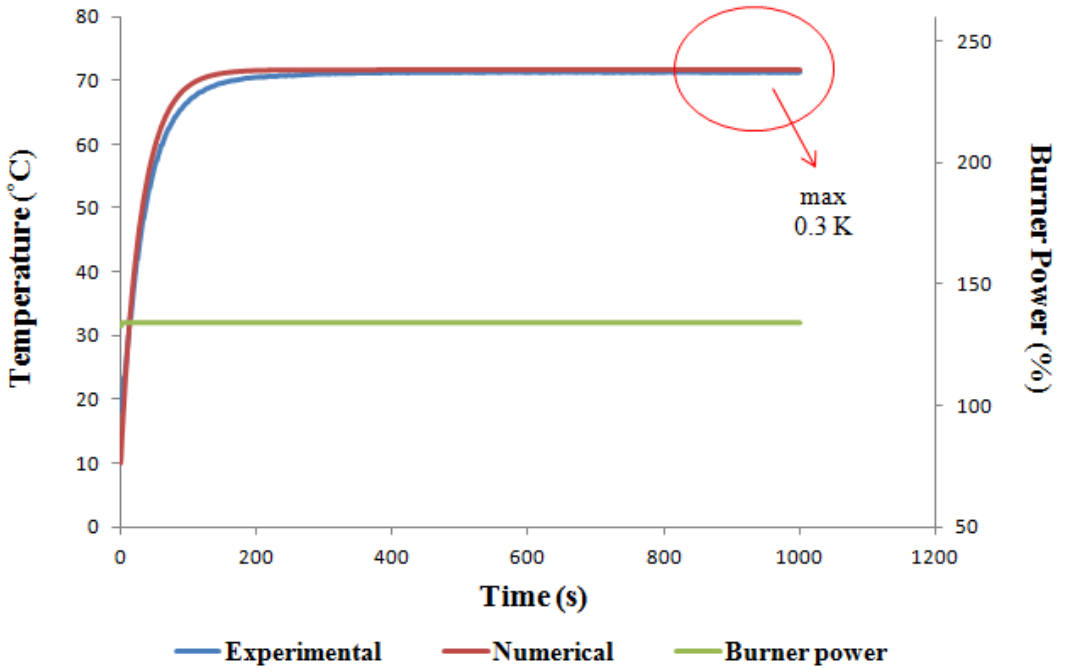

Figure 6.17 Comparison between the numerical and experimental CH water temperature of 24-plate PHE and the conical HC combination at the HC outlet in eco mode at 8.7 l/min DHW flow rate.

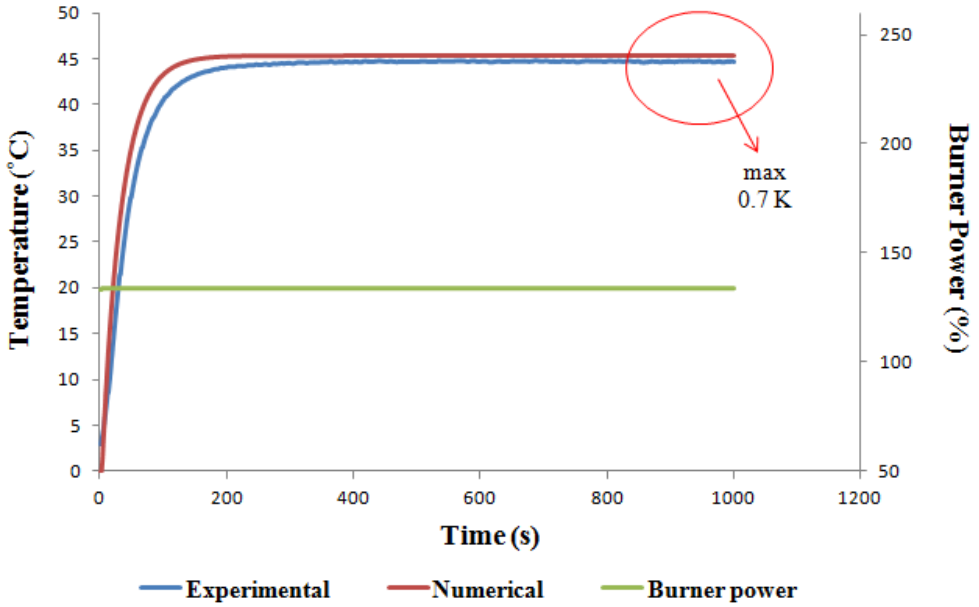

Figure 6.18 Experimental and numerical DHW inlet and outlet temperature difference of the 24-plate PHE and the conical HC combination in eco mode at 8.7 l/min.

Figure 6.19 shows the numerical and experimental DHW outlet and inlet temperature difference of 24-plate PHE and the conical HC combination in comfort mode at 8.7 l/min DHW flow rate.

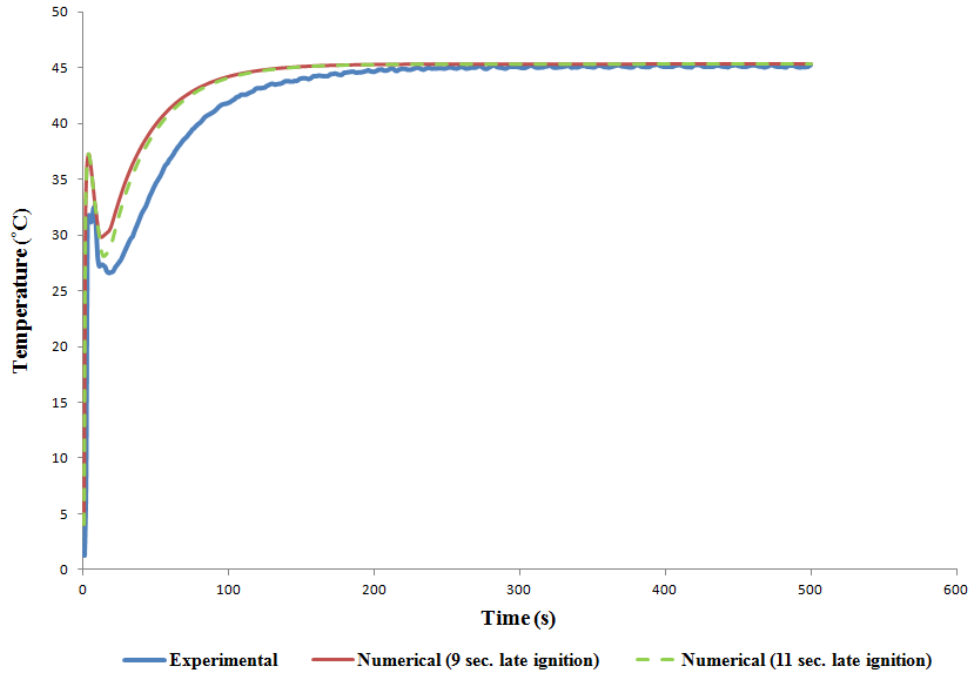

Figure 6.19 Experimental and numerical DHW inlet and outlet temperature difference of the conical HC and 24-plate PHE combination in comfort mode at 8.7 l/min.

Another essential aspect of this study is to observe the experimental and numerical DHW outlet temperature in comfort mode. This part is very difficult to simulate. In a comfort mode, when there is a user demand, the appliance cannot start ignition directly since it has hot water inside. These phenomena are governed by fuzzy logic of the appliance. Then, it is hard for us to predict the appliance behaviour and to see the peaks in DHW outlet temperature. The behaviour of the appliance is tried to be guessed in Figure 6.19 and Figure 6.4. In Figure 6.19, late ignition time effect has been shown on the DHW outlet temperature profile.

Conservation of the energy within the system is also proved for the conical HC and 24-plate PHE combination and for 30 kW heat input as shown in Figure 6.20.

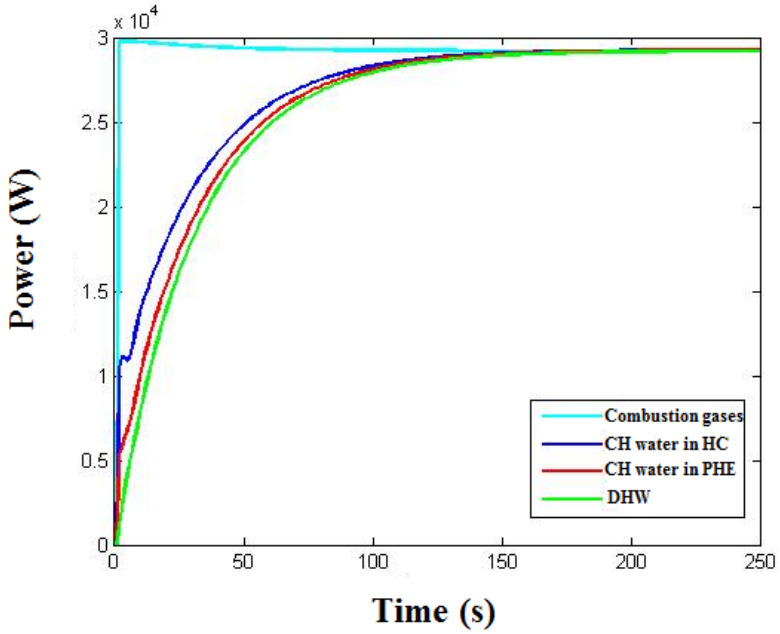

Figure 6.20 Energy transfer rate in the conical HC and 24-plate PHE combination.

Similar to previous combination, stored energy goes to zero while the system becomes steady-state, as shown in Figure 6.21.

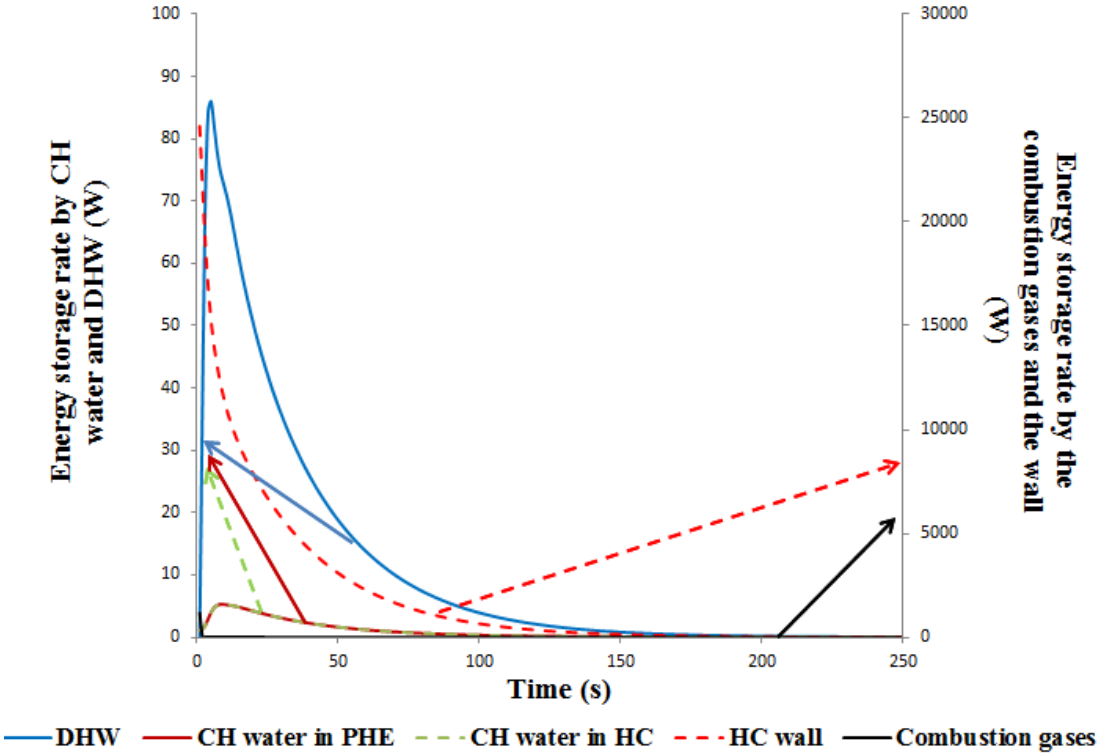

Figure 6.21 Energy storage rate in the components of the conical HC and 24-plate PHE combination at 8.7 l/min.

The numerical results have been verified for different heat exchanger combinations as using same equations just changing the physical values of the parameters. For the flue gas temperature, a very good agreement has been achieved while solving for higher flow rates. However, the results are again satisfactory also for the lower flow rates; at least temperature peaks could be simulated according to the increase and decrease burner power although they are higher when compared to experimental values. As one of the conclusions, measuring and calculating flue gas temperature is a troublesome task.

There is no problem with the other results; all results including the tapping simulation after comfort cycle simulations and calculations of energy balance and storage with respect to time shows that the calculation algorithm is working properly and it can be used to calculate and compare other appliance concept on the theoretical basis.

6.4 Comparison of the Standard Combi Boiler and Primary DHW Concept

In this section the standard combi boiler and the primary DHW concept have been compared in terms of efficiency and the comfort view. DHW outlet temperature of the primary DHW concept has been calculated in eco and comfort mode with a mathematical model created in a similar way of the standard combi boilers. In eco mode, the appliance starts working when it is cold. Figure 6.22 compares the standard combi boiler and primary DHW concept working in the same conditions and eco mode.

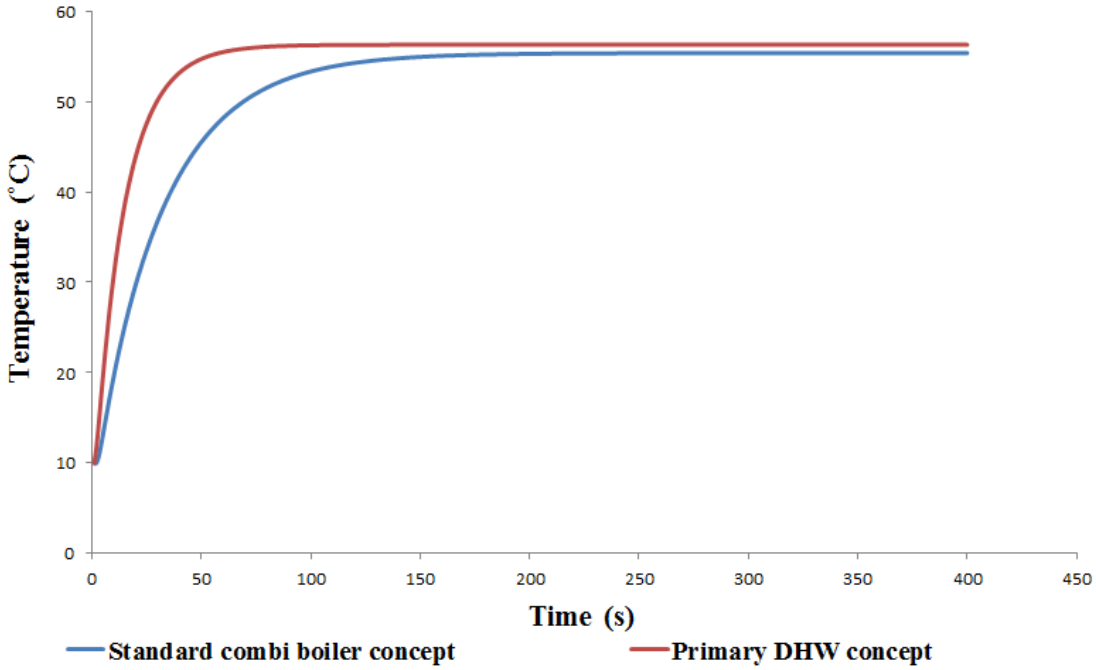

Figure 6.22 Theoretical comparison of the DHW outlet temperature between the primary DHW concept and the standard combi boiler in the eco mode.

Even in eco mode, the primary DHW concept supplies hot water faster compared to the standard combi boiler since the HC is directly used to heat DCW. On the other hand, using only one heat exchanger decreases the thermal inertial effect; thereby lowering the heat retention.

In the comfort mode, the primary DHW concept keeps 60 ˚C DHW inside the HC in case of any user request according to the comparison scenario. Because there is

not a manufactured appliance operating like primary DHW concept; therefore it is only designed and discussed on the paper. To compare it with the standard combi boiler its comfort mode has been built up in a similar way that the standard combi boiler does. In the standard combi boiler concept, it is CH water that is kept for the high comfort level. Figure 6.23 compares the standard combi boiler and primary DHW concept working in the same conditions and eco mode.

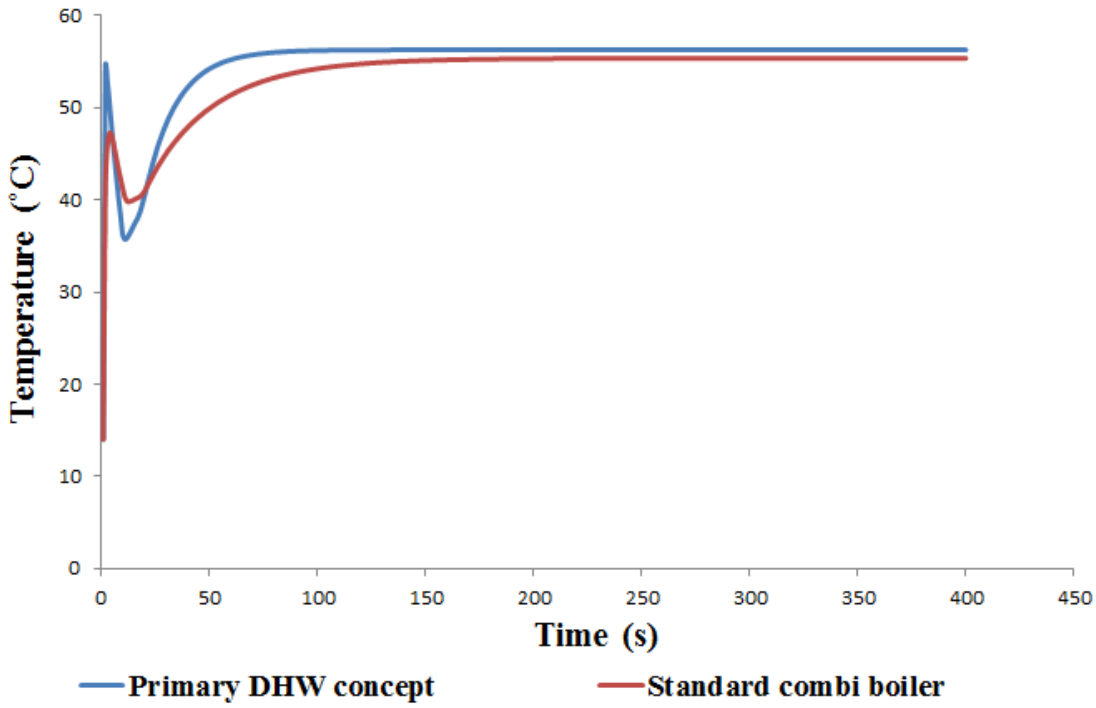

Figure 6.23 Theoretical comparison of the DHW outlet temperature between the primary DHW concept and the standard combi boiler in the comfort mode.

Because of the lower heat retention, DHW outlet temperature decreases in the primary DHW concept more than it does in the standard combi boiler. In other words, late ignition time causes more temperature decrease on the primary DHW concept.

As a result in the primary DHW concept, even in eco mode comfort level is high; but in comfort mode the upper peak increases and the lower peak decreases and it is not a good thing.

From the basic efficiency view, the appliance operates more efficiently in the primary DHW concept. According to the steady-state temperature difference of the appliances, the standard combi boiler operates at 95 % efficiency, whereas the primary DHW concept's efficiency level is 98 %. System losses are decreased due to the usage of single heat exchanger.

Moreover, according to the efficiency tests of the combi boilers (BS EN 13203-2:2006, 2006), mentioned in Chapter 5, efficiency is calculated with respect to the useful and wasted energy defined for each flow rate separately.

A scenario has been created for 8.7 l/min to compare both appliance concept according to theoretical useful and wasted energy view. With detailed explanations, for both of the concepts, the energy is counted as wasted until the difference between DHW inlet and outlet temperature reaches 30 K; meaning that after 30 K temperature difference, the consumed energy will be named as useful.

With reference to the above-mentioned scenario, since primary DHW concept reaches 30 K temperature difference between the DHW inlet and outlet more rapidly as compared to the standard combi boiler, it has a smaller wasted energy/useful energy ratio, 0.362. This ratio is larger in the standard boiler concept, 0.374. A detailed table with the calculation steps about this ratio is given in Appendix B.

As a result, primary DHW concept is superior to the standard combi boiler concept from the view of the wasted energy/useful energy ratio and general efficiency value.

6.5 Parametric Study

As a parametric study part, the common parameters chosen for both of the appliance concepts are as follows: HC wall material, gas volume in the HC, water volume around the HC, and the inlet temperature of the DCW.

The effects of all changes have been shown on the DHW outlet temperature, HC wall, and the flue gas outlet temperature for both appliance concepts.

First parametric change is on the HC material. The proposed types of the HC material are given in Table 6.1. The density change of the types and the resultant mass increase while keeping the volume constant is shown in Table 6.1.

Table 6.1 HC materials used for comparison for both of the appliance concept.

HC wall material	Density (kg/m^3)	Mass (kg)
Pure Aluminum	2702	8.5
Aluminum alloy (Alloy 2024-T6, 4.5 % Cu, 1.5 % Mg, 0.6 % Mn)	2770	8.7
Carbon steels-plain carbon (Mn≤1%, Si≤0.1%)	7854	24.7

Figure 6.24 shows the effect of another aluminum alloy (Alloy 2024-T6, 4.5 % Cu, 1.5 % Mg, 0.6 % Mn), and carbon steels-plain carbon (Mn≤1%, Si≤0.1%) on the DHW outlet temperature. These materials are alternatively suggested to pure aluminum used previously for the HC material of the standard combi boiler model.

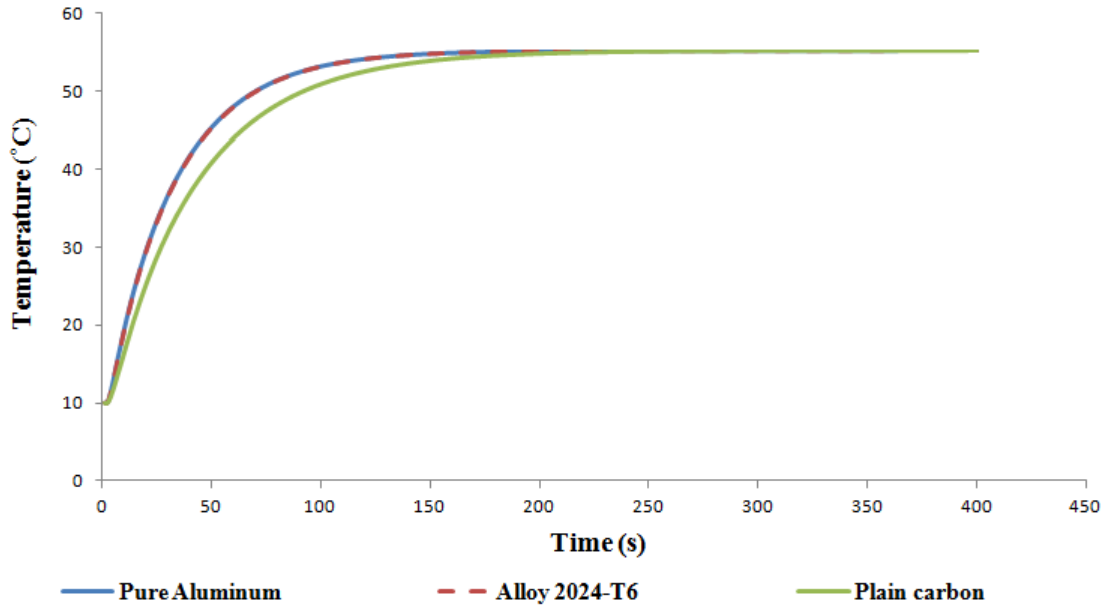

Figure 6.24 Effect of different HC wall materials on DHW outlet temperature of the standard combi boiler concept.

Figure 6.25 shows the effects of using the different materials for the HC on the flue gas outlet temperature of a standard combi boiler.

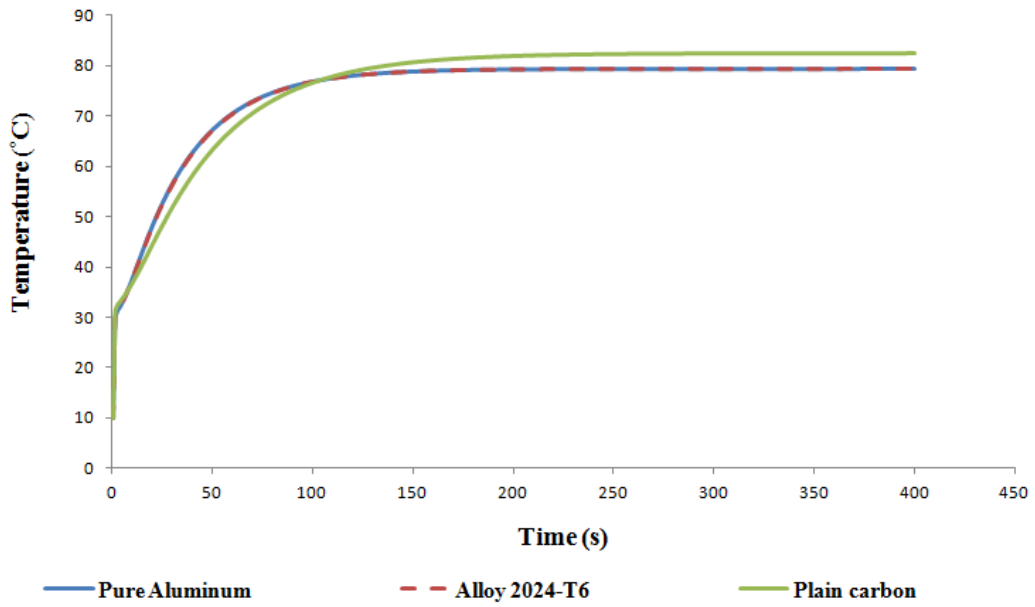

Figure 6.25 Effect of different HC materials on flue gas outlet temperature of the standard combi boiler concept.

Figure 6.26 shows the effects of using different materials for the HC on the wall temperature of a standard combi boiler.

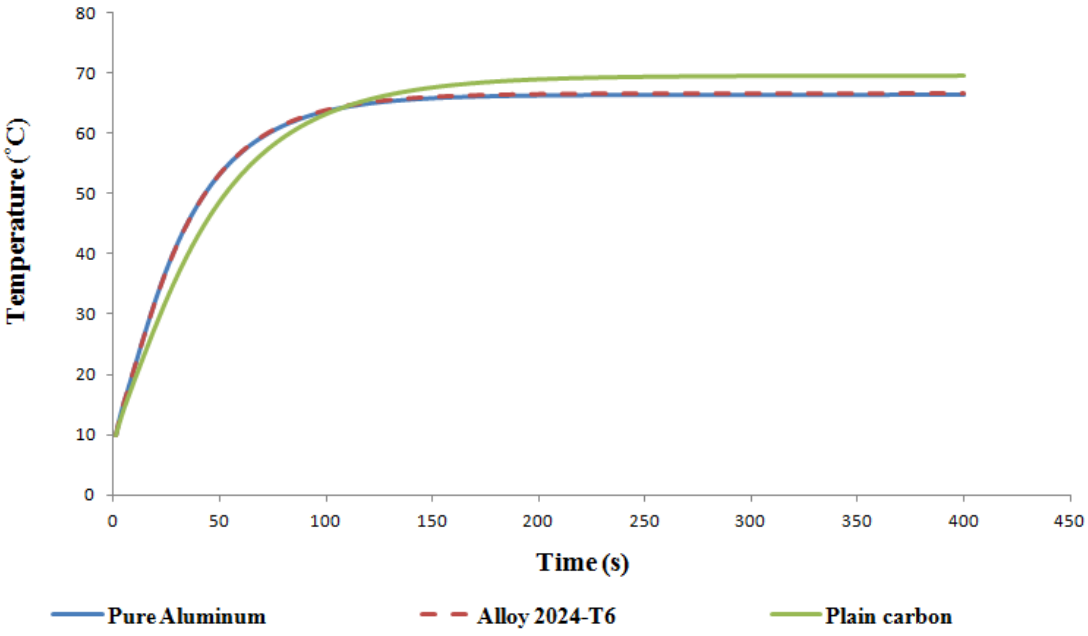

Figure 6.26 Effect of different HC wall materials on the wall temperature of the standard combi boiler.

Since steel has a lower specific heat when compared to the Aluminum alloy and the pure Aluminum, the wall temperature and the flue gas outlet temperature have higher values in Carbon steel for both of the appliance concept.

Figure 6.27 shows the effects of using different materials for the HC on the DHW outlet temperature of a primary DHW concept.

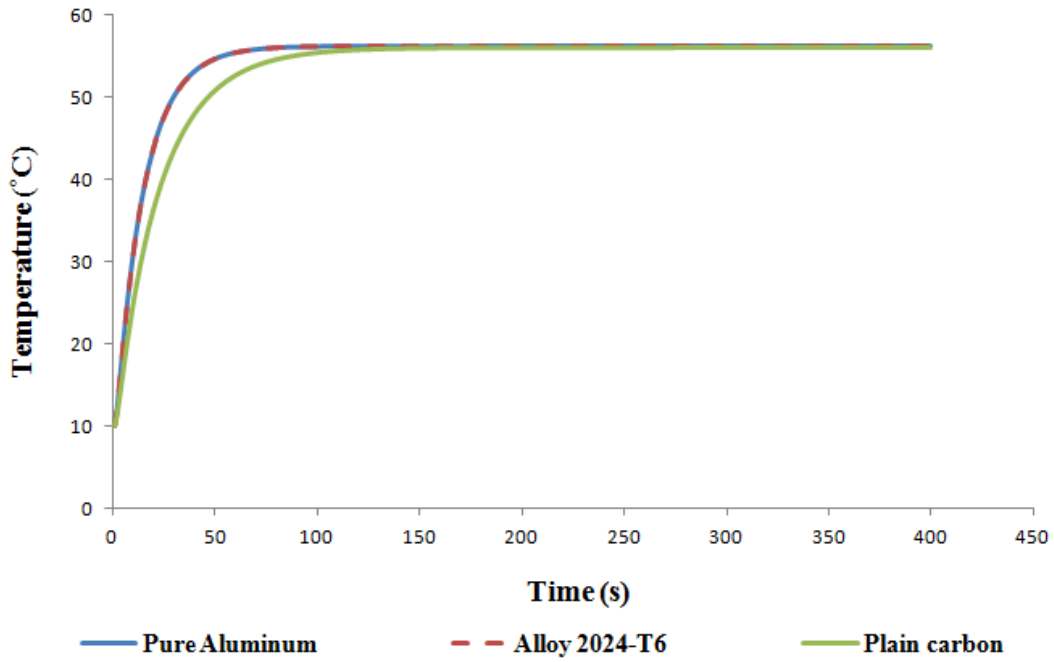

Figure 6.27 Effect of different HC wall materials on DHW outlet temperature of the primary DHW concept.

Figure 6.28 shows the effects of using different materials for the HC on the flue gas outlet temperature of a primary DHW concept.

Figure 6.29shows the effects of using different materials for the HC on the wall temperature of of a primary DHW concept.

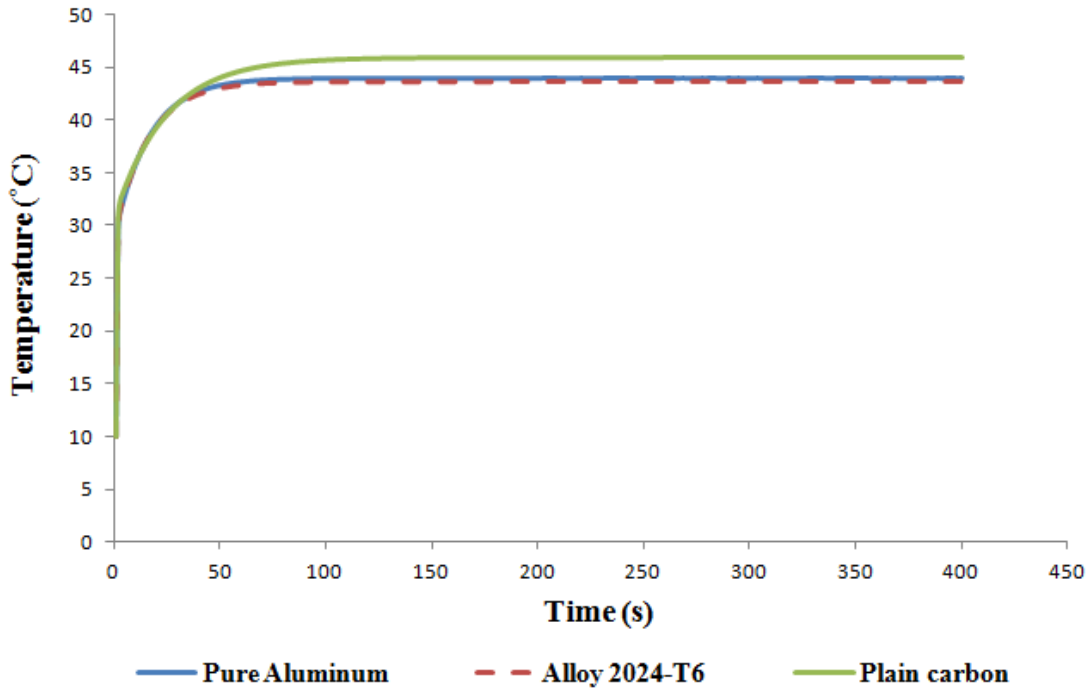

Figure 6.28 Effect of different HC materials on flue gas outlet temperature of the primary DHW concept.

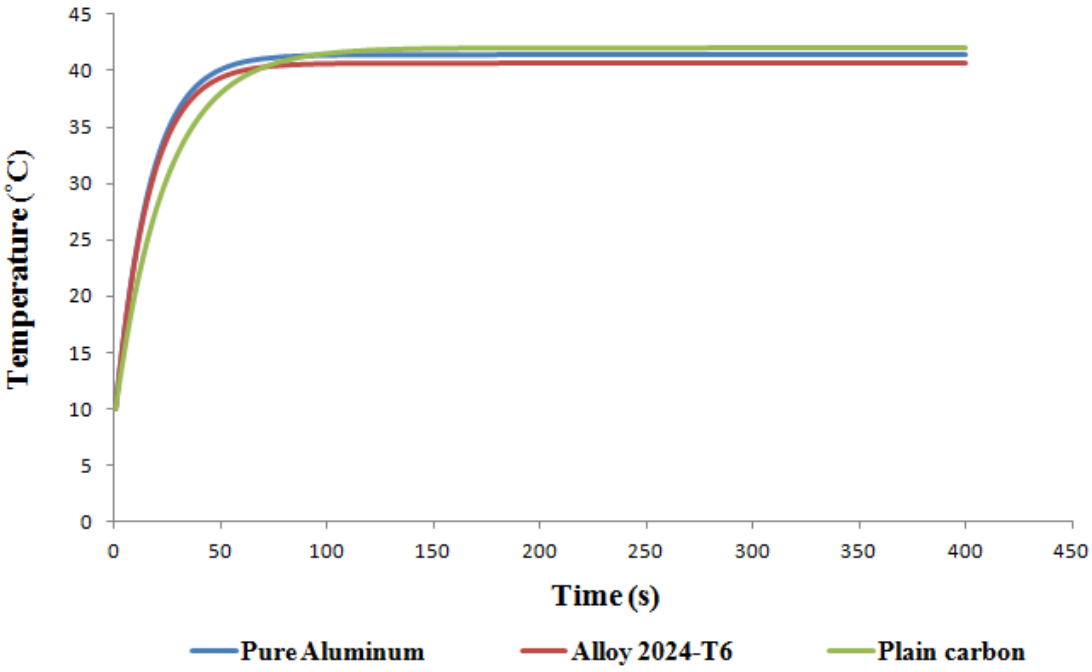

Figure 6.29 Effect of different HC wall materials on the wall temperature of the primary DHW concept.

As a result, for the same volume, since the density is higher in the plain carbon, heat cell mass increases. Additionally thermal conductivity decreases. Then, DHW temperature profile is affected adversely in terms of the transient region for both of the appliance concept.

Pure Al and the mentioned Al alloy (Alloy 2024-T6) have similar properties; therefore there is no noticeable difference between them. Consequently, it is better to use kind of Al alloy as the heat cell wall material for both of the concept for shorter transient region when compared to the carbon steel.

Second parametric study is on the mass of the water around the HC; it is changed by increasing or decreasing the water channel depth. If it is decreased or increased HC mass is also changed; but this amount is ignorable. The most important effect is if it is decreased, the convective heat transfer of the water increased, or the vice versa.

Table 6.2 shows the physical values of the hydraulic diameter, water volume capacity, HC mass, and convective heat transfer coefficient of the water around the HC when the water depth is increased or decreased for the standard combi boiler.

Table 6.2 Resultant changes for different water channel depths in the standard combi boilers.

Water channel depth (mm)	**Hydraulic diameter (mm)**	**Water volume capacity (m^3)**	**HC mass (kg)**	**Convective heat transfer coefficient of the water (W/m^2K)**
6.8	10.9	0.7796	8.4683	16198
7.3	11.5	0.8370	8.5	14632
7.8	12.2	0.8943	8.5317	13326
8.3	12.7	0.9516	8.5634	12221

As shown in Table 6.2, the mass change is negligible. Although, the change in the mass is very little, they have been added to the mathematical model.

A similar table is given in Table 6.3 for the primary DHW concept.

Table 6.3 Resultant changes for different water channel depths in the primary DHW concept.

Water channel depth (mm)	Hydraulic diameter (mm)	Water volume capacity (m^3)	HC mass (kg)	Convective heat transfer coefficient of the water (W/m^2K)
6.8	10.9	0.7796	8.4683	7716
7.3	11.5	0.8370	8.5	6970
7.8	12.2	0.8943	8.5317	6348
8.3	12.7	0.9516	8.5634	5822

Figure 6.30 shows the effects of different water channel depths on the DHW outlet temperature of the standard combi boiler.

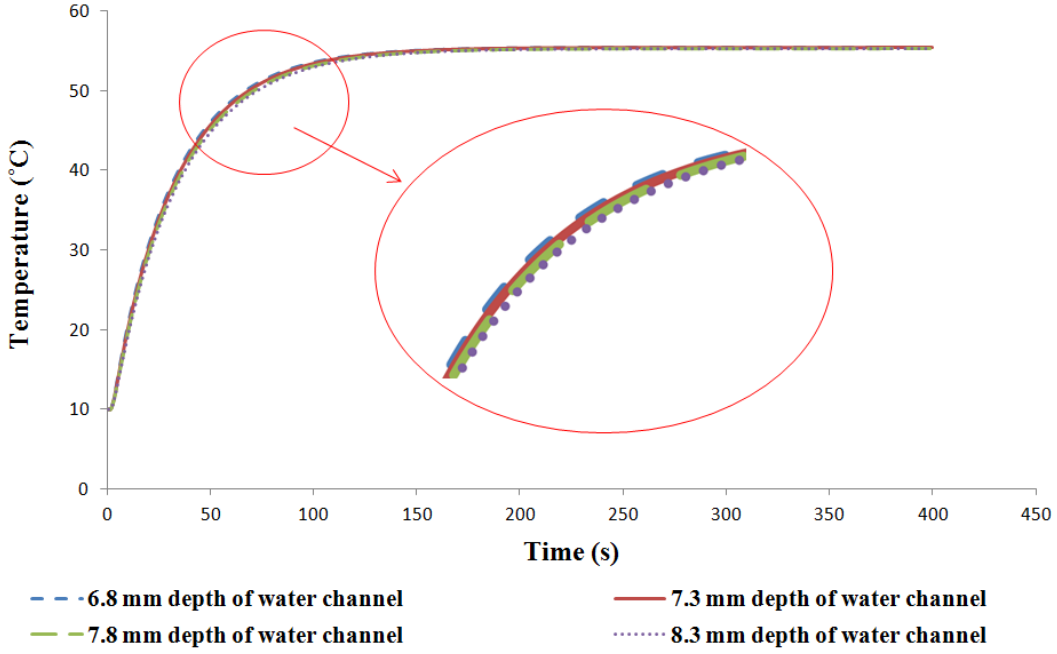

Figure 6.30 Effects of different water channel depths on the DHW outlet temperature of the standard combi boiler.

Figure 6.31 shows the effects of different water channel depths on the flue gas outlet temperature of the standard combi boiler.

Figure 6.32 shows the effects of different water channel depths on the wall temperature of the standard combi boiler.

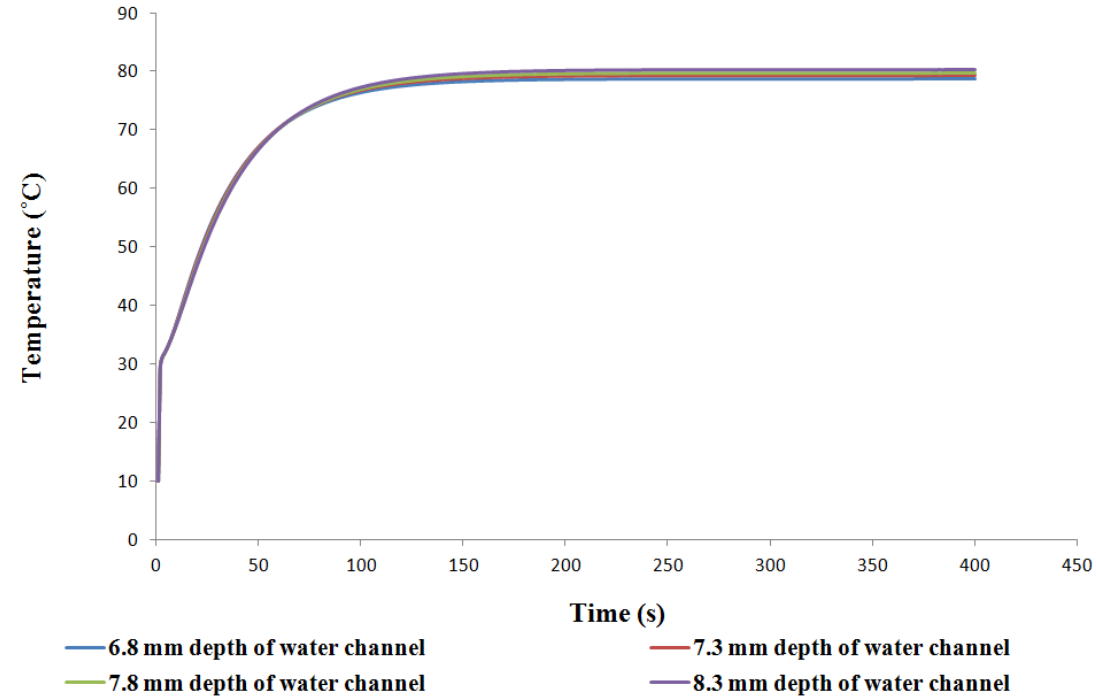

Figure 6.31 Effects of different water channel depths on the flue gas outlet temperature of the standard combi boiler.

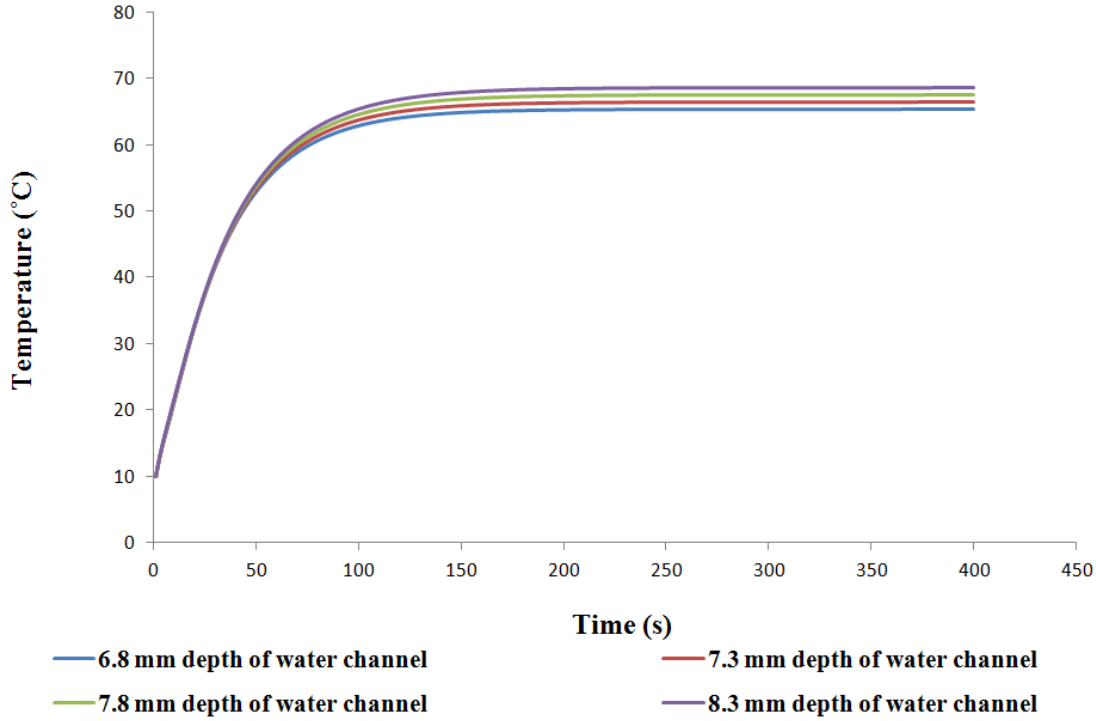

Figure 6.32 Effects of different water channel depths on the flue wall temperature of the standard combi boiler.

As it is shown in the previous figures, the change in the water volume does not have any significant effects on both steady-state temperature profile and duration of the transient region.

Figure 6.33 shows the effects of different water channel depths on the DHW outlet temperature of the primary DHW concept.

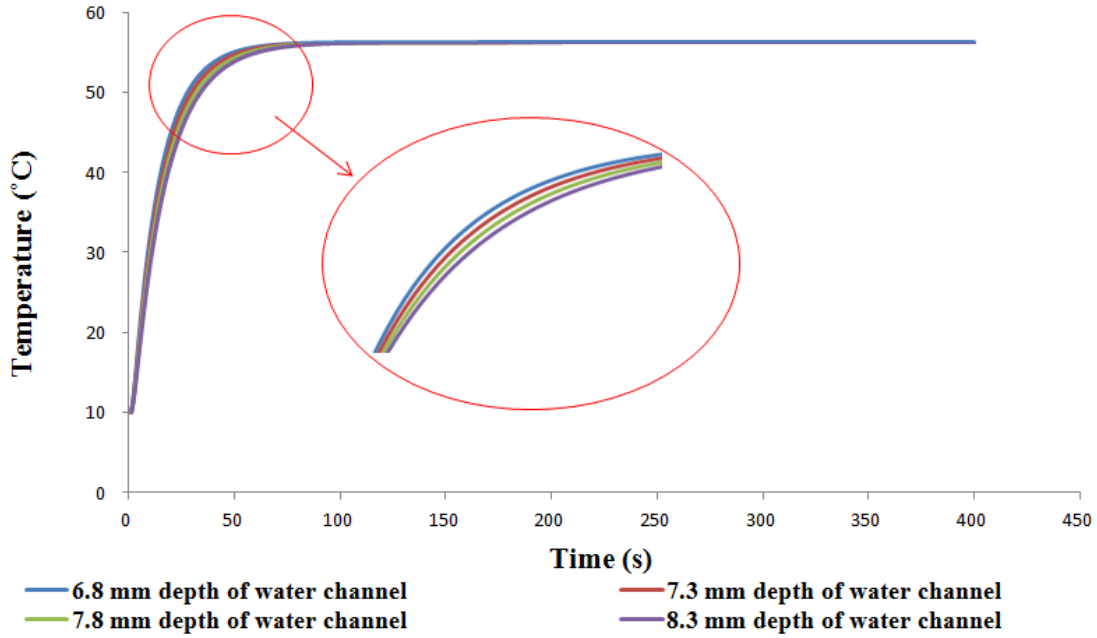

Figure 6.33 Effects of different water channel depths on the DHW outlet temperature of the primary DHW concept.

Figure 6.34 shows the effects of different water channel depths on the flue gas outlet temperature of the primary DHW concept.

Figure 6.35 shows the effects of different water channel depths on the wall temperature of the primary DHW concept.

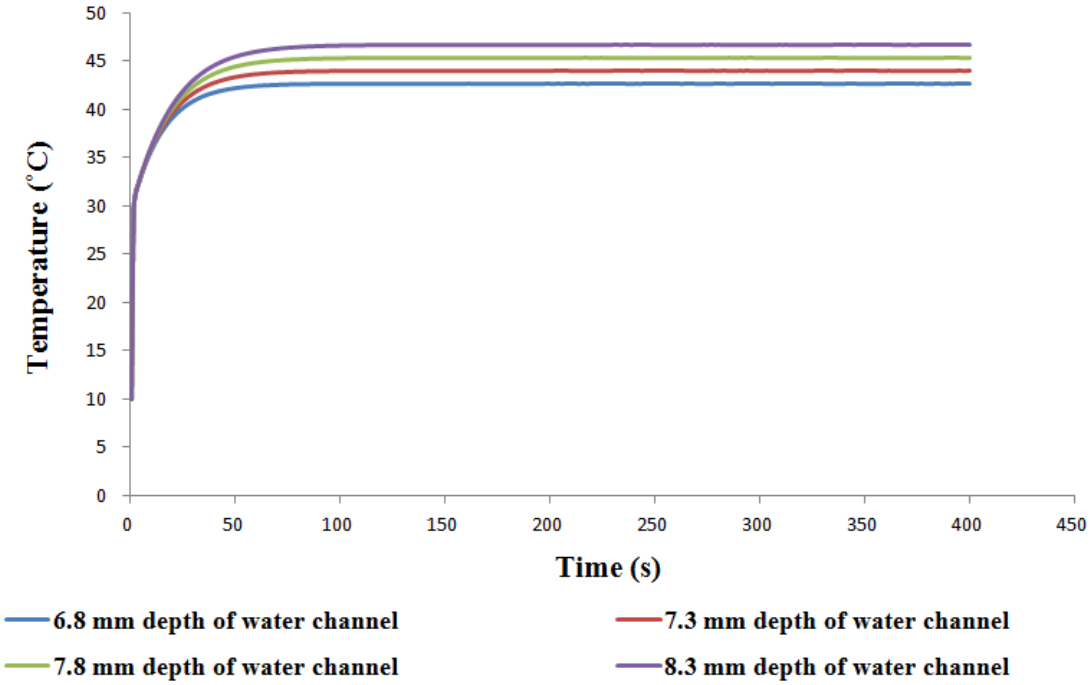

Figure 6.34 Effects of different water channel depths on the flue gas outlet temperature of the primary DHW concept.

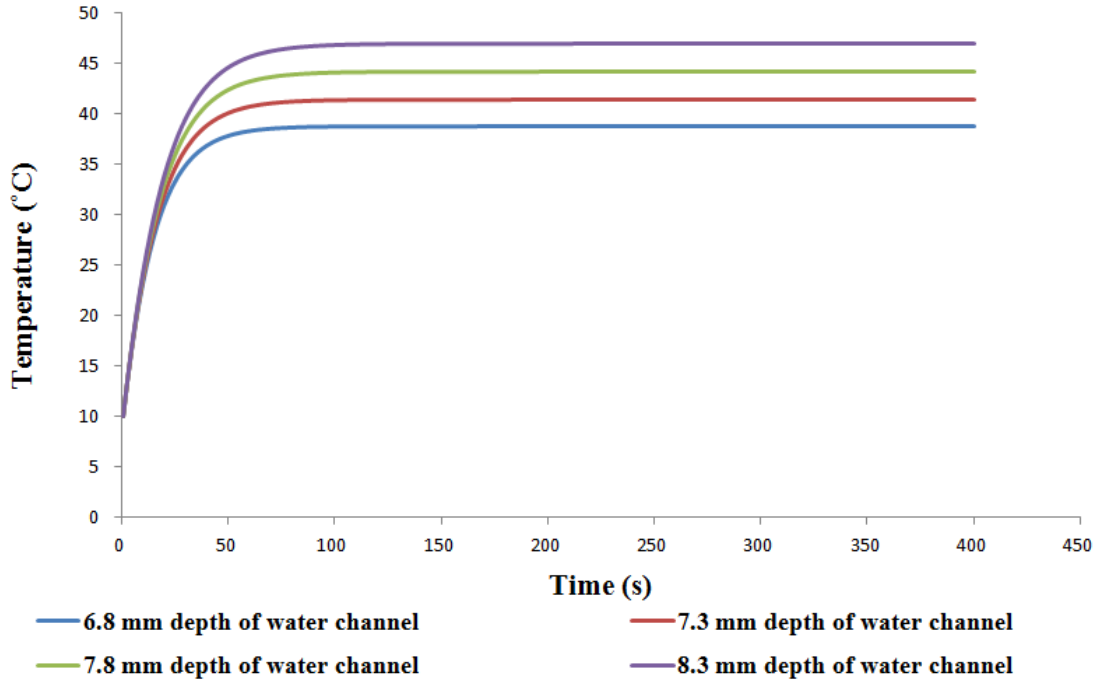

Figure 6.35 Effects of different water channel depths on the wall temperature of the primary DHW concept.

As seen in Figures 6.30- 6.35, for smaller depths, since convective heat transfer coefficient is increased, the heat transfer is also faster. The primary DHW concept is much more affected by the change of the water depth since DHW is directly heated there.

The third parametric study is about the change in the gas volume. Gas volume inside the HC has been increased by decreasing the diameters of the pin fins 1 mm and 2 mm. As a result, the mass of the HC and the convective heat transfer coefficient of the combustion gases decreases for both of the appliance concept.

As shown in the below-given figures, DHW outlet temperature decreases as a result of the decrease in the convective heat transfer coefficient in all appliance concepts.

Table 6.4 shows the changes in the heat transfer coefficient of the flue gas and heat cell mass as a result of decrease in the diameters of the pin fins.

Table 6.4 Resultant changes for different diameters of the pin fins in both of the appliance concept.

Pin fin diameter (mm)	**HC mass (kg)**	**Convective heat transfer coefficient of the gas (W/m^2K)**	**Gas volume (m^3)**	**Internal heat transfer area (m^2)**
11	8.5	113.4	0.0008	0.64
10	7.6	86.6	0.0012	0.56
9	6.8	70.6	0.0015	0.49

According to the flow channel model between the pin fins shown in Figure 4.15, since hydraulic diameter where the flue gas flows increases as the fin diameter is decreased, convective heat transfer coefficient of the flue gas decreases. Furthermore, since there is huge number of pin fins inside the HC, the diameter decrease causes a considerable mass decrease of the HC.

Figure 6.36 shows the effects of the diameter of the pin fins on the DHW outlet temperature of the standard combi boiler.

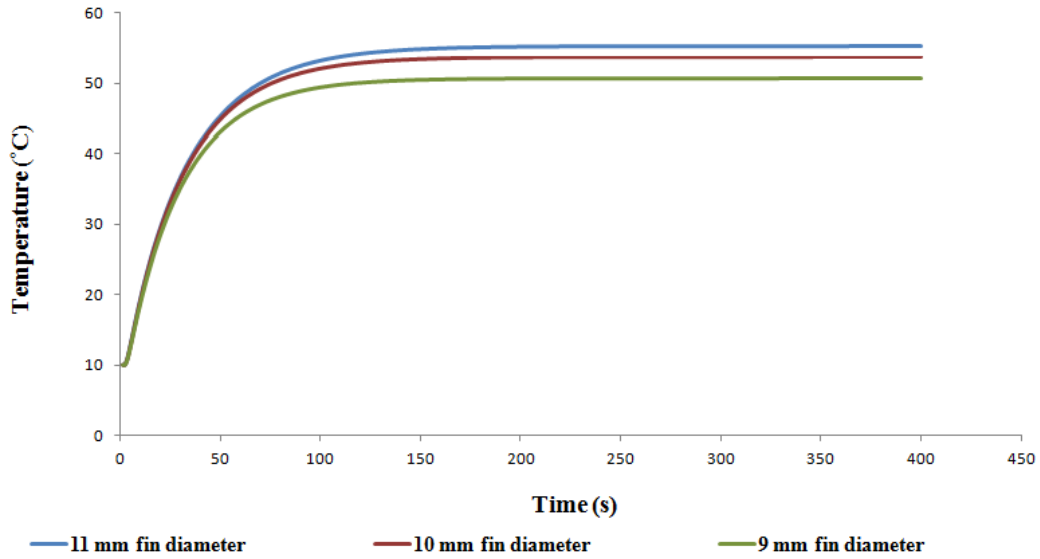

Figure 6.36 Effects of the diameter of the pin fins on the DHW outlet temperature of the standard combi boiler.

Figure 6.37 shows the effects of the diameter of the pin fins on the flue gas outlet temperature of the standard combi boiler.

Figure 6.38 shows the effects of the diameter of the pin fins on the flue gas outlet temperature of the standard combi boiler.

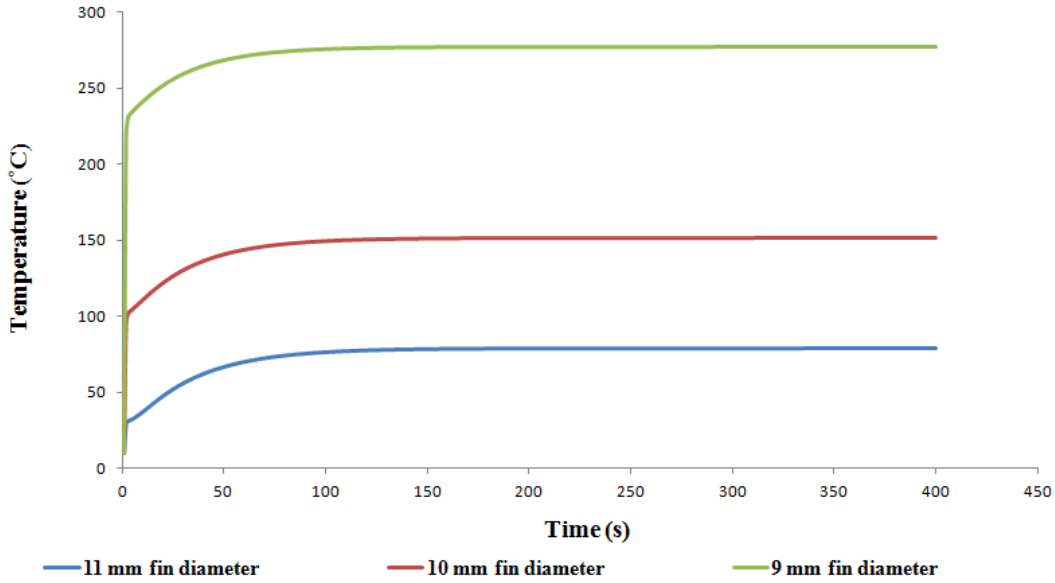

Figure 6.37 Effects of the diameter of the pin fins on the flue gas outlet temperature of the standard combi boiler.

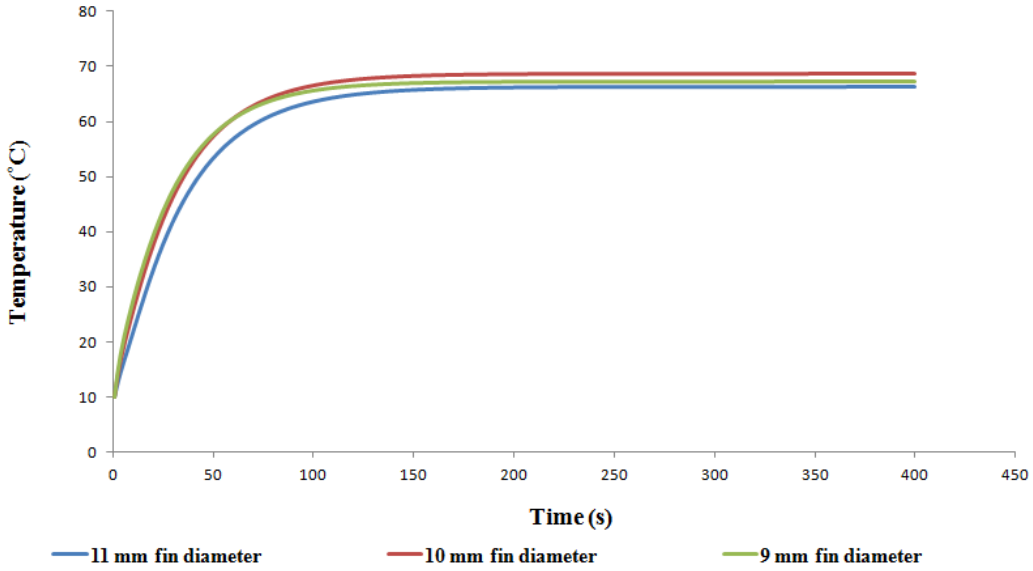

Figure 6.38 Effects of the diameter of the pin fins on the wall temperature of the standard combi boiler.

Figure 6.39 shows the effects of the diameter of the pin fins on the DHW outlet temperature of the primary DHW concept.

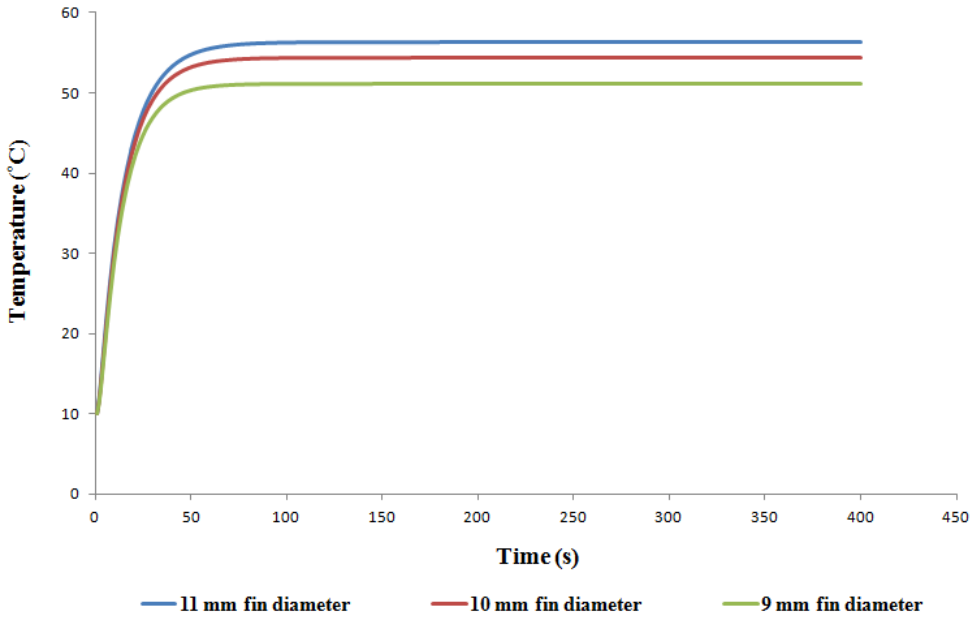

Figure 6.39 Effects of the diameter of the pin fins on the DHW outlet temperature of the primary DHW concept.

Figure 6.40 shows the effects of the diameter of the pin fins on the flue gas outlet temperature of the primary DHW concept.

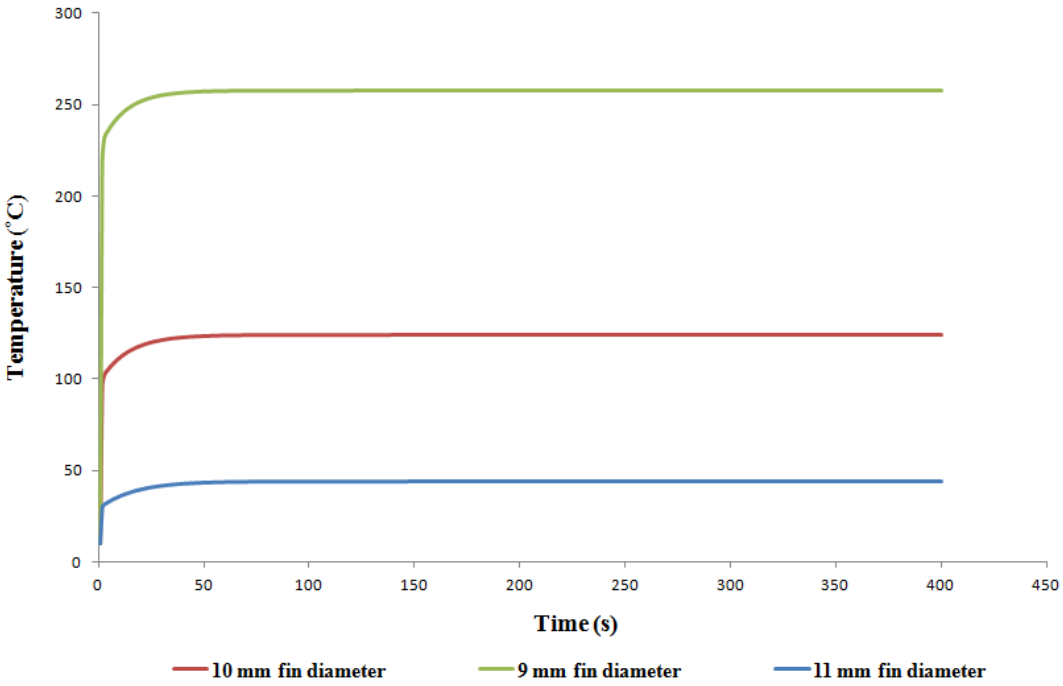

Figure 6.40 Effects of the diameter of the pin fins on the flue gas outlet temperature of the primary DHW concept.

Figure 6.41 shows the effects of the diameter of the pin fins on the wall temperature of the primary DHW concept.

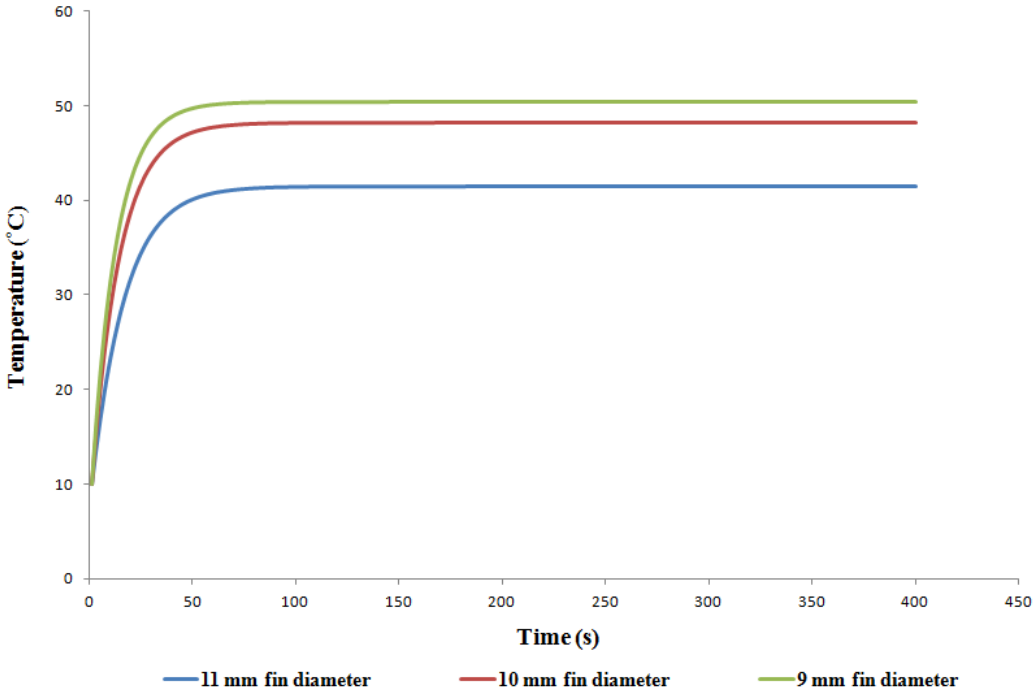

Figure 6.41 Effects of the diameter of the pin fins on the wall temperature of the primary DHW concept.

The effects of the inlet temperatures on the DHW outlet temperature are shown in the Figure 6.42 for the standard combi boiler. Then, Figure 6.43 shows the effects of the DCW inlet temperature on the flue gas outlet temperature of the standard combi boiler.

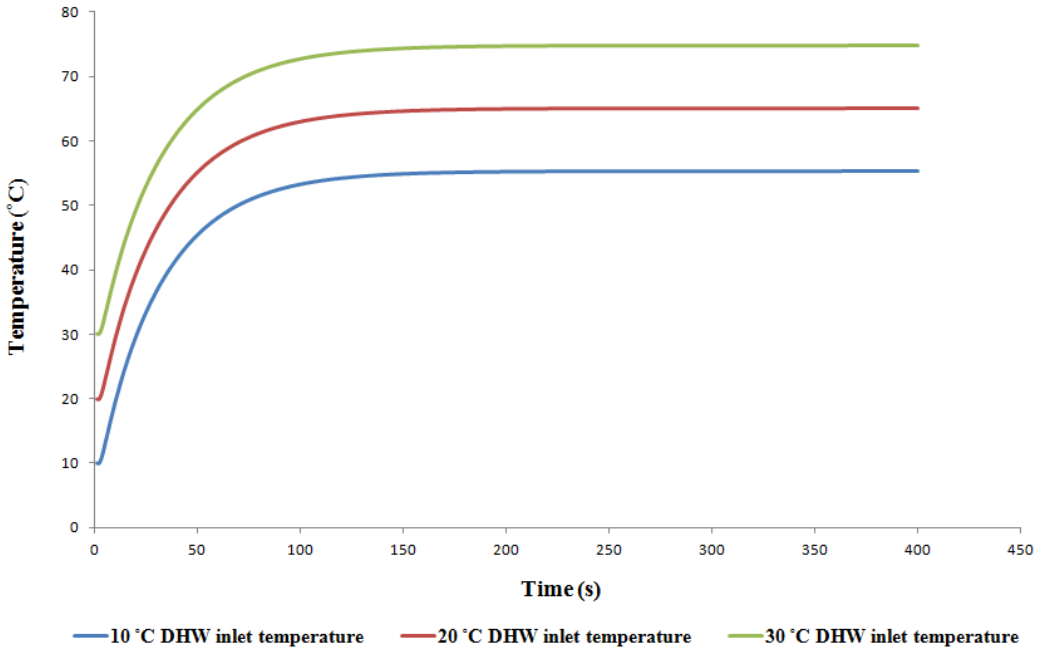

Figure 6.42 Effects of the inlet temperature of the DCW on the DHW outlet temperature for the standard combi boiler.

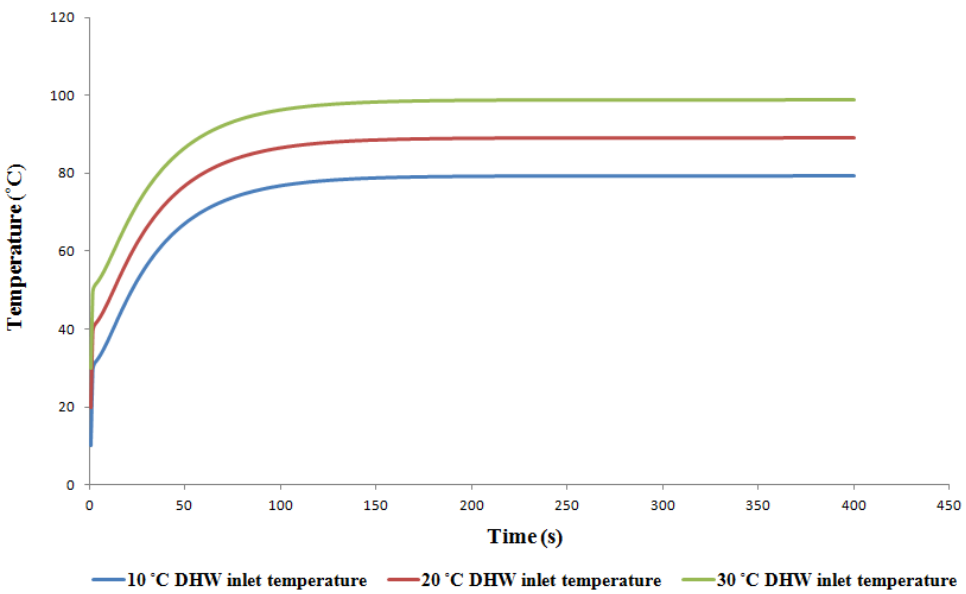

Figure 6.43 Effects of the inlet temperature of the DCW on the flue gas outlet temperature for the standard combi boiler

Figure 6.44 shows the effects of the DCW inlet temperature on the wall temperature of the standard combi boiler.

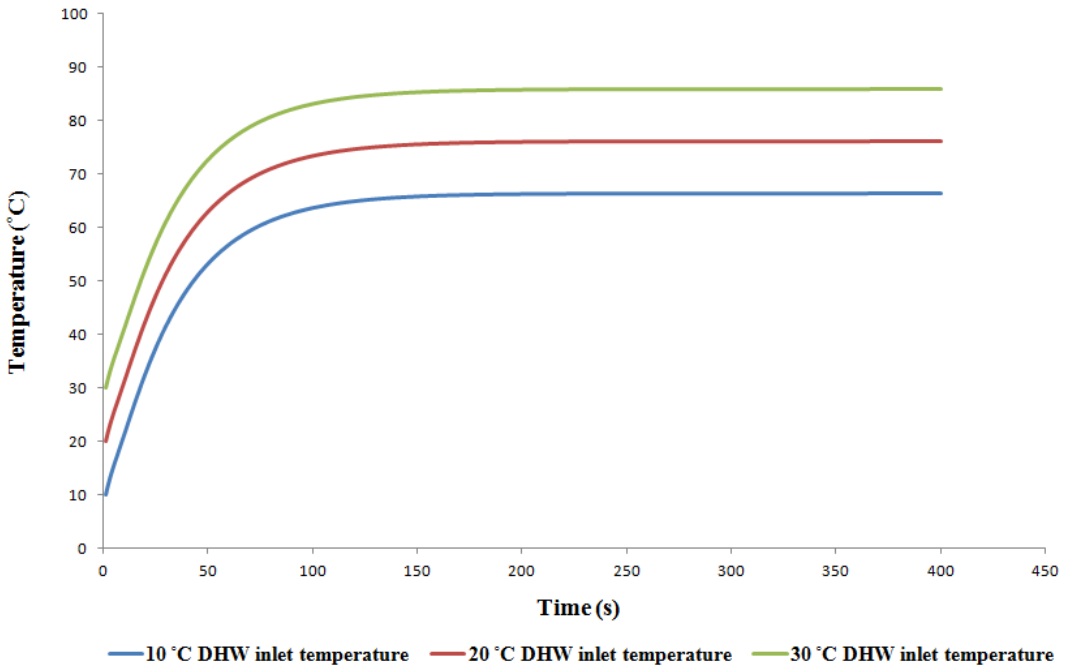

Figure 6.44 Effects of the inlet temperature of the DCW on the wall temperature for the standard combi boiler.

Figure 6.45 shows the effects of the DCW inlet temperature on the DHW outlet temperature of the primary DHW concept.

Figure 6.46 shows the effects of the DCW inlet temperature on the flue gas outlet temperature of the primary DHW concept.

Figure 6.47 shows the effects of the DCW inlet temperature on the wall temperature of the primary DHW concept.

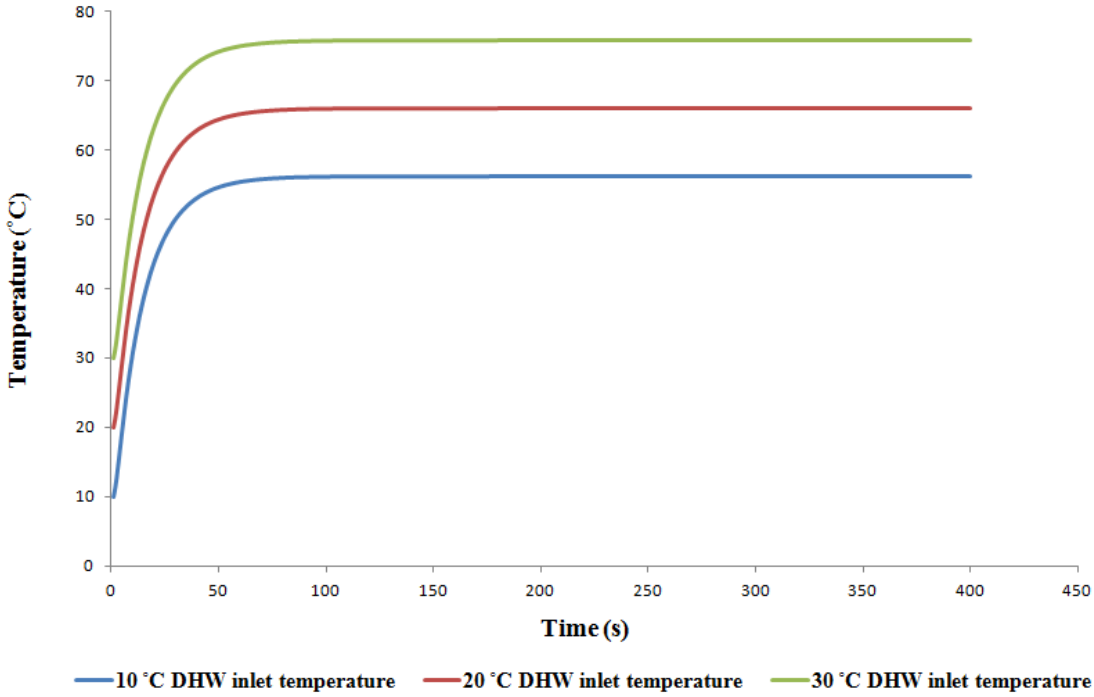

Figure 6.45 Effects of the inlet temperature of the DCW on the DHW outlet temperature for the primary DHW concept.

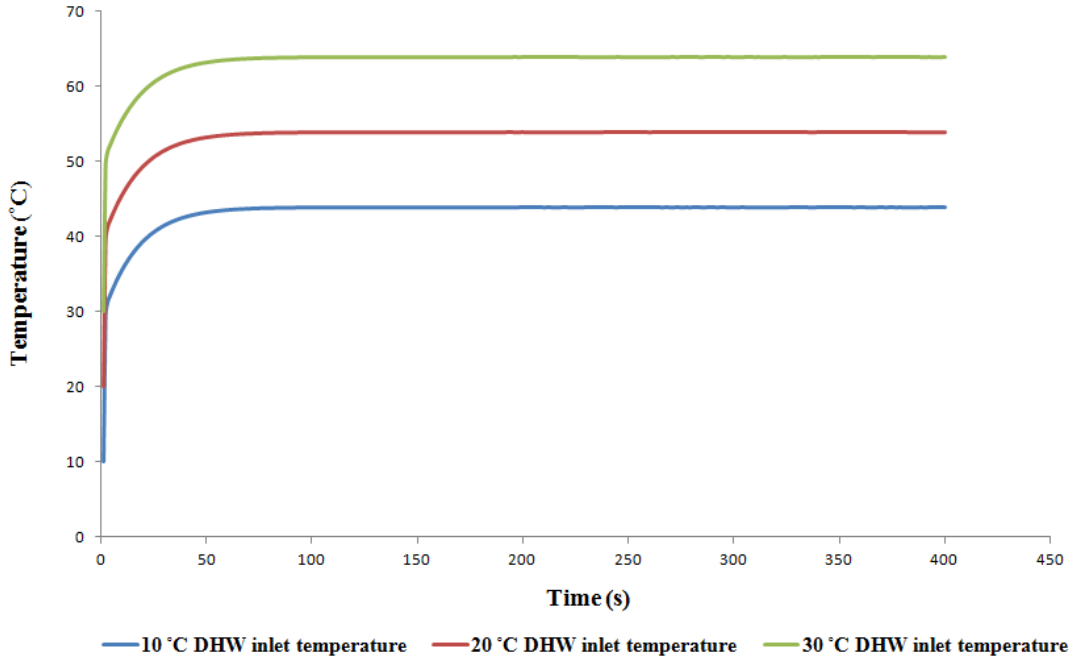

Figure 6.46 Effects of the inlet temperature of the DCW on the flue gas outlet temperature for the primary DHW concept.

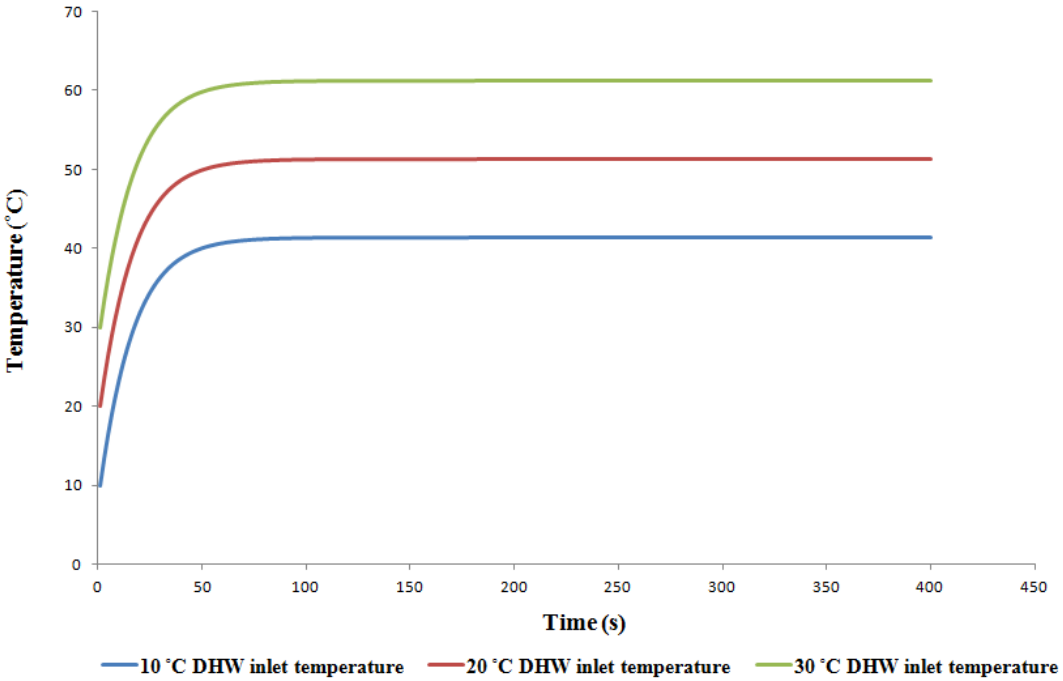

Figure 6.47 Effects of the DCW inlet temperature on the wall temperature of the primary DHW concept.

CHAPTER SEVEN
CONCLUSIONS

In conclusion, after taking everything into consideration, a good agreement is achieved between the numerical and experimental results for both of the heat exchanger combinations (rectangular HC and 26-plate PHE; conical HC 24-plate PHE).

Moreover, conical HC and 24-plate PHE combination has been verified for various flow rates comparing experimental and numerical CH inlet and outlet temperatures, flue gas temperature and inlet and outlet temperature difference of the DHW for the standard combi boiler. Only flue gas outlet temperature has not shown a good agreement for lower flow rates of DHW requirements. However, the calculation algorithm could be used to predict flue gas temperature broadly even in lower flow rates of DHW. All other comparisons have resulted in a very satisfactory consistency. Hence, a calculation algorithm has been obtained for DHW supply function of the combi boiler type heating appliances. Furthermore, power modulation according to the flow rates have been added to the some of the simulations.

The most important part is the verification of the numerical values with the experimental values in comfort working mode. This simulation is also a general representation of one part of the comfort tests according to which the appliances' comfort levels are declared. This test is called as "Waiting Time Test". In this test, it is important to observe the upper and lower peak points and the time interval between the them. According to the measured temperature peak points and the time interval between them, the appliance gets a grade from this test. Since operating the appliance after comfort mode represents "Waiting Time Test", simulation of one of the comfort tests has been also achieved.

As mentioned before, the ignition time cannot easily be predicted when the appliance is hot (keeping hot CH water in the system). Ignition start time is highly dependent upon the software of the appliances and a kind of characteristic property

of the appliances. The temperature of DHW dramatically increases as a result of the hot CH water kept within the system in the comfort working mode. Nevertheless, the appliance cannot directly start ignition because of the logic of the appliance when it is hot. Therefore, DHW outlet temperature starts to decrease till appliance starts ignition. All of these parameters, i.e. ignition time, CH temperature in the system have an important effect on the waiting time test and thus comfort level of the appliance. Using this algorithm, the resultant effects of these kinds of parametric changes can be predicted with the theoretical calculations.

Additionally, two appliance concepts have been compared in terms of comfort and efficiency view. Similar to these comparisons, any design concept or parametric changes could easily be evaluated avoiding the cost of the prototypes of trial-and-error phases.

In this study, only the standard combi boiler and the primary DHW concept have been compared in terms of efficiency and comfort. A similar comfort scenario has been created for the primary DHW concept. In eco mode simulations, when both of the systems start working at the same conditions, the transient region is smaller in primary DHW concept. It is an advantage over the standard combi boilers. In the comfort working mode comparisons of these two appliances, the lower and upper peaks of the DHW outlet temperature profile have been compared. In the comfort mode simulations, upper peak is higher in the primary DHW concept since ready-to-use hot water is kept directly in the HC for higher comfort level. In the standard combi boiler, for higher comfort level, hot CH water is kept in the HC to heat DCW in case a user demand is created. Because of the types of hot water kept in the HC, the upper peak is higher in the primary DHW concept. On the other hand, the lower peak decreases more in this concept since there is only one component resulting in less heat retention. Higher upper peak is not a preferred thing since the user may get very high temperature hot water than the set temperature. It also decreases the comfort level causing damages for the users. Also, if the lower peak on the DHW outlet temperature plot decreases more, the user may feel colder and wait more to get the temperature of the set point.

As efficiency comparison of these both concepts, the primary DHW concept as higher efficiency values since system losses decreases due to the single component. In this investigation, there is another efficiency approach similar to the international standards (BS EN 13203-2:2006, 2006) as useful wasted energy/useful energy ratio. Since DHW temperature increases fast in the primary DHW concept, this ratio is smaller; but both concepts have values very close to each other thereby resulting in 0.01 difference between them.

With these simulations, it will be possible to compare directly the effects of the system parameters on the appliances and calculate the results of the planned changes on the comfort level of the appliances after simulating all six comfort tests. Comfort tests take too much time especially at the design phases of the appliances. Using this practical mathematical model, the designers will have some insight about the comfort levels of the future planned appliances even there is not any prototype to be tested. Consequently, time, prototype costs, and energy will be saved in the laboratory works of the appliances through the results of the preliminary calculations of the comfort tests obtained from the test simulations.

For the parametric investigation, smaller water depths for the channels are useful for fast response of both of the appliance concept; although its effects on the standard combi boiler concept are at the negligible levels. Channel widths have much more effects on the primary DHW concept when compared to the standard combi boiler. Since smaller water depth makes hydraulic diameter smaller resulting in higher convective heat transfer coefficient of the water, transient region diminishes for both of the appliance concept.

As the wall material, Aluminum originated alloys or similar materials having high thermal conductivity are suggested. Transient duration is smaller if Aluminum or its alloy is used for both of the appliance concepts due to higher thermal conductivity. Carbon steel has lower specific heat when compared to the Aluminum alloy or the pure Aluminum. Then, the wall temperature is higher in Carbon steel due to the lower specific heat.

For fin diameters, 11 mm fin diameter, the original fin diameter, is better when compared to the other variations for both of the appliance concept. Although gas volume is increased with the smaller diameters of the fins, the hydraulic channel diameter increases for gas flow thereby resulting in lower heat transfer coefficient of the flue gas. Furthermore, internal heat transfer area decreases. Then, the gas temperature increases at the outlet of the HC for both appliance concepts if the diameters of the pin fins are decreased. As summary, the decrease in the pin fin diameters affects the heat transfer performance of the gas inside the HC negatively. Also, among the investigated parameters, pin fin diameter has the strongest effect on the DHW outlet temperature of both appliance concepts.

The last investigated parameter, DCW inlet temperature, increases the outlet temperature of the DHW in both of the concepts. For a specific DHW set temperature, higher inlet temperature of DCW means less time and energy to reach the set temperature.

As the next steps of this study, all other comfort tests according to (BS EN 13203-1:2006, 2006) other than waiting time test will be simulated. Detailed efficiency test results will be calculated completely covering the international standards (BS EN 13203-2:2006, 2006). Later on, mathematical models of the all other appliance concepts included storage type appliances will be built-up. Their comfort level and efficiency values will be compared on theoretical basis to conclude the most efficient and comfortable appliance type.

REFERENCES

Ataer, A. Ö., İleri, A., & Göğüş, Y. (1995). Transient behaviour of finned-tube cross-flow heat exchangers. *International Journal of Refrigeration, 18 (3),* 153-160.

Atmaca, A. U., Altay, H. M., Ribeiro, B. A. R., Erek, A. (2013). *Modelling of a dual function heating appliance for domestic hot water comfort.* Recent Advances in Fluid Mechanics and Heat & Mass Transfer (Procedings of the 11. International Conference on Fluid Mechanics & Aerodynamics (FMA'13) and Procedings of the 11. International Conference on Heat Transfer, Thermal Engineering and Environment (HTE'13)), ISBN: 978-1-61804-183-8, 117-127.

Basınç düşürücüler, (n.d.). Retrieved December 12, 2012, from http://www.evdeteknik.com/basincdusurucu.html

BS EN 13203-1:2006 (2006). Gas-fired domestic appliances producing hot water-Appliances not exceeding 70 kW heat input and 300 l water storage capacity - Part 1: Assessment of performance of hot water deliveries.

BS EN 13203-2:2006 (2006). Gas-fired domestic appliances producing hot water-Appliances not exceeding 70 kW heat input and 300 l water storage capacity - Part 2: Assessment of energy consumption.

BS EN 483:1999+A4:2007 (2007). Gas-fired central heating boilers – Type C boilers of nominal heat input not exceeding 70 kW.

Bunce, D. J., & Kandlikar, S. G. (1995). Transient response of heat exchangers. *Journal of Heat Transfer, 119,* 729-736.

Galeazzo, F. C. C., Miura, R. Y., Gut, J. A. W., & Tadini, C.C. (2006). Experimental and numerical heat transfer in a plate heat exchanger. *Chemical Engineering Science, 61,* 7133–7138.

Goodwin, D. G. (October 3, 2002). *Cantera C++ user's guide.* Retrieved July 11, 2013, from http://aresinstitute.org/Cantera/cantera-cxx.pdf

Gögüş, Y. A., & Ataer, Ö. E. (1988). Effect of fins on transient behavior of cross-flow air-liquid heat exchangers. *International Refrigeration and Air Conditioning Conference*, 185-192.

Gut, J. A. W., & Pinto, J. M. (2003). Modelling of plate heat exchangers with generalized configurations. *International Journal of Heat and Mass Transfer, 46,* 2571-2585.

High efficiency water heaters, (n.d.). Retrieved April 12, 2012, from http://www.energystar.gov/

Incropera, F. P., Dewitt, D. P., Bergman, T. L., & Lavine, A. S. (2007). *Fundamentals of Heat and Mass Transfer* (6th ed.). USA: John Wiley & Sons, Inc.

Junxiao, S., Guiping, L., & Xiugan, Y. (1998). Transient performances of a two-pass gas-to-gas crossflow heat exchanger. *Journal of Thermal Science, 7 (1),* 67-70.

Kakaç, S., & Liu, H., (2002). *Heat exchangers: selection, rating, and thermal design* (2nd ed.). USA: CRC Press, Taylor & Francis Group

Mishra, M., Das, P. K., Sarangi, S. (2006). Transient behaviour of crossflow heat exchangers due to perturbations in temperature and flow. *International Journal of Heat and Mass Transfer, 49,* 1083–1089.

Research and development roadmap for water heating technologies, (September 30, 2011). Retrieved April 12, 2012, from http://www.ornl.gov/sci/ees/etsd/btric/pdfs/WaterHeatingTechnologiesRoadmap_9-30-2011_FINAL.pdf

Rooke, S. P., Elissa, M. G. (1993). Study of transient behavior of finned coil heat exchangers. *The Fifth Annual Thermal and Fluids Analysis Workshop*, 95-109.

Turns, S. R. (2012). *An introduction to combustion concepts and applications* (3rd ed.). NY: McGraw- Hill.

Types of water heaters, (n.d.). Retrieved April 15, 2012, from http://oee.nrcan.gc.ca/equipment/heating/806#integrated

Ünal, A. (1998). Theoretical analysis of triple concentric-tube heat exchangers, Part 1: Mathematical Modelling. *International Communications in Heat and Mass Transfer, 25 (7)*, 949-958.

Waide, P. (March, 2011). *Opportunities for Success and CO2 Savings from Appliance Energy Efficiency Harmonization- Part2: An Assessment of Test Procedures and Efficiency Metrics.* Retrieved April 12, 2012, from http://www.clasponline.org/en/Resources/Resources/StandardsLabelingResourceLibrary/2011/~/media/Files/SLDocuments/2011-03_HarmonizationStudy/CLASP_HarmonizationStudy_Part2.pdf

APPENDIX

A. Nomenclature

c_p specific heat, J/kg-K

T mean temperature, ˚C

T_{adia} adiabatic flame temperature, ˚C

$\dot{m}$ mass flow rate, kg/s

$A_{sa,g}$ HC inner heat transfer area (from gas domain), m^2

$A_{cs,g}$ cross-sectional area through which flue gas flows, m^2

$A_{sa,wt(hc)}$ HC outer heat transfer area (to the water flowing around the HC), m^2

$A_{cs,wt(hc)}$ cross-sectional area through which HC water (CH water or DCW) flows, m^2

A_o outermost area of HC (contact area with the surrounding air), m^2

$A_{cs,w}$ HC wall cross-sectional area along y_2 direction, m^2

A_{PHE} heat transfer area of one plate, m^2

h_{dcw} convective heat transfer coefficient of the DCW in the HC (primary DHW concept), W/m^2-K

h_g convective heat transfer coefficient of flue gas in the HC, W/m^2-K

$h_{wt(1)}$ convective heat transfer coefficient of CH water in the HC, W/m^2-K

$h_{wt(2)}$ convective heat transfer coefficient of CH water in PHE, W/m^2-K

$h_{wt(3)}$ convective heat transfer coefficient of DHW water in PHE, W/m^2-K

h_∞ natural convection coefficient of surrounding air, W/m^2-K

$U_{dcw\text{-}w}$ overall heat transfer coefficient between the DCW and the HC wall in primary DHW concept, W/m^2-K

$U_{wt(1)}$ overall heat transfer coefficient between the CH water and the HC wall, W/m^2-K

U_{PHE} overall heat transfer coefficient between CH water and DHW in PHE, W/m^2-K

U_g overall heat transfer coefficient between flue gas and HC wall, W/m^2-K

l_{PHE} length of PHE, m

s	HC length, m
z	CH water flow length around HC, m
$R_{t,g\text{-}w}$	total thermal resistance between flue gas and HC wall, K/W
$R_{t,wt(hc)\text{-}w}$	total thermal resistance between HC water (CH water or DCW) and HC wall, K/W
$R_{t,PHE}$	total thermal resistance between CH water and DHW in PHE, K/W
R_0	inner radius of HC wall, m
R_1	average of outer and inner radius of HC wall, m
R_2	outer radius of HC wall, m
R_3	outermost radius of HC
$\dot{Q}_{CH}$	energy transfer rate from CH water to DHW in PHE, J
V_{CHWC}	volume of CH water per channel of PHE, m^3
V_{DHWC}	volume of DHW per channel of PHE, m^3
n	total number of CVs
t	time
t_{final}	final time
Nu	Nusselt number, $[hD_h / k]$
Re	Reynolds number, $[(4m)/(\pi D_h \mu)]$
Pr	Prandtl number, $[c_p \mu / k]$ or $[\nu / \alpha]$
ΔT_{lm}	logarithmic mean temperature difference, K
U_{HC}	overall heat transfer coefficient of the heat cell, W/m^2K
A_{HC}	average heat transfer area from gas to water in the heat cell, m^2
μ_w	dynamic viscosity at plate width inside gasket, Pa.s or Ns/m^2
μ	dynamic viscosity at average inlet temperature (of any fluid under investigation), Pa.s or Ns/m^2
D_{hp}	hydraulic diameter of the water channels in PHE, m
G	mass velocity through a channel, kg/m^2s
A_{ch}	one channel flow area, m^2
A_1	single-plate effective heat transfer area, m^2
A_{1p}	projected plate area, m^2
p_p	plate pitch, m

t_p	plate thickness, m
b_m	mean channel flow gap, m
LHV	lower heating value or net calorific value, MJ/m^3 or MJ/kg
$\dot{n}$	molar rate, kmol/s
W	molecular weight, kg/kmol
V	measured volumetric rate, m^3/h
$\dot{Q}_i$	nominal heat input rate, kW
h	convective heat transfer coefficient, W/m^2K
k	thermal conductivity, W/mK
L	length of the water channel in the HC, m
c_p	specific heat of the fluid under investigation, J/kgK
C_f	correction factor obtained from the calibration curve of the gas meter (Related calibration curve is given in Appendix C)
L_p	projected plate length, m
L_w	plate width inside gasket
t_g	gas temperature at the gas meter, ˚C
p_g	gas pressure at the gas meter, mbar
p_a	atmospheric pressure at the time of the test, mbar
D_h	hydraulic diameter a channel in the HC, m
a	length of the flow channel of the flue gas, m
b	width of the flow channel of the flue gas, m
A_c	flow cross-sectional area, m^2
P_h	wetted perimeter, m
H_{reac}	reactant mixture enthalpy, kJ
H_{prod}	product mixture enthalpy, kJ
P	pressure, atm
h_{reac}	absolute enthalpy of the reactants on a mass basis, kJ/kg
h_{prod}	absolute enthalpy of the products on a mass basis, kJ/kg
N_i	mole numbers of any species (i), kmol or mol

$\bar{h}_i$	absolute enthalpy of any species (i) on a mole basis, kJ/kmol
$\bar{h}^0_{f,i}$	enthalpy of formation at standard reference state on a mole basis, kJ/kmol
A_{total}	total surface area of the fins and the prime surface, m^2
A_f	surface area of a single fin, m^2
A_b	the area of the prime surface where fin array are attached, m^2
Z	total number of the fins
D_{fin}	diameter of a pin fin, m
L_{fin}	length of a pin fin, m
L_c	corrected fin length, m
$\dot{Q}_{gas}$	energy transfer rate from combustion gases to the water around the HC, W

Subscripts/Superscripts:

m	number of the CV under study
p/p+1	present/previous time step
h	hot
c	cold
D	hydraulic diameter
w	heat cell wall
wt	water
g	flue gas (combustion gases)
wt(1)	CH water in HC
wt(2)	CH water in PHE
wt(3)	DHW in PHE
dcw	domestic cold water in HC (in primary DHW concept)
∞	surrounding air
f	fuel
a	air
is	initial state

fs	final state
O_2	Oxygen
N_2	Nitrogene
ff	fin

Greek Symbols:

η_{fin}	overall surface efficiency
η_{fs}	fin efficiency (the performance of a single fin)
ρ	density, kg/m^3
λ	excess air coefficient
Φ	ratio of effective to projected area of corrugated plate

Abbreviations:

CH	central heating
DHW	domestic hot water
DCW	domestic cold water
PHE	plate heat exchanger
P-HE	primary heat exchanger
S-HE	secondary heat exchanger
HC	heat cell
HE	heat exchanger
CV	control volume
CHWC	central heating water channel
DHWC	domestic hot water channel
BC	boundary condition
IC	initial condition

B. Wasted Energy/Useful Energy Ratio

Table B.1 DHW outlet temperatures of both appliance concept with respect to time

DHW outlet temperature in the primary DHW concept (˚C)	DHW inlet and outlet temperature difference in the primary DHW concept (˚C)	Heat gain of DHW for DCW of the primary DHW concept (W)	DHW outlet temperature in thestandard combi boiler (˚C)	DHW inlet and outlet temperature difference in the standard combi boiler (˚C)	Heat gain of DHW for DCW of the standard combi boiler (W)
10,000	0,000	0,000	10,000	0,000	0,000
11,724	1,724	1044,744	10,000	0,000	0,000
14,181	4,181	2533,819	10,672	0,672	407,413
16,877	6,877	4167,885	11,811	1,811	1097,395
19,573	9,573	5802,083	13,147	3,147	1907,337
22,160	12,160	7370,229	14,519	4,519	2738,935
24,594	14,594	8845,352	15,864	5,864	3553,940
26,861	16,861	10219,531	17,169	7,169	4345,418
28,964	18,964	11493,778	18,439	8,439	5114,702
30,909	20,909	12673,018	19,671	9,671	5861,741
32,709	22,709	13763,649	20,864	10,864	6584,529
34,373	24,373	14772,376	22,013	12,013	7281,144
35,913	25,913	15705,687	23,118	13,118	7950,959
37,338	27,338	16569,646	24,180	14,180	8594,584
38,658	28,658	17369,830	25,201	15,201	9213,270
39,882	29,882	18111,336	26,183	16,183	9808,415
41,016	31,016	18798,812	27,128	17,128	10381,331
42,068	32,068	19436,498	28,039	18,039	10933,206
43,044	33,044	20028,263	28,916	18,916	11465,128
43,951	33,951	20577,645	29,763	19,763	11978,111
44,793	34,793	21087,878	30,579	20,579	12473,098
45,575	35,575	21561,927	31,368	21,368	12950,960
46,302	36,302	22002,511	32,129	22,129	13412,497
46,978	36,978	22412,126	32,865	22,865	13858,441
47,606	37,606	22793,064	33,576	23,576	14289,464
48,191	38,191	23147,436	34,264	24,264	14706,188
48,735	38,735	23477,184	34,929	24,929	15109,189
49,241	39,241	23784,099	35,572	25,572	15499,003
49,713	39,713	24069,833	36,194	26,194	15876,134
50,152	40,152	24335,899	36,796	26,796	16241,051
50,560	40,560	24583,711	37,379	27,379	16594,200
50,941	40,941	24814,575	37,943	27,943	16935,999
51,296	41,296	25029,693	38,488	28,488	17266,849
51,627	41,627	25230,179	39,017	29,017	17587,129
51,935	41,935	25417,060	39,528	29,528	17897,199
52,223	42,223	25591,291	40,024	30,024	18197,405
52,491	42,491	25753,754	40,503	30,503	18488,080
52,741	42,741	25905,267	40,968	30,968	18769,538

According to the scenario of the useful and wasted energy, the energy gain by DCW has been counted as wasted energy till the DHW inlet and outlet temperature difference reaches 30 K for both of the appliance concept. Then these points have been signed with yellow in Table B.1. Average of the wasted energy till this point is

10027.7 W for the primary DHW concept, whereas it is 9997,6 W for the standard combi boiler as signed with green in Table B.1. In a similar way, average useful energy is counted as 27687 W for the primary DHW concept and 26671,1 W for the standard combi boiler according to the calculations for 400 second including the steady-state conditions. Resultantly, wasted energy/useful energy ratio is 0.36 for the primary DHW concept and 0.37 for the standard combi boiler.

C. Calibration Curve of the Gas Meter

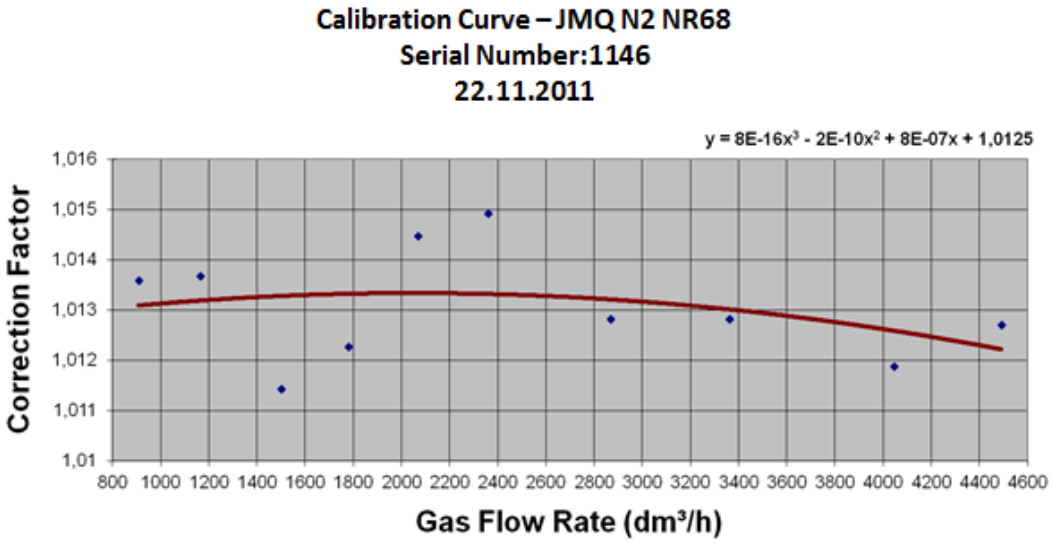

Figure B.1 Calibration curve of the gas meter